A Non-Contact Structural Health Monitoring Method Based on Radio Frequency Signal Analysis

Alexander Amies

A thesis presented for partial fulfilment of the

requirements for the degree of Doctor of Philosophy

in

Mechanical Engineering

at the

University of Canterbury

Christchurch, New Zealand

July 2018

Abstract

Structural health monitoring (SHM) is a group of technologies enabling the monitoring of structural motion during external loading. This loading is often caused by earthquakes. SHM provides understanding of the severity and location of damage to a structure without requiring visual structural inspection. The technologies used to perform SHM require input measurements taken from the structure during seismic events.

Many modern implementations of SHM instrumentation networks use accelerometers or strain gauges to obtain data. For parametric SHM methods in particular, this data must be converted to displacement to determine the severity of structural property changes. This necessity means filtering must be applied to structural acceleration data, which removes crucial response information that can indicate damage. A method of directly measuring displacement was thus sought.

Research into methods of direct measurement of displacement indicated frequency-modulated continuous wave (FMCW) radar was suitable. This technology uses mixing of transmitted and reflected signals with time-varying frequency to determine signal time-of-flight. Simulation of this technology in a 1D channel indicated the method would be precise enough for SHM data collection. Research indicated interstorey drift ratios (IDRs) as small as 0.2 % would need to be detected to identify slight damage. Sim-

ulation showed that with the use of signal processing techniques, a sub-millimetre target displacement precision could be obtained, which is much smaller than the 5 mm displacement resolution requirement found in literature.

A hardware prototype was constructed for experimental testing on a shake table. This prototype was constructed with components that allowed for maximum configurability to test radar systems with different input parameters. The table was driven with historical earthquake acceleration data. The mean equivalent IDR error found with the use of cross-correlation and multitaper signal processing methods was 0.05 %, indicating the concept of radar-based SHM was viable.

A pair of structural instrumentation schemes using FMCW radar sensors were devised. The first of these methods requires the placement of two radar transceiver units in adjacent corners of a floor, and two corner reflectors in opposite corners. The second method uses a single transceiver unit placed in the centre of a floor, with two corner reflectors placed in upper adjacent corners. The former method allows for more precise monitoring, while the latter method is suitable for structures with significant centrally-located structural material or in situations where cost is a limiting factor.

The possibility of using existing wireless local area network (WLAN) hardware for SHM purposes was investigated. It was found that the IEEE 802.11 5 GHz band had suitable bandwidth for implementing FMCW radar-based SHM. Simulation of a system using standard-compliant transmission demonstrated that cheap installations of SHM are possible using this method, allowing the use of SHM to become more widespread and thus public safety to be improved.

Publications

Over the course of this research, a number of papers have been published. The research demonstrated in these papers is based on the work presented in this thesis.

Journal Papers

- **Amies, AC**, Pretty, CG, Rodgers, GW, Chase, JG (2018). "Improving the precision of a radar-based structural health monitoring system." [Draft completed]

- **Amies, AC**, Pretty, CG, Rodgers, GW, Chase, JG (2018). "Experimental validation of a radar-based structural health monitoring system," *IEEE/ASME Transactions on Mechatronics*. [Under review]

Conference Papers

- **Amies, AC**, Pretty, CG, Rodgers, GW, Chase, JG (2018). "Shake table testing of a radar-based structural health monitoring method," *2018 14th IEEE/ASME International Conference on Mechatronic and Embedded Systems and Applications (MESA)*, Oulu, Finland, 2-4 July 2018.

- **Amies, AC**, Pretty, CG, Rodgers, GW, Chase, JG (2016). "Simulating and testing a non-contact structural health monitoring system," *2016 12th IEEE/ASME International Conference on Mechatronic and Embedded Systems and Applications (MESA)*, Auckland, New Zealand, 29-31 August 2016.

- **Amies, AC**, Pretty, CG, Rodgers, GW, Chase, JG (2016). "Development of a non-contact, non-line of sight displacement sensor for structural health monitoring," *2016 New Zealand Society for Earthquake Engineering (NZSEE)*, Christchurch, New Zealand, 1-3 April 2016.

- **Amies, AC**, Pretty, CG, Rodgers, GW, Chase, JG (2015). "A continuous wave radar technique for structural health monitoring," *2015 9th International Conference on Sensing Technology (ICST)*, Auckland, New Zealand, 8-10 December 2015.

Acknowledgments

I would like to express my sincere thanks to my supervisory team consisting of Dr. Chris Pretty, Distinguished Professor Geoff Chase, and Associate Professor Geoff Rodgers. Their invaluable expertise, resources, and access have given me the tools I have needed to conduct this research. I am grateful for the inspiration they have provided me with to create something new in structural health monitoring, a field I previously knew nothing about.

My thanks must also go to the technical support I have received, not only from my supervisory team, but also from Julian Murphy and Scott Amies. Their decades of experience helped me solve problems in ways I could not have managed myself.

As well as those at the University of Canterbury who have supported me, I would like to thank the University of Auckland for access to their shake table to carry out my experimental work. My research was also generously supported by a Mechanical Engineering Doctoral Scholarship and a College of Engineering Fees Scholarship, without which I would not have been able to complete my Ph.D.

I would also like to thank the many other students in E209, who have provided me with technical and emotional support throughout our shared struggle. The opportunity to

vent frustrations to those who understand the difficulties of research was crucial, as was the ability to, when necessary, take my mind off my own project to learn about their work. The camaraderie of the students in that environment makes postgraduate research easy to recommend to others.

Finally, and most importantly, I must thank my parents. Without their continued love, support, and patience, I would not have been able to complete the work in this thesis. I am forever indebted for the opportunities they have provided me to live a rewarding life.

Contents

Abstract ii

Publications iv

Acknowledgments vi

Contents viii

List of Figures xii

List of Tables xvii

List of Abbreviations xix

1 Introduction 1

1.1 Problem 1

1.2 Preface 2

2 Literature Review 5

2.1 Introduction 5

2.2 Structural Health Monitoring 6

2.2.1 Parametric Methods 7

2.2.2 Non-Parametric Methods 13

2.2.3 Implications for Sensor Requirements 15

2.2.4 Requirements for Damage Detection 16
2.2.5 Existing Methods for Structural Instrumentation 21
2.3 Indoor Positional Tracking Methods 25
2.3.1 Generic Wireless Local Area Network Positioning 25
2.3.2 Global Positioning System 28
2.3.3 Radar 32
2.3.4 Indoor Multi-Target Tracking Methods 38
2.4 Context of Problem Definition 39
2.5 Summary 40

3 Simulating a Radar-Based Structural Health Monitoring Method 43
3.1 Introduction 43
3.2 Simulation Method 44
3.2.1 Static Target Modelling 45
3.2.2 Seismic Motion Modelling 48
3.3 Results 51
3.4 Discussion 54
3.5 Summary 55

4 Development of a Prototype Radar Structural Health Monitoring Sensor 58
4.1 Introduction 58
4.2 Design Requirements 59
4.3 Components Selected 63
4.4 Reflector Design 67
4.5 Summary 68

5 Shake Table Validation of Prototype Radar Sensor 71
5.1 Introduction 71
5.2 Method 72
5.3 Tested Data Sets 76

5.4 Signal Processing Methods 78
5.4.1 'Peak' Method 79
5.4.2 'Quad' Method 81
5.4.3 'QuadF' Method 82
5.4.4 'MT' Method 83
5.4.5 Data Processing for System Validation 87
5.4.6 Comparison to Accelerometers 92
5.5 Results 92
5.6 Discussion 94
5.7 Summary 100

6 Sensor Placement and Identification in a Multistorey Structure 102
6.1 Introduction 102
6.2 Requirements 103
6.3 Placement Options 107
6.3.1 Mapping Interstorey Diagonal Displacements to Three Dimensions 108
6.3.2 Centrally-Located Transceiver Monitoring 115
6.3.3 Method Comparison 118
6.4 Summary 122

7 Utilising Existing Wireless Protocols for Structural Displacement Measurement 123
7.1 Introduction 123
7.2 Existing Protocols 124
7.3 Simulation 127
7.3.1 Method 127
7.3.2 Results 130
7.3.3 Discussion 131
7.4 Summary 134

8 Conclusions **135**

9 Future Work **138**

References **142**

List of Figures

2.1 A diagram of a building before (black) and during or after (red) a seismic event. The quantities to used to calculate the interstorey drift ratio ($\delta_2 = (d_2 - d_1)/h_2$) are indicated in blue. 17

2.2 An example from Naeim, Hagie, and Alimoradi (2005) of a fragility function determining the likelihood of cracking at multiple damage states. . . . 19

2.3 Construction of the L1 and L2 GPS signals (Dana, 2000) 29

2.4 An example of how frequency-modulated continuous wave signals change in frequency over time. The transmitted signal is shown in red, and the reflected and received signal is shown in green, indicating the delay between the two signals. The difference in frequency between the two signals is shown in blue, indicating that the signals have mostly a constant frequency difference, where the frequency difference is proportional to the time it takes for the wave to return. 33

2.5 The hypothetical beat spectrum of a radar system. Frequency a may correspond to the target, while b could be the same target as observed by signals travelling along a different path. 37

3.1 The data used to simulate a single degree of freedom (DOF) structure, taken from the 2010 Canterbury, New Zealand earthquake. 49

3.2 Impulses representing the beat signal Discrete Fourier Transform (DFT) are shown in blue, and a quadratic interpolation of the three points centred about the DFT peak shown in red. The peak of this interpolation provides a better estimate of the reflector distance than the raw DFT peak. . . . 50

3.3 Beat signal for a simulated static target ($d = 10\,\mathrm{m}$, $(f_1 - f_0) = 700\,\mathrm{MHz}$, $T_{\mathrm{mod}} = 5\,\mathrm{ms}$, AWGN SNR = 20 dB). 52

3.4 Displacement estimation accuracy is improved with increased frequency sweep bandwidth. In each case, $T_{\mathrm{mod}} = 5\,\mathrm{ms}$, and $f_1 = 1\,\mathrm{GHz}$. 53

3.5 A comparison between 'Peak' (blue) and 'Quad' (red) methods with different amounts of zero-padding (relative to T_{mod}). The quadratic interpolation method is consistently better, and zero-padding the signal improves the detection accuracy. 53

3.6 The tracking of the displacement of a target driven with structural response data (blue) with a system using the 'Peak' method (red). 56

3.7 The tracking of the displacement of a target driven with structural response data (blue) with a system using the 'Quad' method (red). 56

3.8 The tracking of the displacement of a target driven with structural response data (blue) with a system using the 'MT' method (red). 57

3.9 The tracking of the displacement of a target driven with structural response data (blue) with a system using the 'CorrMT' method (red). 57

4.1 The functional layout of the FMCW system used to validate this SHM approach. 63

4.2 The interface for the LMX2492EVM Fractional PLL device to configure the transmitter frequency modulation parameters. 64

4.3 The horizontal radiation pattern for a range of broadcast frequencies for the Aaronia HyperLOG 60180 antenna (reproduced from Aaronia (2014)). 65

4.4 The interface for the Logic Pro 16 when configured to capture analog signals. 66

4.5 Components of the FMCW radar prototype, including (a) the PLL and VCO, (b) the signal mixer, (c) and the ADC. 67
4.6 Initial verification of the prototype, with components connected in (a) and detecting a nearby static reflector in (b). 69
4.7 Corner reflectors reflect incoming beam paths off each of the three internal faces before returning the beam in a direction parallel to the path in which it entered the reflector. Note that regardless of the entry angle, the beam travels the same distance before it exits the reflector. 70
4.8 The corner reflector fixed to a shake table. 70

5.1 Plan view of the FMCW radar validation experimental layout, with a corner reflector fastened to the shake table and the monitoring equipment placed off-structure. 73
5.2 The prototype FMCW system set up to detect the motion of a shake table, and the reflector fastened to the table (far right). 74
5.3 The FFT spectrum of the REHS strong motion recording (red) and the corresponding FFT spectrum of the response of a 2.0 s period single DOF structure (blue) for this input ground motion. 75
5.4 The Christchurch Resthaven (REHS) ground displacement data. 77
5.5 The Christchurch Cathedral College (CCCC) ground displacement data. 77
5.6 The Canterbury Botanical Gardens (CBGS) ground displacement data. . 78
5.7 The Papanui High School (PPHS) ground displacement data. 78
5.8 The Christchurch Hospital (CHHC) ground displacement data. 79
5.9 Linear variable differential transformer (blue) and radar 'CorrMT' method (red) data (a) before and (b) after time synchronisation. 88
5.10 An example of a hypothetical 2D structure with a radar transceiver placed in the lower left corner and a reflector in the upper right corner. The inter-storey diagonal displacement, x, is represented in blue. 89

5.11 The REHS acceleration-derived displacement data (blue) and radar-derived data (red), compared to the linear variable differential transformer (LVDT)-derived displacement (black, dashed). 94
5.12 The CCCC acceleration-derived displacement data (blue) and radar-derived data (red), compared to the LVDT-derived displacement (black, dashed). 95
5.13 The CBGS acceleration-derived displacement data (blue) and radar-derived data (red), compared to the LVDT-derived displacement (black, dashed). 95
5.14 The PPHS acceleration-derived displacement data (blue) and radar-derived data (red), compared to the LVDT-derived displacement (black, dashed). 96
5.15 The CHHC acceleration-derived displacement data (blue) and radar-derived data (red), compared to the LVDT-derived displacement (black, dashed). 96
5.16 A comparison of sweep spectra from simulation (blue) and experimental (red) data. In both cases, the FFT method was used. 97

6.1 Empirical damage state data based on (a) interstorey drift ratio, (b) load cycles, and (c) joint shear strain engineering demand parameters with associated coefficients of determination (Pagni & Lowes, 2006). 106
6.2 The definition of North-South and West-East axes in a three dimensional, multistorey structure. 107
6.3 The interstorey diagonal displacement, shown as x, of a hypothetical two dimensional structure. 109
6.4 The definition of interstorey diagonal displacements in a three dimensional structure. 111
6.5 An artificially generated example of a beat spectrum containing two prominent reflecting targets. 114
6.6 The definition of interstorey centre-to-corner displacements in a three dimensional structure. 116

7.1 A frequency upsweep when the frequencies are limited to the centre frequencies of the channels available to IEEE 802.11-compliant hardware in the 5 GHz band. 128

7.2 The created spectrum for 5.0 GHz channel 56, which was run through an inverse FFT for chirp generation. 129

7.3 The simulated tracking (red) using 'CorrMT' of a single DOF target driven with structural response data (blue). The target is tracked using a WiFi-based FMCW radar system. 131

7.4 Another example of simulated tracking (red) using 'CorrMT' of a single DOF target driven with structural response data (blue). The target is tracked using a Wi-Fi-based FMCW radar system with non-ideal broadcast channels. 132

List of Tables

2.1 Requirements of proposed structural health monitoring system 41

3.1 A simulated FMCW system using 2010 Canterbury earthquake data . . 54

4.1 The components selected for the prototype FMCW system. 68

5.1 Mean absolute interstorey diagonal displacement errors as a relative percentage 93

5.2 Mean interstorey drift ratio errors as absolute difference in IDR 93

5.3 IDR errors at peak interstorey drift as absolute difference in IDR 93

5.4 Accelerometer errors 94

6.1 Prototype transceiver unit cost 121

7.1 IEEE 802.11 WLAN channels in the 2.4 GHz band 125

7.2 IEEE 802.11 WLAN channels in the 5 GHz band 126

List of Abbreviations

ANN artificial neural network

AWGN additive white Gaussian noise

DFT Discrete Fourier Transform

DM damage state

DOF degree of freedom

EDP engineering demand parameter

EMD empirical mode decomposition

ERA Eigensystem Realisation Algorithm

FE finite element

FFT Fast Fourier Transform

FIR finite impulse response

FMCW frequency-modulated continuous wave

GNSS global navigation satellite system

GPS Global Positioning System

HMM hidden Markov model

ICCD interstorey centre-to-corner displacement

IDD interstorey diagonal displacement

IDR interstorey drift ratio

IF intermediate frequency

IIR infinite impulse response

LMS least mean square

LOS line of sight

NF noise figure

NLOS non-line of sight

PCB printed circuit board

PDF probability density function

PLL phase-locked loop

RF radio frequency

RSS received signal strength

SHM structural health monitoring

SNR signal-to-noise ratio

SV space vehicle

TOF time-of-flight

UWB ultra-wide bandwidth

WLAN wireless local area network

Electrical Devices

ADC analog-to-digital converter

ASIC application-specific integrated circuit

FBG fiber Bragg grating

FPGA field-programmable gate array

LVDT linear variable differential transformer

MEMS Micro-Electro Mechanical System

VCO voltage-controlled oscillator

Cardinal Directions

N-S north-south

W-E west-east

Organisations

IASC-ASCE International Association for Structural Control-American Society of Civil Engineers

IEEE Institute of Electrical and Electronics Engineers

Strong Motion Sites

CBGS Canterbury Botanical Gardens

CCCC Christchurch Cathedral College

CHHC Christchurch Hospital

PPHS Papanui High School

REHS Christchurch Resthaven

CHAPTER 1

Introduction

1.1 Problem

Structural health monitoring (SHM) is a group of technologies that enables the monitoring of motion during structural loading, which leads to understanding of the severity and location of damage to a structure with measured motion data. Determination of damage otherwise requires the removal and visual inspection of structural members. This process is time-consuming and expensive in the aftermath of seismic activity, because above certain force and moment magnitudes all structures in the vicinity of the earthquake's epicentre require this inspection. Monitoring is used to provide similar information without the need for human intervention.

Contemporary technologies can struggle to obtain measurements of structural displacement, instead measuring structural strain or acceleration and obtaining estimates of displacement indirectly. This process is complicated by the necessity of baseline correc-

tion of the derived displacement due to the double integration of acceleration. This problem limits these systems' ability to accurately track displacement. In addition, many contemporary methods which directly measure displacement require structural modification for installation. This necessity limits their ability to be retrofitted to existing structures.

This thesis attempts to provide a proof-of-concept for a method of non-contact SHM which measures structural displacement directly. The use of a radio frequency (RF) approach, namely frequency-modulated continuous wave (FMCW) radar, is novel in the context of active structural monitoring for seismic events. Research has been undertaken to determine the precision of such a system, the radar parameters required to enable it to function, and the limitations of this method of monitoring.

1.2 Preface

SHM is a collection of methods that determine structural damage, particularly during earthquakes. Detection of damage is crucial because after incurring damage, a structure's properties change. These changes reduce the resillience of a structure in the event of subsequent seismic events. The SHM process can be performed using either parametric or non-parametric methods. The former group of methods attempts to deduce changes in modal parameters based on the difference between modelled and measured responses in a structure during a seismic event. The latter group typically use time domain analysis of structural motion data to determine damage without prior knowledge of structural performance. In either case, knowledge of structural displacement is important for determining severity and locality of damage.

Radar is a well-researched electromagnetic wave-based technique used to detect the

presence of objects and their distance from a transmitting and receiving unit. This unit transmits radio waves of known frequencies and compares these waves to received echoes to determine the distance to nearby reflective objects. There are numerous methods used to determine the distance to reflectors, including time of flight of the signal, and frequency analysis of a frequency modulated radar signal (Brooker, 2005; Jenn, 2007). This thesis presents a method employing the latter technique to provide direct displacement measurements for SHM.

There are numerous metrics used as inputs to models of structural damage, and among these is the interstorey drift ratio (IDR). This metric measures how far one level of a multistorey structure is displaced from its resting position relative to the storey below it, and the distance separating the two storeys. Larger IDR measurements naturally correlate with more severe damage (Chase, Hudson, Lin, Elliot, & Sim, 2005; H. Kim & Adeli, 2004).

Modern methods of measuring displacement typically utilise accelerometers, and then doubly-integrate to obtain displacement estimates. This method is susceptible to integral drift errors (Thenozhi, Yu, & Garrido, 2012), resulting in damaging motion potentially going undetected if a structure resettles in a different position after a seismic event. The ability to measure structural displacement avoids the need for baseline correction (Boore, Stephens, & Joyner, 2002; Chiu, 1997). This research is thus focused on a non-contact method of measuring structural displacement directly.

There are currently existing types of SHM sensors. These sensors include devices capable of measuring impedance (Hoshyarmanesh, Abbasi, Moein, Ghodsi, & Zareinia, 2017), accelerometers (Li, Li, & Song, 2004; Moyo, Brownjohn, Suresh, & Tjin, 2005), and displacement measuring sensors, such as non-contact line scanners (Jeon et al., 2014; Nayyerloo, 2011; Nayyerloo et al., 2011) and directly-connected linear variable differ-

ential transformer (LVDT) methods. The latter method requires space in the structure for the system to be installed, and can be damaged during earthquakes. To incorporate these methods in a structure, allowances would need to be made for the placement of these sensors. This requirement makes such designs less robust and difficult to retrofit to existing buildings. A non-line of sight (NLOS), non-contact method was desired, and radar was identified as a suitable technology for this purpose.

In order to obtain displacement measurements, FMCW radar can be used. This method transmits a signal with time-varying frequency, and compares the returned echo of the signal with the transmitted signal at the same instant by multiplying (or heterodyning) the two signals to obtain a beat signal. The fundamental frequency of this mixed signal is proportional to the signal time-of-flight. From this value, a distance can be obtained. The parameters of the FMCW system, including bandwidth, centre frequency, modulation sweep time, and signal amplification, determine how successful the system is at detecting small perturbations in distance and at detecting distant objects.

This thesis explores how such a system would be implemented, and its suitability for SHM. The relationship between radar distance measurements and IDR is explained, and what that relationship means for the FMCW system's resolution requirements is explored. The FMCW system is tested in simulation, and the results of the simulation are used to justify the chosen parameters for a hardware prototype. This prototype was then designed, built, and tested using a shake table to verify that sufficiently accurate IDR measurements could potentially be obtained by an installation of this SHM method. An implementation strategy for FMCW radar SHM sensors is presented, in addition to an investigation into the suitability of generic WiFi hardware for this method of instrumentation.

CHAPTER 2

Literature Review

2.1 Introduction

This chapter presents a review of the literature on structural health monitoring (SHM) including the requirements of SHM systems, and measures and metrics which best assess structural damage. Further, the particular ranges of values used for these metrics were identified to determine the necessary limits of operation of any proposed SHM sensor method. From this information, the limitations of contemporary SHM were identified, allowing for the identification of a method of motion detection which was both novel and a solution for the limitations of existing research.

The ability to determine structural displacement directly, in a non-contact manner, was seen as being the most potentially beneficial to the general SHM field. The ability to retrofit accurate displacement sensors to existing structures in a simple and cost-effective manner would enable instrumentation for numerous structures, making such

monitoring essentially ubiquitous. In turn, it would help enable identification of structures that through design error or age, are unable to withstand damaging earthquakes. The literature review conducted in this chapter sought to identify the possible methods to achieve this goal.

2.2 Structural Health Monitoring

There are numerous approaches taken to the assessment of damage in structures after seismic events. Knowledge of structural damage must be gained in the immediate aftermath of such events to determine the safety of reoccupation. There is a class of post-event inspection techniques which use ultrasonic, electromagnetic, and radiography methods to assess damage in a non-destructive manner (Chang & Liu, 2003). These methods require direct access to the structure to perform, compromising inspector safety, and are time-consuming and costly to execute. These methods are also only able to identify surface-level damage and cannot detect yielding or loss of stiffness. To circumvent these issues, SHM is used to provide information about structures without the need for human intervention.

SHM uses sensor networks to monitor the behaviour of structures during loading, particularly caused by seismic events. The data collected by these sensors is used to estimate structural properties and condition relative to a baseline prior the earthquake or other environmental load. Any changes reflect the damage in the structure to varying levels of identification, ranging from the identification of the presence of damage, to the quantification of that damage and thus the expected lifetime of the structure. These vibration-based methods are typically used for global damage identification (Fritzen, 2014). The structural behaviour is used as an input to either a parametric or non-parametric method to determine this damage.

2.2.1 Parametric Methods

Parametric methods of determining damage require an understanding of structural dynamics. Typical dynamic systems are represented by modal parameters, which are altered by structural deformation. Methods which utilise changes in these properties to determine damage typically revolve around the identification of natural frequency, mode shapes, and modal damping (Doebling, Farrar, Prime, & Shevitz, 1996; Yan, Cheng, Wu, & Yam, 2007; Zou, Tong, & Steven, 2000). Because of its simplicity of measurement, natural frequency changes have been used as a damage metric in a number of applications (Brincker, Zhang, & Andersen, 2000; Doebling et al., 1996; Qiao, Esmaeily, & Melhem Hani, 2012). However, natural frequency has been shown to be lacking in the required sensitivity to be suitable as a damage identification in large structures (J.-T. Kim, Ryu, Cho, & Stubbs, 2003).

Mode shape has been shown to be more sensitive to localised damage than natural frequency. Particularly, damage present at locations on a structure where its mode shape function changes rapidly is more easily identifiable using mode shape analysis (Khoo, Mantena, & Jadhav, 2004; Maia, Silva, Almas, & Sampaio, 2003). However, due to the difficulty of precisely measuring mode shapes compared to measuring natural frequency, this method requires a larger number of sensors to achieve suitable SHM and is therefore more costly to implement. Measurement of natural frequency or mode shape to determine damage also requires primarily linear behaviour in dynamic response. These methods are therefore prone to allowing non-linear response due to damage to remain undetected, limiting their effectiveness (Chase, Hwang, Barroso, & Mander, 2004).

Use of the Eigensystem Realisation Algorithm (ERA) is a typical approach taken to identify structural damage using time-domain response data. In this scenario, a Hankel

matrix is generated to realise a linear model for the dynamical system (Juang & Pappa, 1985). The matrix is of the form:

$$\begin{bmatrix} y(k) & y(k+1) & \cdots & y(k+n-1) \\ y(k+1) & y(k+2) & \cdots & y(k+n) \\ \vdots & \vdots & \ddots & \vdots \\ y(k+n-1) & y(k+n) & \cdots & y(k+2n-2) \end{bmatrix} \tag{2.1}$$

where $y(k)$ is the k^{th} state measurement of the structure, such as acceleration. This matrix is used to generate the system output, from which the eigenvalues of the time-domain response data are extracted to determine the natural frequencies and mode shapes of the structure. This process has been further investigated by Bernal and Gunes (2000) and Luş, Betti, Yu, and De Angelis (2004) with the latter approach using a Kalman filter estimator for basline model identification before using a least squares approach to optimisation of the state space model. Caicedo, Dyke, and Johnson (2004) note that the accuracy of the approach is dependent on sensor noise, resolution, and linearity, in addition to model error. The extraction of free-response time series data from SHM systems which record motion during seismic events can be challenging, adding to the difficulty of minimising model error.

Parametric methods include finite element (FE) approaches, in which system parameters are altered based on differences between the mathematical structural model and measurements taken from the monitored structure (Brownjohn, Xia, Hao, & Xia, 2001; Cunha & Caetano, 2006; Jaishi & Ren, 2005). The model is developed from the results of an initial impulse test to determine the structural response in an output degree of freedom (DOF) relative to the magnitude of input. A number of update methods are employed to achieve a closer relationship in mass, stiffness, and damping characteristics

between the structure and its FE model. These approaches include sensitivity function (Fritzen, Jennewein, & Kiefer, 1998) and response surface methods (Ren & Chen, 2010). The changes in monitored parameters can be directly linked to damage (Mottershead, Link, & Friswell, 2011).

Changes in modal parameters can be challenging to interpret and relate to a damage mapping (Mottershead & Friswell, 1993), thus leading to the development of methods which use baseline mass, stiffness, and damping properties of structures as models for comparison. A parametric approach used for near-real-time SHM utilises the comparison of model-based behaviour with monitored structural motion. This is achieved using adaptive least mean square (LMS) filtering to transform the monitored structural data to minimise the error between true behaviour and modelled behaviour. The remaining error, between the model and reality can be attributed to changes in structural parameters, indicating a damage state. The behaviour of a structure due to external loading can be modelled (Chase et al., 2004):

$$\boldsymbol{M} \cdot \ddot{v} + \boldsymbol{C} \cdot \dot{v} + \boldsymbol{K} \cdot v = -\boldsymbol{M} \cdot \mathbf{1}\ddot{x}_g \tag{2.2}$$

Here, $\boldsymbol{M}$, $\boldsymbol{C}$, and $\boldsymbol{K}$ are the mass, damping and stiffness parameters of the structure, $\ddot{x}_g$ is the ground acceleration applied to the structure, $\mathbf{1}$ is a column vector of ones with length equal to the number of floors in the structure, and v, $\dot{v}$, and $\ddot{v}$ are the structure's displacement, velocity, and acceleration respectively.

The model defined by Chase et al. (2004) is a simplified version of the approach taken by Bouc (1967) and Wen (1976). This model is expressed in the form:

$$m\ddot{v}(t) + c\dot{v}(t) + \alpha\frac{F_y}{Y}v(t) + (1-\alpha)\frac{F_y}{Y}h(t) = -m\ddot{x}_g \tag{2.3}$$

where v, $\dot{v}$, and $\ddot{v}$ are the displacement, velocity, and acceleration of the structure. The structural parameters m and c are the mass and equivalent viscous damping respectively, while F_y and Y are the yield force and displacement of the structure. $\ddot{x}_g$ is the ground acceleration applied to the structure. The parameter h is the hysteretic displacement, where $\dot{h}$ is expressed by:

$$\dot{h}(t) = \dot{v}(t)\left\{A - \left|\frac{h(t)}{Y}\right|^n (\beta \text{sign}\,(\dot{v}(t)h(t)) + \gamma)\right\} \tag{2.4}$$
$$A > 0, \beta > 0, -\beta < \gamma \leq \beta, n \geq 1$$

where the parameters A, β, γ, and n are the Bouc-Wen model parameters of stiffness, fatness, pinching, and abruptness. Equations (2.3) and (2.4) indicate that the structure's response to external forces has some hysteretic property. Structural motion and thus indicators of damage are therefore dependent on instantaneous displacement, velocity, and acceleration. It follows that to obtain information regarding structural damage through motion and deformation analysis, accurate tracking of displacement is required.

In the general case in Equation (2.2), the kinematic inputs are vector quantities where each element corresponds to the motion of the ith storey to the ground, resulting in, for a three storey structure:

$$\begin{bmatrix} m_1 & 0 & 0 \\ 0 & m_2 & 0 \\ 0 & 0 & m_3 \end{bmatrix} \begin{bmatrix} \ddot{v}_1 \\ \ddot{v}_2 \\ \ddot{v}_3 \end{bmatrix} + \begin{bmatrix} c_1 + c_2 & -c_2 & 0 \\ -c_2 & c_2 + c_3 & -c_3 \\ 0 & -c_3 & c_3 \end{bmatrix} \begin{bmatrix} \dot{v}_1 \\ \dot{v}_2 \\ \dot{v}_3 \end{bmatrix} + \begin{bmatrix} k_1 + k_2 & -k_2 & 0 \\ -k_2 & k_2 + k_3 & -k_3 \\ 0 & -k_3 & k_3 \end{bmatrix} \begin{bmatrix} v_1 \\ v_2 \\ v_3 \end{bmatrix} = - \begin{bmatrix} m_1 \\ m_2 \\ m_3 \end{bmatrix} \ddot{x}_g \quad (2.5)$$

Damage resulting from external loading causes a change in structural parameters, in particular natural frequency and stiffness. These changes in behaviour require a re-modeled structure with the form:

$$\boldsymbol{M} \cdot \ddot{v} + \boldsymbol{C} \cdot \dot{v} + (\boldsymbol{K} + \Delta\boldsymbol{K}) \cdot v = -\boldsymbol{M} \cdot \boldsymbol{1}\ddot{x}_g \quad (2.6)$$

The additional parameter $\Delta\boldsymbol{K}$ contains the information relating to structural parameter changes and may be time-variant. The goal of SHM systems is to provide the v, $\dot{v}$, and $\ddot{v}$ data such that, with knowledge of ground motion and initial structural parameters, the structural changes post-event can be identified. From these changes, damage existence, location, and severity are determined.

The example three storey structure model presented in Equation (2.5) therefore also has some $\Delta\boldsymbol{K}$ which can be reparameterised to allow for changes to properties of independent storeys to be isolated:

$$\Delta \boldsymbol{K} = \alpha_1 \begin{bmatrix} 1 & 0 & 0 \\ 0 & 0 & 0 \\ 0 & 0 & 0 \end{bmatrix} + \alpha_2 \begin{bmatrix} 1 & -1 & 0 \\ -1 & 1 & 0 \\ 0 & 0 & 0 \end{bmatrix} + \alpha_3 \begin{bmatrix} 0 & 0 & 0 \\ 0 & 1 & -1 \\ 0 & -1 & 1 \end{bmatrix} = \begin{bmatrix} \alpha_1 + \alpha_2 & -\alpha_2 & 0 \\ -\alpha_2 & \alpha_2 + \alpha_3 & -\alpha_3 \\ 0 & -\alpha_3 & \alpha_3 \end{bmatrix} \quad (2.7)$$

In Equation (2.7), the time-varying scalar parameters α_i are equal to the independent floor stiffness changes Δk_i, thus meaning that the change in stiffness can be equated to:

$$\Delta \boldsymbol{K} = \begin{bmatrix} \Delta k_1 + \Delta k_2 & -\Delta k_2 & 0 \\ -\Delta k_2 & \Delta k_2 + \Delta k_3 & -\Delta k_3 \\ 0 & -\Delta k_3 & \Delta k_3 \end{bmatrix} = \sum_{i=1}^{3} \alpha_i \Delta K_i \quad (2.8)$$

Equation (2.6) can then be rearranged as such:

$$\boldsymbol{M} \cdot \ddot{v} + \boldsymbol{C} \cdot \dot{v} + \boldsymbol{K} \cdot v + \sum_{i=1}^{n} \alpha \Delta K_i v = -\boldsymbol{M} \cdot \boldsymbol{1} \ddot{x}_g = \boldsymbol{F} \quad (2.9)$$

The model error due to non-linear effects for an n-storey structure can be thus expressed as:

$$\begin{aligned} y_k &= \boldsymbol{F} - \boldsymbol{M} \cdot \ddot{v} - \boldsymbol{C} \cdot \dot{v} - \boldsymbol{K} \cdot v \\ &= \sum_{i=1}^{n} \alpha \Delta K_i v \end{aligned} \tag{2.10}$$

The equivalence in Equation (2.10) shows that the determination of instantaneous structural damage at time k using this model is dependent on the time-varying displacement of the structure.

An adaptive LMS filter was then employed, with filter coefficients varied to minimise the non-linear error. The difference between the noisy input data $\hat{y}_k$ and the filter output constituted the error which could be attributed to change in structural stiffness α_i. This method enabled individual stiffness changes to be identified, and thus the position of damage was able to be located. The method was validated using a range of damage patterns on an International Association for Structural Control-American Society of Civil Engineers (IASC-ASCE) benchmark structure.

2.2.2 Non-Parametric Methods

While parametric methods combine the structural response data gained from SHM sensors with excitation data to identify the damage state of a structure based on predetermined structural parameters, non-parametric methods aim to provide indications of structural damage without necessary prior knowledge of structural performance. Typical applications of these methods involve the time-domain analysis of system response data. From this analysis, features characteristic of a change in structural property can be identified.

One example of non-parametric SHM is empirical mode decomposition (EMD), in which underlying basis functions of a signal are extracted from time series data to reveal the modes of system response (Huang et al., 1998). Periodic frequency domain analysis of these basis functions using the Hilbert transform allows for the change in modes during a seismic event to be investigated, allowing non-linearities in structural response to be identified. One proposed application of EMD has verified its suitability for damage identification in an SHM context (Roveri & Carcaterra, 2012). A system which relies on EMD for damage identification cannot be fully automated. Each identified mode requires analysis of its relevance to structural behaviour, from which a judgement of damage location and severity can be made.

Wavelet-based methods are also used to evaluate a structure's response to seismic loading. This method is a generalised form of a windowed Fourier transform which allows non-stationary signal's dominant modes to be tracked in time (Torrence & Compo, 1998). A set of basis functions which make up the modes of a wavelet-transformed signal can also be identified using this method, which has been used as a method of structural damage assessment (Hou, Noori, & Amand, 2000; H. Kim & Adeli, 2004; Sun & Chang, 2002). This method has also been used in a parametric sense to determine instantaneous damping coefficients in an experimental six-storey frame structure, with the conclusion that changes in damping are a better indicator of damage than modal frequency (Curadelli, Riera, Ambrosini, & Amani, 2008).

Artificial neural networks (ANNs) have been developed to interpret structural response data for the categorisation of damage. This method requires the training of an interconnected system of nodes and weights with patterns of structural damage, such that both undamaged and damaged structural states can be recognised. Once fully trained, the ANN can provide a probabilistic estimate of a finite group of damage states based on input signals collected from SHM equipment. Implementations by Mangal, Idichandy,

and Ganapathy (1996) and Masri, Smyth, Chassiakos, Caughey, and Hunter (2000) have shown that a number of ANN structures, including back-propagation and adaptive resonance theory, are suitable for use in an SHM context.

ANN-based methods are considered to be suitable in situations where a large training dataset is available. Without this data, there is no way to determine a suitable algorithm for damage classification due to the complex, non-linear structure of ANNs. ANN methods are useful in situations where prior knowledge of the behaviour of the monitored structure is unknown, due to the non-specific nature of training datasets.

Particle filters are also used to obtain state variables from observation variables in an SHM context. Zheng, Shi, Lu, Hong, and Shen (2013) propose a particle probability hypothesis density filter method for the positional tracking of multiple targets in a multipath environment. This method was simulated to demonstrate that up to three targets in a high-clutter environment could be tracked with suitable precision.

2.2.3 Implications for Sensor Requirements

The preceding review of contemporary SHM literature highlights a major gap in current technology. Parametric methods of SHM can relate changes in stiffness and other structural parameters to the floor-to-floor displacement the structure undergoes during an earthquake. Hence, measured displacement is required for damage detection. Robust sensing methods typically use accelerometers for instrumentation. The acceleration reported by these devices must be doubly-integrated to obtain displacement. The result of this process is an integral drift resulting from introduced constants of integration.

To remove the drift, baseline correction algorithms have been introduced. These algo-

rithms often include some form of high-pass filtering to remove the drift, because the drift is lower in frequency than the oscillatory ground motion and structural response. However, these algorithms are thus unable to preserve non-linear changes in structural behaviour. The loss of non-linearities in the input data significantly compromises SHM's ability to detect structural parameter degradation, because these non-linearities are often a key indicator of such change.

Non-parametric methods which analyse natural frequency and mode shapes from acceleration data have been shown to be inferior damage detection methods when compared to parametric methods. This difference is due to mode shapes' lack of sensitivity to damage (J.-T. Kim et al., 2003). For SHM with desirable sensitivity and precision, it is thus necessary to be able to directly measure structural displacement. This thesis aims to find a method of achieving this goal.

2.2.4 Requirements for Damage Detection

To determine the requirements for a sensor system to be able to provide useful data for SHM, the metrics used must be understood. The model described by Chase et al. (2004) indicates that the stiffness of particular storeys on a structure is related to the difference in displacement between adjacent levels. This common metric is the interstorey drift ratio (IDR). This metric expresses the "difference in lateral displacements in between two consecutive floors normalized by the [interstorey] height" (Miranda & Akkar, 2006). The instantaneous IDR of the i^{th} floor, δ_i, is given by the formula:

$$\delta_i = \frac{(d_i - d_{i-1})}{h_i} \tag{2.11}$$

where d_i is the distance from the rest position the floor has travelled, and h_i is the height of the i^{th} floor above the floor below (Miranda, 1999). A diagram showing the parameters of this metric in a hypothetical 2D structure is presented in Figure 2.1. Typically, due to the commonly perpendicular arrangement of members in a structure, structures are assigned IDRs for motion in perpendicular directions, nominally north-south (N-S) and west-east (W-E).

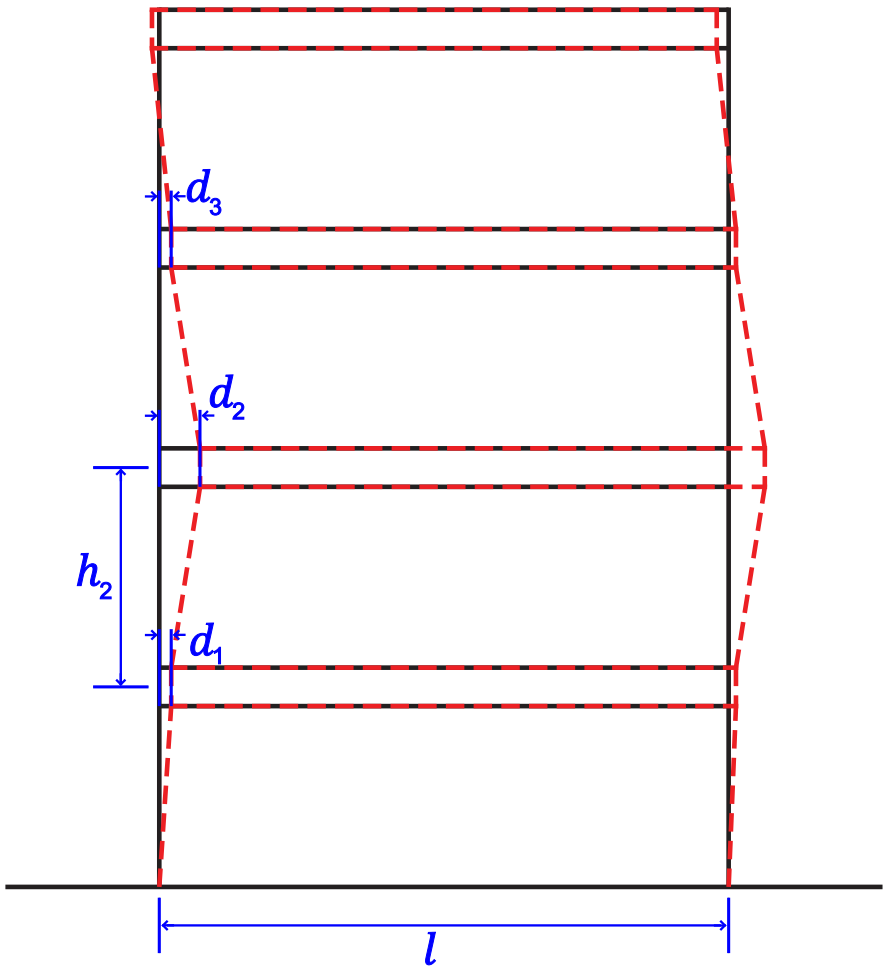

Figure 2.1: A diagram of a building before (black) and during or after (red) a seismic event. The quantities to used to calculate the interstorey drift ratio ($\delta_2 = (d_2 - d_1)/h_2$) are indicated in blue.

An SHM system should be able to measure drift amounts as small as those which would cause negligible damage to the structure, and as large as those which would cause catastrophic structural failure. The former limit ensures that small amounts of damage to the

structure can be tracked; it is unnecessary to exceed the latter limit as SHM is only concerned with ensuring that a building is able to be evacuated and strengthened before the point of catastrophic failure. These limits, in displacement terms, are dependent on the sizes of the structures being monitored due to the relationship in Equation (2.11).

A previous study (C. Zhou, Chase, Rodgers, Xu, & Tomlinson, 2015) has indicated that model-based SHM methods use an IDR threshold for determining whether certain deformations should be used for post-yielding stiffness estimation. The lower this threshold is set, the less precisely the post-yielding stiffness can be estimated for particular levels of sensor noise. For all levels of sensor noise, it was shown that stiffness estimations were poor when this threshold was dropped below 0.5 %. Hence, IDRs below this value are less important for the detection of damage in SHM.

The range of values which need to be within an SHM method's scope of measurement can be obtained from previous studies into damaging structural displacement. Fragility functions are used to provide a probabilistic measure of damage based on structural response data. These functions assume generic behaviour and a generic structure, meaning that the metrics do not necessarily indicate damage versus the structure's initial state, and are thus not suitable as an SHM method for a single given structure. However, the range of damaged samples can be used in a broader sense to learn what the range of damaging IDRs is.

Figure 2.2 shows how fragility functions map engineering demand parameters (EDPs) to multiple discrete outcomes, indicating a variability in damage severity. These fragility functions have been defined through the manual categorisation of samples taken from structures into four damage states, designated DM_1 to DM_4, ascending in order of severity.

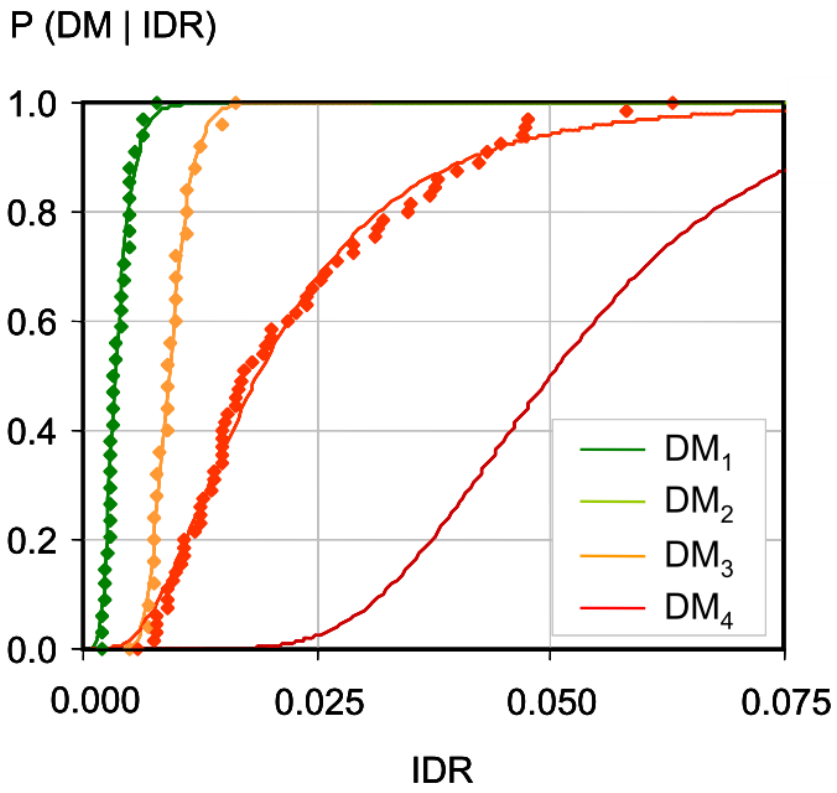

Figure 2.2: An example from Naeim et al. (2005) of a fragility function determining the likelihood of cracking at multiple damage states.

An IDR of below 0.5% (Naeim et al., 2005) or 1.0% (Priestley & Kowalsky, 2000) is considered to be undamaging, so any proposed method should be able to measure at least as accurately as the lower of these values. Similarly, IDR values in the range of 1.5 % to 2.0 % (Jiang & Kubo, 2008; Naeim et al., 2005) are considered to be severely damaging to a structure. An SHM technique should therefore be able to accurately measure IDR values in the range 0.2 % to 2.5 % to ensure that any potentially damaging drift can be measured. SHM is typically used on inhabitable buildings (which are assumed to have minimum horizontal dimensions as small as 5 m) and some larger structures, such as dams or bridges (which are assumed to have maximum horizontal dimensions as large as 10 km), so an SHM technique could be required to measure drifts as small as 10 mm and as large as 250 mm (Naeim et al., 2005).

In addition to lower and upper limits for drift detection, a proposed SHM system must

also be able to detect drift to a fine enough resolution to provide sufficiently detailed information for damage analysis. Pagni and Lowes (2006) indicate that 12 damage states are suitable for classifying damage in structures, and these states correspond to IDRs in the range 0 % to 6 %, implying that an IDR resolution of 0.5 % is sufficient for classification. However, improvements on this figure would limit the risk of quanitisation error dominating any small variation in detected drift. Ideally, resolutions of 0.2 % or smaller should be able to be achieved by a proposed SHM method.

The displacement data for each point on the structure ideally needs to be measured continuously by any proposed SHM method so that the time-variant stress on the structure can be examined. Within the time series output, the maximum displacements from the structure's resting state should be able to be extracted so that the maximum IDR can be checked. Ultimately, SHM data's validity is dependent on the accuracy of its displacement measurements; as such, measurement accuracy should be prioritised over time resolution if a trade-off between the two exists. While time-series data may be useful for structural integrity analysis, peak measurements of a structure's IDR can reveal how severely a structure has been damaged, and is the prevailing metric used in literature.

Some methods of automated damage assessment rely on wavelet transforms to identify probable damaging motion (Al-Khalidy et al., 1997; Hou et al., 2000; Naeim et al., 2005; Sun & Chang, 2002). This involves the transformation of the time-series structural displacement data onto a basis of wavelets known to characterise damage. For this method to be successfully applied, it is noted by Al-Khalidy et al. (1997) that an increased input sampling rate can improve the detection of impulses, leading to improved damage assessment accuracy. If the data output from the proposed SHM method is to be useful for both parametric and non-parametric methods, it should be able to record measurements sufficiently quickly. This figure is in the region of 50 Hz (G.-D. Zhou & Yi, 2013).

Knowledge of the numerical requirements of an SHM system allow for definition of success criteria for a proposed sensor. If the proposed method is able to collect data corresponding to drift ratios as small as 0.2 % and as large as 2.5 %, and collect drift data at least 50 times per second, then it can be seen to be suitable in this context. Beyond these minimal suitability criteria, metrics such as accuracy, precision, robustness, cost, and installability can be used to compare a proposed method to existing technology.

2.2.5 Existing Methods for Structural Instrumentation

Numerous sensing methods are currently either deployed or undergoing research to attempt to provide useful structural data for SHM. Lynch and Loh (2006) provide a thorough review of wirelessly-deployed sensor modules, with a particular focus on accelerometer-based sensors. These methods use structural member acceleration and force loading. These wireless sensors are autonomous data acquisition nodes capable of running independently with their own power source, and the ability to broadcast their data to each other to enable the holistic collection of structural motion data. These sensors are able to perform on-board data analysis to allow for the near-real-time evaluation of structural motion, and thus structural integrity.

Because these systems produce acceleration data, they require the transformation to another metric for use in SHM. To make the transformation from acceleration to drift, the data must be doubly-integrated:

$$
\begin{aligned}
a(t) &= \frac{dv(t)}{dt} \\
v(t) &= \frac{dd(t)}{dt} \\
\therefore a(t) &= \frac{d^2d(t)}{dt^2} \\
d(t) &= \int \left[\int a(t)\, dt \right] dt
\end{aligned} \tag{2.12}
$$

This double integration process introduces non-linear terms due to constants of integration, known as integral drift. This error can be corrected to an extent using numerical techniques such as proposed by Thenozhi et al. (2012), but the error cannot be removed entirely. The resulting uncertainty is a particular problem when non-linear displacement and/or residual displacement occur, which is the case where greatest accuracy is desired. Accelerometer-based methods are therefore inferior at obtaining structural drift information than methods which measure displacement directly.

Accelerometer-based methods are implemented using discrete sensors placed at different locations on a structure. Wireless communication is typically used to transmit acceleration data to a central node for analysis. An example application of this method, presented by Jo et al. (2011), is the monitoring of the Jindo bridge in South Korea, with particular regard to the bridge's cable tension. A total of 113 sensor nodes were used for full SHM, each of which contained sensors, a microcontroller, and energy harvesting components.

Existing final implementations of SHM methods include Kinemetrics' OASIS platform for post-earthquake building occupancy resumption assessment. This method primarily uses accelerometers in conjunction with displacement transducers, wind sensors, and strain gauges to mathematically derive kinematic quantities relating to structural

motion for the purpose of visualising damage severity and location (Kinemetrics, 2013). This method requires on-site computation to provide data and visualisations in real-time.

Other methods exist, which measure joint shear strain with the use of strain gauges. These methods attempt to provide data for strain-based models. Typical applications of this method use fiber Bragg grating (FBG) devices to identify the strain that specific structural members have undergone. FBGs work by reflecting specific wavelengths of light transmitted through them. When undergoing deformation, the reflected wavelength varies, allowing the magnitude of deformation to be estimated and the strain to thus be calculated.

Majumder, Gangopadhyay, Chakraborty, Dasgupta, and Bhattacharya (2008) note that, as is typical in strain gauge implementations, temperature compensation must be used to isolate changes in reflected wavelength that are due to material strain rather than temperature variation. This process is performed using a number of different methods, including the use of two separate FBGs of different wavelengths inscribed in the same fibre (Song, Lee, Choi, & Lee, 1997), and the use of long-period gratings due to their relative sensitivity to temperature variation. Chan et al. (2006); Li et al. (2004); Moyo et al. (2005) provide evidence of applications of these sensors for SHM purposes. These sensors are reported to have a strain estimation error of 5 %.

In addition to methods which measure acceleration and strain, there is some existing research into methods which attempt to measure structural displacement directly. Linear variable differential transformer (LVDT) sensors are one such possible method, and have been used in SHM installations on bridges (Brownjohn, 2007) and buildings (Kuang et al., 2016; Sridhar et al., 2013; C. Zhou, Chase, Rodgers, Kuang, et al., 2015). These devices operate by the variation of primary-to-secondary coil ratio in a trans-

former with one primary and two secondary windings, where the winding ratio varies depending on the position of the sensor. While these sensors are able to provide direct displacement measurements, fixing them to structures is challenging due to their need to be fastened to a reference point, and the nature of the sensor requires the distance between the fixed and target locations to match the sensor (Lee & Shinozuka, 2006). They are relatively fragile.

Other tools which have undergone evaluation of potential efficacy include laser line-scanners (Nayyerloo et al., 2011). These devices use line-scanning cameras to track the motion of a target at a fixed point on the structure. By measuring the horizontal and vertical perturbations of the target, relative displacement information between the camera location and target can be ascertained. This data can then be converted to drift for the purposes of SHM. The reported error obtained from the use of this method was 3 % (Nayyerloo et al., 2011). While this method and LVDT implementations are both able to produce structural displacement data as required, they have the downside of requiring an unimpeded path between the fixed location and tracked target. This requirement means that structures must be either designed around, or modified for, their installation, limiting the retrofittability of these SHM methods.

None of the methods discussed in this section fully fit the criteria outlined in Section 1.1. While some methods were able to provide directly-obtained displacement data, allowing more precise drift-based parametric methods to be utilised, these methods lack the ability to be simply retrofitted to existing structures. Other devices, which are sensor nodes with either accelerometer or FBG strain gauges used to obtain loading or deformation data, are simple to retrofit due to their small form factor and ability to collect and transmit data wirelessly, but do not collect data which can be used with drift-based parametric methods. It was clear from this research that a gap in the current knowledge-base existed. As such, a non-contact, displacement-based method of

SHM was sought.

2.3 Indoor Positional Tracking Methods

The reviewed literature around contemporary and in-development SHM methods indicated particular problems with the data they provide. The inability of modern methods to provide accurate structural displacement estimations without significant computation, while also being simple and cheap to retrofit to existing structures, prompted research into technology suitable to meet these needs. There are numerous spatial location schemes for indoor applications which have been implemented using radio frequency (RF) signals. RF-based methods were seen to be able to fill the non-contact requirement of the novel SHM system. These methods were thus evaluated for their potential efficacy in an SHM context, particularly with regard to their ability to precisely track small drifts.

2.3.1 Generic Wireless Local Area Network Positioning

Wireless local area network (WLAN)-based positioning can be performed using IEEE 802.11-compliant technology, as reported by Sayrafian-Pour and Perez (2007). The research indicated that using the received signal strength property of signals transmitted from a number of different points in a room, the position of an object could be estimated to within $\pm 2.02\,\mathrm{m}$, on average. This capability could be further improved by varying the output signal strengths of the transmitters based on an object's position in the network. Another paper (Lanzisera, Lin, & Pister, 2006) indicated time-of-flight could be used with similar hardware to achieve comparable levels of accuracy (1 m outdoors, and 3 m indoors). While these techniques would be suitable for simple object tracking, their

inaccuracy would lead them to be unsuitable for SHM.

Research by Thorbjornsen, White, Brown, and Reeve (2010) specifically focuses on a time-of-flight (TOF)-based ranging scheme tested using a narrow-band Texas Instruments CC2430 2.4 GHz transceiver. A ranging algorithm was implemented on both an initiator and receiver device, and the two-way range between the devices was calculated. The accuracy was enhanced by comparing the initiator and receiver signal frequencies to measure the sub-clock rate phase offset of the signals. Indoor testing of this scheme focused on stationary targets resulted in a peak error of 3.2 m. A linearly moving target had roughly double the distance error, due to the time-varying channel. Thus, this method would also be unsuitable for SHM applications.

Doppler shift analysis of transmitted 2.4 GHz signals has been shown to be sufficient in accuracy to observe human gestures (Pu, Gupta, Gollakota, & Patel, 2013). The technology, using high-end IEEE 802.11-compliant routers, was shown to provide gesture recognition of a set of 12 gestures, which was accurate at least 88% of the time. This level of accuracy indicated such a method may be useful in detecting displacement to sufficiently accurate levels for SHM, and provides an avenue for further research in this application.

According to Kushki, Plataniotis, and Venetsanopoulos (2012), there are four signal features which can be used for positioning:

Angle of arrival

This feature measures the direction of the signal as it is received at the antenna. Two distinct three-dimensional angles are required to obtain a three-dimensional position, as the intersection between the two paths from transmitter to receiver gives a unique location. This method requires a specialised antenna to obtain the

received angle, creating an additional hardware cost.

Time of arrival

This feature measures the time of travel from the signal's transmitter to its receiver by using knowledge of the signal's speed. Three distances are required to compute a three-dimensional position. The receiver and transmitters must be precisely synchronised, which is difficult to achieve in WLANs (Küpper, 2005).

Time difference of arrival

This feature uses multiple receivers to measure the difference of arrival times for a signal. Three or more differences are required to compute a receiver's position using hyperbolic lateration (Küpper, 2005). Ideally, this method requires perfect synchronisation between the transmitters and receivers.

Received signal strength (RSS)

This feature uses a device to measure the power of the signal observed at the receiver. It is appropriate for WLAN, as no additional hardware is required. However, modelling of the properties of RSS is required. Ideally, the signal power drops at a rate inversely proportional to the square of the distance from the transmitter. In reality, large- and smaller-scale propagation effects alter the RSS of a signal.

The large-scale propagation effects are caused by path loss and shadowing, and can be modelled statistically by the equation (Kushki et al., 2012):

$$P_r(\text{dB}) = P_t(\text{dB}) + 10\log_{10} K - 10\gamma \log\left(\frac{d}{d_0}\right) - \psi(\text{dB}). \tag{2.13}$$

In this equation, K is a constant dependent on antenna and channel character-

istics, d_0 is a reference distance for the antenna far-field, and γ is the path loss component, typically $\gamma = 2$ for free-space and $2 \leq \gamma \leq 6$ for a multi-storey office building (Kushki et al., 2012). Training data is typically used to model the path loss.

The small-scale propagation effects are due to the reflection and refraction of a signal in the environment, and are not modelled due to the complexity of the time-varying channel.

The use of these methods of displacement detection with WLAN is made more challenging by the mulitpath environment present in structures. To account for this additional complication, there are a number of different approaches to positional tracking which can be used. Typically, these techniques must rely on probabilistic approaches due to the unpredictable nature of the channel (Kushki et al., 2012).

2.3.2 Global Positioning System

Global Positioning System (GPS) is a method of positioning, which a SHM method could utilise if it was fast enough for real-time monitoring. First, the operation of GPS was investigated. The Federal Radionavigation Plan (2000) specifies two services, with figures 95% accurate (Dana, 2000):

- Precise Positioning Service (22 m horizontal accuracy, 27.7 m vertical accuracy, 200 ns time accuracy)

- Standard Positioning Service(100 m horizontal accuracy, 156 m vertical accuracy, 340 ns time accuracy

There are also several different schemes used to express the accuracy of the received measurements (Dana, 2000). Two separate carrier signals are used by the orbiting satellites (known as space vehicles (SVs)) to transmit data:

- L1 frequency: 1575.42 MHz, for the navigation message and the Standard Positioning Service code signals.

- L2 frequency: 1227.60 MHz, for measuring ionospheric delay for Precise Positioning Service equipped receivers.

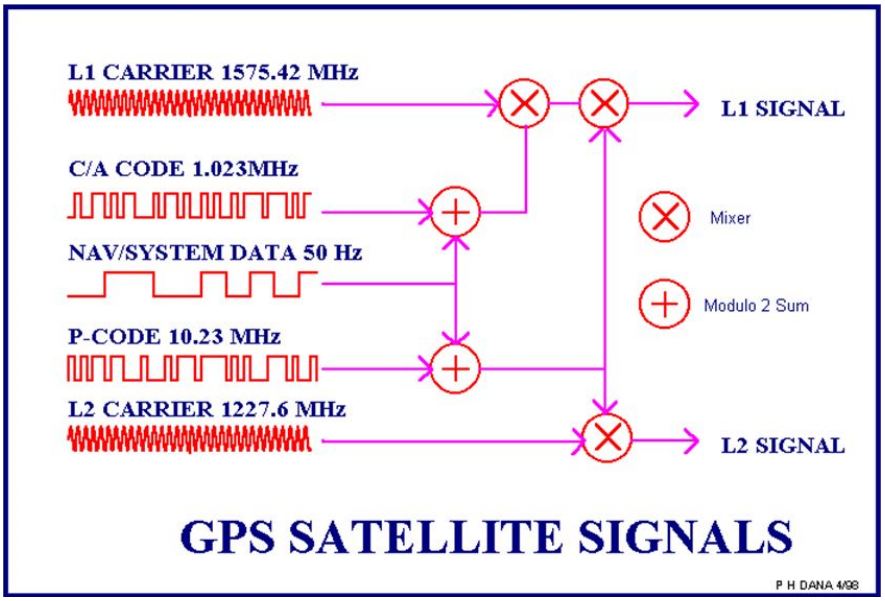

Figure 2.3: Construction of the L1 and L2 GPS signals (Dana, 2000)

The construction of these signals is shown in Figure 2.3. Some of the transmitted data does not need to be continuously collected. SV ephemeris data can realistically be used for days with limited error (Dana, 2000). Equally, the almanac data, which provides information about the approximate orbital paths of the SVs and is used to calculate the communication Doppler shift, can be valid for several months.

The messages are essentially an implementation of a time-difference-of-arrival scheme using positioning data of the SVs (McNeff, 2002). The receiver produces replicas of the

Coarse Acquisition and Precise codes for the purposes of navigation. These codes are both pseudorandom noise. The former can be obtained either by utilising a lookup table of precomputed codes (the modern method for receivers with large amounts of available memory; 32 1023-bit sequences must be stored), or by using a shift register implementation. This implementation shifts code chips in time by slewing the shift register control clock. The generated, or stored, code is shifted along the received signal until full correlation is acquired, indicated by maximum signal power, and the sending SV can be identified.

The 50 Hz Navigation Signal is demodulated from the GPS carrier signal using a bi-phase locked loop. The Doppler Shifted carrier frequency is also obtained using the phase-locked loop (PLL). The pseudorandom noise code start position at the time of full correlation is the time of arrival of the SV pseudorandom noise at the receiver. This quantity, known as the pseudo-range, is "a measure of the range to SV offset by the amount to which the receiver clock is offset from GPS time" (Dana, 2000). The receiver's estimated position is calculated by finding an intersection of these pseudo-ranges from different SVs during the same epoch. These measurements are used together with orbital elements from ephemeris data to compute the SV positions in three dimensions.

Three SVs are required for the computation of Earth-centred, Earth-fixed coordinates, and a further SV to compute the time. The latter computation allows a cheap onboard clock to be used. In short, by knowing the position of an SV, calculated from its almanac and ephemeris data, and the time a signal took to reach the receiver, the overlapping spheres of several SVs can be combined to locate the receiver in 3D space.

Due to the channel shading, which occurs as GPS signals pass through materials such as those in buildings, as would occur in potential targets of structural health monitoring, some solutions using this technique use repeaters to create a local GPS-based position-

ing system (Ozsoy, Bozkurt, & Tekin, 2013). The repeaters used by Ozsoy et al. (2013) used amplifiers to compensate for indoor signal loss and the event of the near-far problem, which prevents weak signals from being detected in the presence of much stronger signals. This technique enabled distance to be measured to an accuracy of 0.5 m to 5.0 m depending on the test object's distance from the repeaters (Jardak & Samama, 2009; Ozsoy et al., 2013).

Accuracy of off-the-shelf GPS receivers for indoor positioning without the use of repeaters is insufficient for a SHM application. The findings of Piras and Cina (2010) indicate the accuracy of such a system is only 5 m to 8 m, which is around three orders of magnitude too low for this application. The main causes attributed to this inaccuracy are low signal-to-noise ratio (SNR) and high levels of multipath interference. These factors arise due to the indoor environment.

A hybrid, or assisted model proposed by Geok, Choy, and Peng (2009) uses a combination of both GPS signals and triangulation from cellular base stations. The non-linear distance equations in this model can be solved using a traditional Taylor series expansion, or by substitution and expansion. The latter of these methods provides more accurate positioning data. The best-case accuracy of this method was found to range from 0.6 m to 36 m (Geok et al., 2009).

Dedicated SHM systems using Differential GPS have been an area of active research since 2002 (Çelebi & Sanli, 2002). This research has shown that GPS systems with sampling rates in the range 10 Hz to 20 Hz can be used for long-term monitoring of structures. Displacement data obtained from these sensors is claimed to have a margin of error of less than 10 mm. A more contemporary review of devices to suitable for Differential GPS by Kaloop, Elbeltagi, Hu, and Elrefai (2017) highlights that high-precision systems have resolutions in the range 3 mm to 5 mm for static measurement, and 10 mm

to 20 mm for dynamic targets.

Due to the slow acquisition speed of GPS systems, monitoring of slow-period structures using this method requires verification. Research by Moschas, Avallone, Saltogianni, and Stiros (2014) and Yigit and Gurlek (2017) shows that structures with periods in the range 1 Hz to 3 Hz can be monitored using global navigation satellite system (GNSS)-derived point positioning. The latter source indicates that the method is suitable for non-parametric analysis of suspension bridges and highway viaducts. Research by Jo, Sim, Tatkowski, Spencer, and Nelson (2012) demonstrates a method to use combinations of cheap GPS chips found in mobile phones, which typically have a resolution of a few metres, placed in dense arrays for improved positioning precision. Results of this research showed that resolutions as low as 200 mm to 300 mm can be achieved using this method, and that resolution improves with the number of sensors used. These methods all require unimpeded line of sight (LOS) to GPS satellites, allowing them to be used to measure overall structural drift, but limiting their effectiveness for the measurement of IDRs.

2.3.3 Radar

Radio Detection and Ranging, or radar, is an object detection system based analysis of reflections of RF signals. Frequency-modulated continuous wave (FMCW) is a particular radar technique which is potentially sufficiently accurate for use in SHM. FMCW is a relatively simple form of radar that has been used in a number of applications, but not yet in SHM. This system relies on observing the frequency shift of a transmitted and received signal to calculate the signal's time-of-flight and hence if the expected distance is known, the difference can be calculated. Figure 2.4 diagramatically shows how such a procedure can be performed in a simple case.

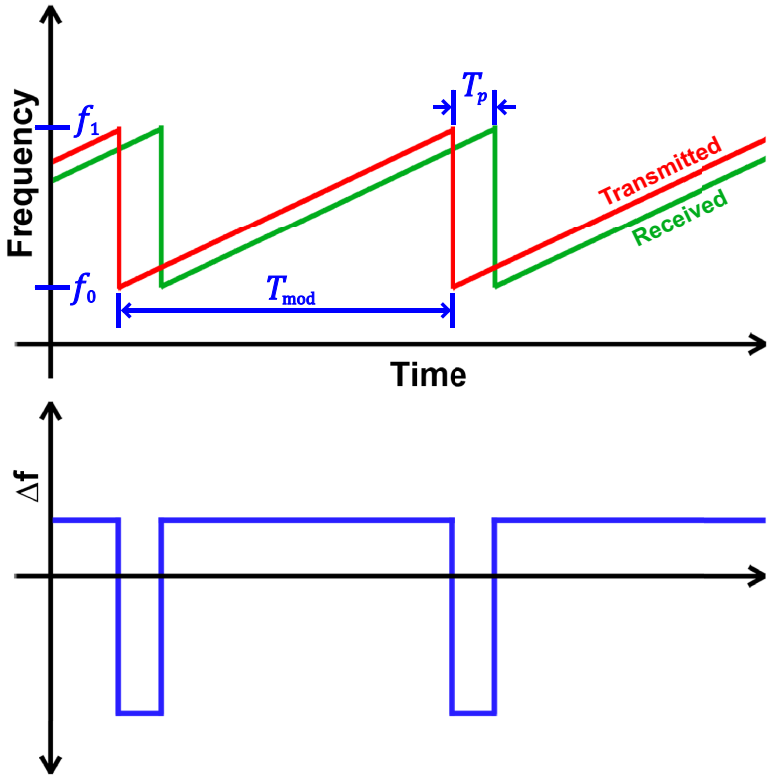

Figure 2.4: An example of how frequency-modulated continuous wave signals change in frequency over time. The transmitted signal is shown in red, and the reflected and received signal is shown in green, indicating the delay between the two signals. The difference in frequency between the two signals is shown in blue, indicating that the signals have mostly a constant frequency difference, where the frequency difference is proportional to the time it takes for the wave to return.

FMCW radar systems transmit a signal with a frequency which changes over time. For example, a system can use a triangular modulation, in which the signal's frequency increases linearly from a lower frequency bound (defined as f_0) to an upper frequency bound (defined as f_1). Once the transmitter modulator output reaches the upper bound, it immediately reverts to the lower bound and continues transmitting. The behaviour of the transmitter is shown in Figure 2.4.

The reflected signal is received some time after it was transmitted. The delay means that at the instant the reflected signal arrives at the receiving antenna, the transmitting antenna is sending a signal with a higher frequency. The frequency difference between the signals is proportional to the delay time, and thus the distance the reflected signal

travelled. The transmitted and received signals are defined:

$$\begin{aligned} v_{\mathrm{FM}}(t) &= A_c \cos\left[\omega_c(t) + \frac{A_b}{2}t^2\right] \\ v_{\mathrm{FM}}(t - T_p) &= A_c \cos\left[\omega_c(t - T_p) + \frac{A_b}{2}(t - T_p)^2\right] \end{aligned} \tag{2.14}$$

where A_c is the transmitted signal amplitude, $\omega_c(t)$ is the carrier signal frequency, A_b is the rate of increase of the frequency sweep, and T_p is the time taken for the signal to arrive at the receiver Brooker (2005). These signals can be heterodyned using a mixer to produce the beat signal defined:

$$\begin{aligned} v_{\mathrm{out}}(t) &= v_{\mathrm{FM}}(t) \times v_{\mathrm{FM}}(t - T_p) \\ v_{\mathrm{out}}(t) &= \frac{A_c^2}{2}\left[\cos\left(m_{\mathrm{out}}t + A_b t^2 + \phi_u\right) + \cos\left(A_b T_p t - \phi_u\right)\right] \end{aligned} \tag{2.15}$$

The phase shift for each cosine term in Equation (2.15), ϕ_u, is equal to $(A_b/2)\,T_p^2 - \omega_c T_p$. The first cosine term in Equation (2.15) has a linearly increasing frequency, $m_{\mathrm{out}} = 2\omega_c - A_b T_p$, which is approximately twice as large as the carrier frequency, and can thus be filtered using a low-pass filter. This leaves the second cosine term, which has a frequency defined:

$$f_r = \frac{A_b T_p}{2\pi} \tag{2.16}$$

f_r is proportional to the signal propagation time between the transmitter and receiver. This relationship allows the reflector distance to be identified using the FMCW formula Brooker (2005); Deacon, Hunt, Koenigsknecht, Leonard, and Oakley (2011):

$$x = \frac{c \times T_{\text{mod}}}{2\,(f_1 - f_0)} f_r \tag{2.17}$$

where c is the speed of signal transmission, and T_{mod} is the period over which the linear frequency sweep occurs.

In practical cases, multiple reflections additively contribute to the captured beat signal with differing A_c values. Hence, identification of the f_r relating to the target reflector is non-trivial, though naïve peak finding can provide a reasonable estimate in ideal cases.

The distance resolution's theoretical limitation is dependent on the discretisation of the heterodyned signal. The Discrete Fourier Transform (DFT) process has a frequency bin resolution of $\Delta f = \frac{1}{T}$, where $T = T_{\text{mod}}$ is the duration of the signal collected. From Equation (2.17), it follows that:

$$\begin{aligned} \Delta x &= \frac{c \times T_{\text{mod}}}{2(f_1 - f_0)} \Delta f_r \\ &= \frac{c \times T_{\text{mod}}}{2(f_1 - f_0)} \frac{1}{T_{\text{mod}}} \\ &= \frac{c}{2(f_1 - f_0)} \end{aligned} \tag{2.18}$$

Equation (2.18) implies a relationship between increased frequency modulation bandwidth and improved distance resolution. Sensor resolution with analog frequency mod-

ulation can thus be improved infinitely with increasing sweep bandwidth. Practical sweep generators are non-linear (i.e. stepped), which limits the effective precision capabilities of an FMCW system Brooker (2005). Increasing T_{mod} can mitigate non-linearities, however this increase results in a trade-off between spatial and temporal resolution. Because building responses typically fall within the 0.2 Hz to 20 Hz range, SHM applications require $T_{\mathrm{mod}} \leq 20\,\mathrm{ms}$, limiting the achievable displacement resolution.

A number of tests using different chirp bandwidths will need to be carried out in order to find an accurate SHM method. Some ultra-wide bandwidth (UWB) ranging techniques proposed by (Garmatyuk, Schuerger, Kauffman, & Spalding, 2009), (Garmatyuk & Kauffman, 2009), and (Saddik, Singh, & Brown, 2007) indicate range resolutions of 300 mm, which would be insufficient for SHM purposes without the introduction of signal processing techniques to more precisely determine f_r. Additionally, due to the non-ideal channel, which includes such effects as multipath signal propagation and signal attenuation, the received signal may not have a single, easily-detected frequency. The received signal should undergo spectral analysis, as shown in Figure 2.5, so that the correct frequency can be detected and therefore the exact range can be calculated.

There has been significant research in this field. A hybridised system based on FMCW and interferometry (Wang, Gu, Inoue, & Li, 2013) shows that such a scheme can achieve instantaneous displacement measurements with an accuracy of 16.5 mm, and continuous tracking measurements with an accuracy of 2 mm. Another hybridised system which combines FMCW and two-tone continuous wave radar shows that 50 mm is an achievable level of accuracy (Zhang, Li, & Wu, 2008). A non-hybridised system with an algorithm for improving FMCW radar's inherent range resolution limitations (Ko, Cheng, & Su, 2008) showed that accuracy to within 70 mm could be achieved. Another FMCW radar-based tracking system specifically focused on tracking indoor targets (Gierlich, Huttner, Dabek, & Huemer, 2007) showed that three-dimensional loca-

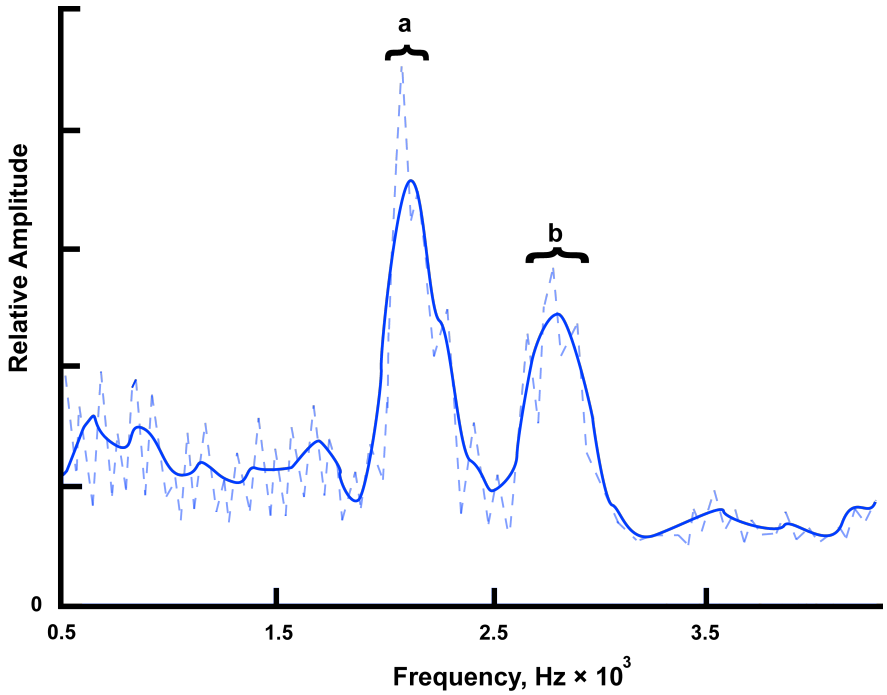

Figure 2.5: The hypothetical beat spectrum of a radar system. Frequency a may correspond to the target, while b could be the same target as observed by signals travelling along a different path.

tions can be tracked to within 28 mm. The research and experimentation in (Garmatyuk, Schuerger, & Kauffman, 2011), based on discoveries presented by Antonik, Griffiths, Weiner, and Wicks (2001), show that despite using a software-defined system with a range resolution of 300 mm, more closely-spaced targets can still be resolved.

There are existing examples of systems which utilise FMCW radar for displacement detection in structures (Gentile, 2009; Mayer, Yanev, Olson, & Smyth, 2010; Rice, Li, Gu, & Hernandez, 2011). These devices are placed off-structure and measure the displacement of specific points of the structure. While this method provides a metric for structural deformation, it does not directly relate to the IDR metric for which parametric SHM methods exist. The accuracy levels found in this previous research were considered to be promising; FMCW has the potential for use a technique to perform SHM. This potential is particularly helped by knowledge of the structural coupling of a monitored building, giving FMCW a distinct advantage in the complex indoor environment. Additional information about the relative position of points in a structure can be used to

improve accuracy towards the 10 mm target previously mentioned.

2.3.4 Indoor Multi-Target Tracking Methods

The use of RF methods for tracking positions on a structure either requires careful time or spatial separation of targets, or a method of separating targets through filtering. This section details the tracking problem and its proposed solutions.

The tracking problem involves analysing the state space sequence $\{\mathbf{x}_k, k \in \mathbb{N}\}$ from a probabilistic perspective. The degree of belief in the state, $\mathbf{x}_k$, must be recursively calculated with regards to the measurement data, $\mathbf{z}_{1:k}$, meaning the conditional probability density function (PDF), $p(\mathbf{x}_k|\mathbf{z}_{1:k})$, must be constructed. This PDF is obtained "in two stages: prediction and update" (Arulampalam, Maskell, Gordon, & Clapp, 2002). The prediction stage utilises the Chapman-Kolmogorov equation to obtain the prior PDF of the kth state, while Bayes' rule is used to update the prior "update" stage. However, the solution is not practically obtainable using this method. Some methods can find the solution under certain restrictions, while others can approximate the solution if it is otherwise intractable.

A Kalman filter approach should be used if certain restrictive assumptions hold, and no algorithm can perform better in a linear Gaussian environment. The main assumption is the PDF at every posterior time step is "Gaussian and, hence, parameterised by a mean and covariance" (Arulampalam et al., 2002). The PDF at time step k can also be assumed to be Gaussian if the measurement and state noise signals are "drawn from Gaussian distributions of known parameters," and the state derivation and measurement functions are known to be linear. This method can require non-existent matrix inverses to be calculated.

An alternative to the Kalman filter method is the grid-based method. It can be computed "if the state space is discrete and consists of a finite number of states" (Arulampalam et al., 2002). This method assumes that the previous and current time step PDFs are known.

If the state derivation and measurement functions can not be linearised, then an extended Kalman filter can be implemented by locally linearising the functions with a first-order Taylor expansion. This method approximates the PDF $p(\mathbf{x}_k|\mathbf{z}_{1:k})$ to be Gaussian. If it is non-Gaussian, then either a grid-based or particle filter can be used for better performance. The grid-based method can be used if the state space is continuous, but decomposable into N_s "cells". The probabilities are based on the central point of each cell, and integrated over the region.

This method has two key disadvantages. The state space must be dense, which causes long computation times, but finite. Second, the state space is predefined, which prevents uneven partitioning to create better resolution in areas of high probability density. Hidden Markov model (HMM) filters, which utilise the Viterbi algorithm, are an application of the approximate grid-based method (Ardo, Astrom, & Berthilsson, 2007; Arulampalam et al., 2002).

2.4 Context of Problem Definition

Research into non-contact position techniques that do not require an unimpeded transmission path has shown RF-based approaches may be suitable for indoor positioning. In particular, radar-based approaches appear to have the ability to meet SHM requirements. Other RF-based approaches to positioning in indoor, multipath environments, including WLAN and GPS methods, appear to lack the precision required to determine

interstorey drift.

Specifically, the use of FMCW radar seems appropriate for a non-contact displacement-measuring SHM system. Rather than unmodulated continuous wave radar, which uses the properties of the Doppler shift to identify the target's velocity, the modulated version uses beat frequencies to determine the signal's TOF, which is linearly related to the target's displacement. This approach allows displacement to be directly measured, allowing displacement-based SHM to be used. The characteristics of this method enable static and slow-moving objects to be ignored, allowing for precise location of a structural target.

2.5 Summary

The current state of research in SHM has been analysed in this literature review. Parametric methods of SHM were shown to require data reflecting changes in structural displacement. Typical modern approaches achieve this by taking acceleration data and doubly-integrating. This process requires baseline correction to remove integral drift. Baseline correction methods are unable to preserve non-linear behaviour, meaning that data fed into parametric SHM methods does not contain a vital indicator of structural change. Non-parametric SHM methods including eigenvalue-based approaches and wavelet methods attempt to ascertain damage from natural frequency and modal parameters. These inputs lack sensitivity to damage compared to structural kinematics.

A need was thus identified for a method of structural instrumentation which measures displacement directly. The IDR metric was shown to be the required data input for model-based SHM methods. This metric is a height-normalised measure of the relative displacement between adjacent floors of a structure. The range of parameters indica-

Table 2.1: Requirements of proposed structural health monitoring system

Parameter	Required Value
Minimum change in displacement	5 mm
Minimum IDR	0.2 %
Maximum change in displacement	250 mm
Maximum IDR	2.5 %
Minimum IDR resolution	0.2 %
Minimum sample rate	50 Hz
Maximum transmitter-reflector distance	100 m

tive of damage was identified, so potential sensing methods could be evaluated for their efficacy in an SHM context. The sample rate required for monitoring of damaging motion was also identified. These parameters are summarised in Table 2.1.

Numerous non-contact approaches to indoor positioning and displacement measurement were investigated. These methods included WLAN-based methods, namely angle of arrival, time of arrival, time difference of arrival, and received signal strength. These methods were not deemed to be able to provide sufficient displacement accuracy, particularly considering the highly multipath environment with significant propagation effects that an SHM system would be required to operate in. GPS-based approaches for indoor positioning were also considered, and while these systems are able to track objects within a cluttered environment, they lack the precision to track structural features undergoing anything but significantly damaging levels of displacement in a real-time.

Radar was determined to be a suitable method to perform SHM in a non-contact manner. FMCW radar in particular provides displacement data which is able to be used with interstorey drift-based SHM. With appropriate sweep time and bandwidth configurations, radar is theoretically able to measure the displacement of a target to a level of precision necessary for the detection of small IDRs. Additionally, continuous wave radar is able to identify static and slow-moving objects that do not correspond to a target in motion, and is therefore well-suited to tracking objects in a noisy, multipath environment. Previous research into this field has demonstrated that using radar to

monitor structures with off-structure sensors can work, however a seismic monitoring device requires more permanent sensor positioning. The findings of this literature review necessitated the simulation of an FMCW radar system to confirm its suitability for tracking seismic-related structural motion, and further, the need to develop and validate a radar-based SHM system to meet the requirements outlined in Table 2.1.

CHAPTER 3

Simulating a Radar-Based Structural Health Monitoring Method

3.1 Introduction

Reviewed literature indicated that a non-contact structural health monitoring (SHM) approach was potentially viable. The viability of any method based on the transmission of radio frequency (RF) waves was seen to be determined by the displacement resolution achievable with the method, and by the ability for wave penetration through a cluttered environment to be achieved. As presented in the previous chapter, SHM requires interstorey drift ratios (IDRs) in the range $0.2\,\% \leq \delta_i \leq 2.5\,\%$ to be detected at a rate of $f_s \geq 50\,\text{Hz}$ (Al-Khalidy et al., 1997; Hou et al., 2000; Naeim et al., 2005; Sun & Chang, 2002)

for use in automated damage assessment models. The ability of a frequency-modulated continuous wave (FMCW) radar system to perform within these parameters therefore needed to be verified.

An initial verification was conducted in simulation to justify the construction of a hardware prototype. Such a simulation was required to determine the hardware parameters necessary for the previously mentioned SHM requirements to be met. These hardware parameters, specifically the values of f_0, f_1, and T_{mod}, were required to be known before hardware construction could begin, because of the limitations of available components.

This chapter details the software written to conduct the necessary simulation. It explains how the virtual FMCW radar system was designed, and how its performance with different values of f_0, f_1, and T_{mod} was evaluated. The limitations of the simulation process are explained. From these evaluations, the potential efficacy of an FMCW radar SHM system is determined.

3.2 Simulation Method

Simulation was undertaken using MATLAB 2014a (The MathWorks, Natick, MA, USA). This software was chosen due to its ability to perform matrix- and vector-level operations on large arrays, as would be required to simulate high-frequency signals.

So that the abilities of millimetre-wave radar implementations could be properly evaluated, a determination was made to scale the frequencies and distances of the simulated system. To use the FMCW radar method naïvely without any additionally signal processing, the distance resolution of the system must be in the order of millimetres. Using

the FMCW resolution Equation (2.18) established in Chapter 2, the required radar sweep bandwidth $f_1 - f_0$ for a 10 mm resolution is 30 GHz.

To simulate such signals, a sampling rate of around 20 times in excess of this figure must be used. This requirement means that single sweeps require more RAM to store than is available in a typical PC. The FMCW radar Equation (2.17) states that there is an inversely proportional relationship between the radar sweep bandwidth $f_1 - f_0$, and the measured distance, x. The bandwidths tested were thus able to be reduced by a factor of 1000, and to complement this adjustment, the distances and resolutions measured by the systems were increased by the same factor.

To verify that the simulated FMCW radar system was able to measure displacements correctly, a static target placed a fixed distance from the transceiver along a 1D channel was simulated. Once this had been verified, a time-variant distance vector mapped to real structural motion data was used as the target for testing purposes.

3.2.1 Static Target Modelling

Initially, a frequency upsweep generator function was created, as detailed in Listing 3.1. This function was able to generate a sine wave vector with an arbitrary initial phase and selected initial and final frequencies, as well as a specified modulation time. Using this function, a wrapper function which was able to generate a sweep beginning at an arbitrary time `T_offset` was created, and is shown in Listing 3.2.

```
function [chirp, f_inst, phi_end] = ...
    ChirpLinear(f_0, f_1, f_s, T_mod, T_pad, phi_start)
% ChirpLinear

% Number of samples of a sweep in the chirp
```

```
N_sweep = round(T_mod * f_s);
N_pad = round(T_pad * f_s);

if (N_sweep > 0)
    % Generate the instantaneous frequencies at each point in time,
    % increasing for N_sweep points
    f_inst = [linspace(f_0, f_1, N_sweep) zeros(1, N_pad)];

    % Since (in continuous time) instantaneous frequency is derivative of
    % phase, its integral must be computed to get the phase for sin().
    phi = 2 * pi * cumsum(f_inst) / f_s + phi_start;

    chirp = sin(phi);
    phi_end = mod(phi(end), 2 * pi);
else
    chirp = zeros(1, N_pad);
    f_inst = zeros(1, N_pad);
    phi_end = phi_start;
end
```

Listing 3.1: Chirp generator

```
function [chirp, f_inst, phi_end] = ...
    ChirpLinearDelayed(f_0, f_1, f_s, T_mod, T_pad, phi_start, t_offset)
% ChirpLinearDelayed

% The offset time should be relative to a single chirp period
t_offset = mod(t_offset, T_mod);

% The number of samples the time offset corresponds to
N_offset = floor(t_offset * f_s);

% If N_offset is not greater than zero, then there is no delay and an
% undelayed chirp can be computed
if (N_offset > 0)
    % The periods of the first and second sections of the delayed chirp
```

```
    T_first = T_mod - t_offset;
    T_second = t_offset;

    % The start frequency of the first chirp section and the stop frequency
    % of the second chirp section
    f_start = f_0 + N_offset * (f_1 - f_0) / (round(T_mod * f_s) - 1);
    f_stop = f_0 + (N_offset - 1) * (f_1 - f_0) / (round(T_mod * f_s) - 1);

    % Generate the two chirp sections
    [chirpStart, f_instStart, phi] = ChirpLinear(f_start, f_1, f_s, ...
        T_first, T_pad, phi_start);
    [chirpEnd, f_instEnd, phi] = ChirpLinear(f_0, f_stop, f_s, ...
        T_second, 0, phi);

    % The combination of the two chirp sections
    chirp = [chirpStart chirpEnd];
    f_inst = [f_instStart f_instEnd];
    phi_end = phi;
else
    [chirp, f_inst, phi_end] = ChirpLinear(f_0, f_1, f_s, T_mod, T_pad, ...
        phi_start);
end

end
```

Listing 3.2: Chirp generator with some arbitrary time offset

An arbitrary number of signal sweeps were then generated, as shown in Listing 3.3. The transmitter output vector, `signalTx`, was used to create the received signal `signalRx` by adding a delay proportional to the simulated target distance. This process was performed by simply adding a vector of zeros to the beginning of `signalTx`, with the length of that vector determined using a simple $t = \frac{d}{v}$ equation and assuming signal propagation speed equal to the speed of light. The transmitter and receiver signals were then mixed to form `signalMix`, as shown in Listing 3.4. A Fourier transform was then

applied to the heterodyned signal, and from this, the peak frequency was able to be identified and converted to a target displacement using Equation (2.17).

```
% Generate a chirp signal of the required number of sweeps
signalTx = zeros(1, N_tx);
t_tx = linspace(0, 1 / f_d, N_tx);
f_tx = zeros(1, N_tx);
phi = phi_offset;
for I = 1:(f_s / f_sweep):N_tx
    I_end = round(I + f_s / f_sweep - 1);
    [signalTx(I:I_end), f_tx(I:I_end), phi] = ChirpLinearDelayed(f_0, ...
        f_1, f_s, T_mod, T_pad, phi, t_detectorOffset);
end
signalTx = signalTx(1:N_tx);
f_tx = f_tx(1:N_tx);
```

Listing 3.3: Filling the transmitter output with chirps

```
% Perform hardware FMCW steps
N_delay = round(2 * d / c / (1 / f_s));
channel = zeros(1, N_delay);
signalRx = [zeros(1, ceil(N_delay)) signalTx(1:end-ceil(N_delay))];
signalRx = awgn(signalRx, 20);
signalMix = signalTx .* signalRx;

% Perform the hardware sampling, simulating the ADC process
signalMixSampled = signalMix(round(1:(f_s / f_adc):length(signalMix)));
N_mixSampled = length(signalMixSampled);
```

Listing 3.4: Generating and heterodyning the mixed signal

3.2.2 Seismic Motion Modelling

Once a static target was able to be simulated, the system had to be tested using real structural data to verify its efficacy in an SHM context. To perform this, the code pre-

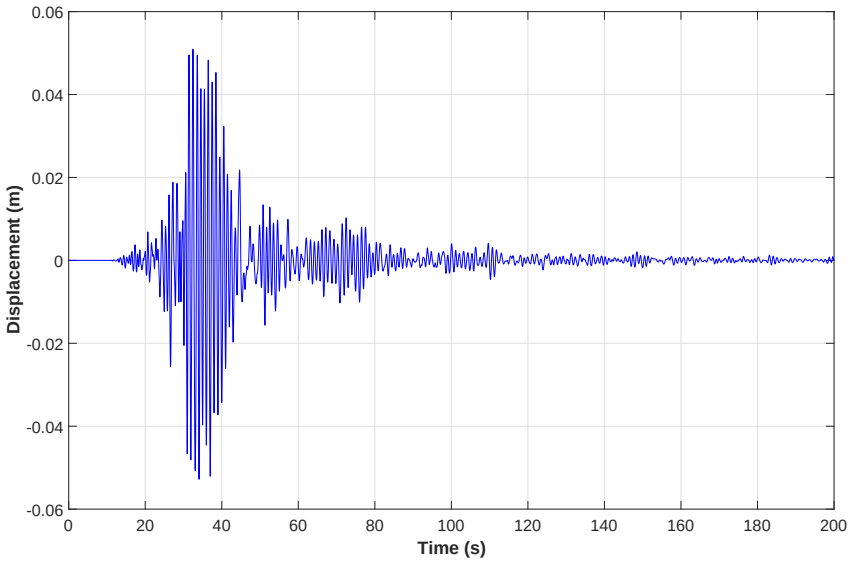

Figure 3.1: The data used to simulate a single degree of freedom (DOF) structure, taken from the 2010 Canterbury, New Zealand earthquake.

sented in Section 3.2.1 was altered so that the size of the delay zero-vector varied depending on some motion data. This motion data was obtained from a structure in the Christchurch Botanic Gardens with a 1.0 s response period during the 2010 Canterbury, New Zealand earthquake, and is shown in Figure 3.1.

The variable delay was created by scaling and recentering the motion record to a suitable distance expected to be measured by an FMCW radar SHM system. `signalRx` was then generated by delaying `signalTx` element-wise, as shown in Listing 3.5.

```
d = (d_amp .* x1' + d_mean) .* bw_ratio;

N_delay = round(2 * d / c / (1 / f_s)); % FMCW equation
N_channel = ceil(max(d) / c * f_s);

delayIndices = (J - 1) * N_dSamplesPerSweep + floor(((1:N_tx) - 1) / f_s * f_s_d) +
    1;
delays = (1:N_tx) + N_delay(delayIndices);
signalRx(delays) = signalTx;
```

Listing 3.5: Generating a variable-distance target

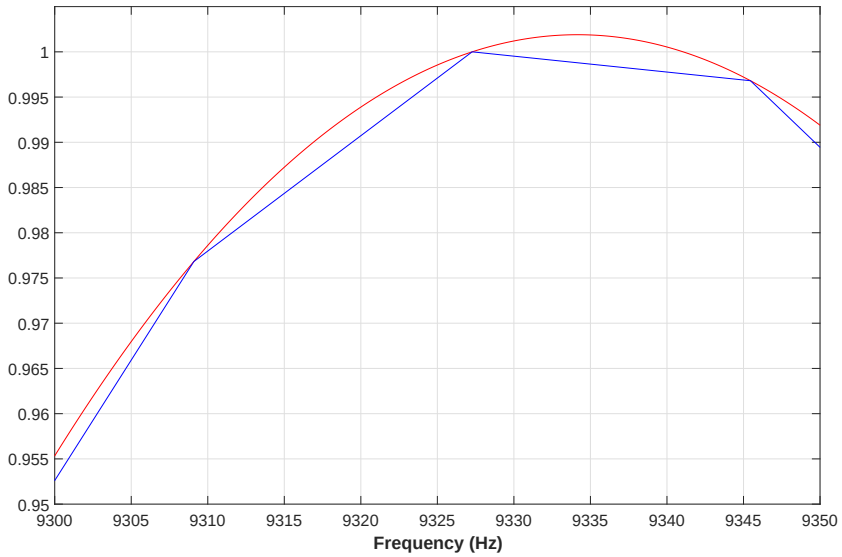

Figure 3.2: Impulses representing the beat signal DFT are shown in blue, and a quadratic interpolation of the three points centred about the DFT peak shown in red. The peak of this interpolation provides a better estimate of the reflector distance than the raw DFT peak.

To test the ability of the simulated system, various signal processing techniques were used. The most significant of these techniques was additional zero-padding of the mixed signal before obtaining its spectrum for peak analysis. This was carried out by supplying a non-zero time to the `T_pad` parameter of the `ChirpLinearDelayed` function. This lengthened the spectrum vector output of the Discrete Fourier Transform (DFT), but also introduced a sinc function to the spectrum. Further signal processing techniques were used to circumvent the spread of spectral energy.

The basic method of naïve peak finding (simple maximum location) of the spectrum is referred to as the ‘Peak’ method. The first of the additional techniques used to improve distance estimation accuracy was the quadratic interpolation of the frequencies adjacent to the peak (‘Quad’); the peak of the quadratic fitting these points was then selected as the beat frequency. Figure 3.2 depicts this method.

The second method used the multitaper (‘MT’) method of spectral analysis (Thomson,

1982). Simple single taper smoothed methods, as applied in the previous distance estimation methods, are limited by a compromise between the frequency estimation variance and bias caused by spectral leakage (Park, Lindberg, & Vernon, 1987). Due to the multipath interference encountered in real-world implementations of radar SHM, the ability to optimise this compromise enabled a less biased spectrum to be found.

The final distance estimation method used a cross-correlation between the multitaper frequency spectra of each displacement measurement and the spectrum of the initial measurement, assumed to correspond to zero displacement ('CorrMT'). The correlated spectral ranges were limited to frequencies corresponding to distances of $\pm 1.5\,\mathrm{m}$ either side of the expected distance. The frequency offset corresponding to the peak of each cross-correlation was converted to a distance offset, which created time series distance offset data for plotting and error calculation.

3.3 Results

Simulation of a static target at distance $d = 10\,\mathrm{m}$ with a bandwidth of $(f_1 - f_0) = 700\,\mathrm{MHz}$ and $T_{\mathrm{mod}} = 5\,\mathrm{ms}$ yielded a peak in the DFT spectrum at the expected frequency of 9.33 kHz. Depictions of the heterodyned signal in the time and frequency domains can be seen in Figure 3.3.

Simulation of a moving target was performed using a range of frequency sweep bandwidths. The effects of varying the sweep bandwidth on the mean relative error between the original data and the tracked distance can be seen in Figure 3.4. In each case, the modulation time T_{mod} was held at 5 ms, and the peak modulation frequency $f_1 = 1\,\mathrm{GHz}$. The starting modulation frequency was varied in the range $f_0 = 0\,\mathrm{MHz}$ to 900 MHz.

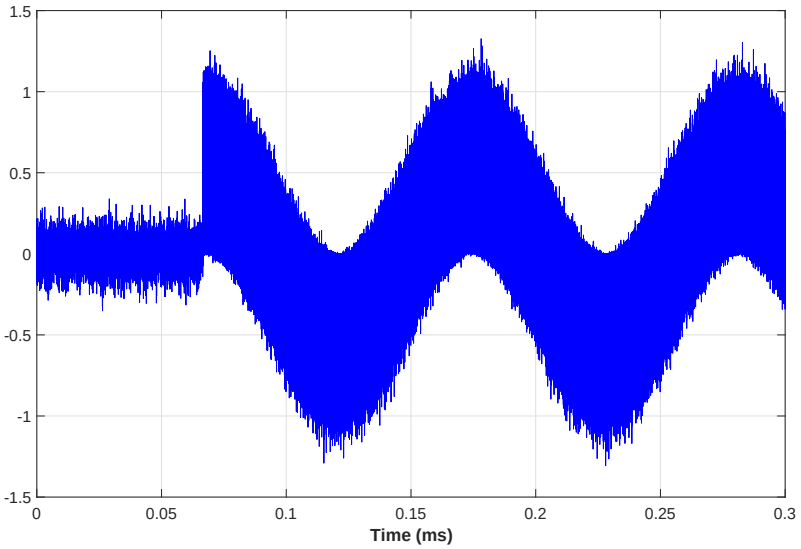

(a) Time domain

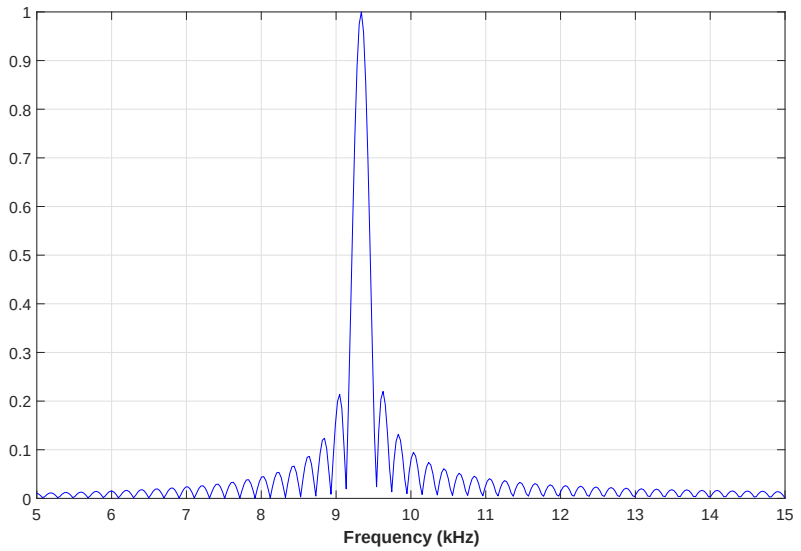

(b) Frequency domain

Figure 3.3: Beat signal for a simulated static target ($d = 10\,\mathrm{m}$, $(f_1 - f_0) = 700\,\mathrm{MHz}$, $T_{\mathrm{mod}} = 5\,\mathrm{ms}$, AWGN SNR $= 20\,\mathrm{dB}$).

An analysis of the effects of adding zero-padding to the heterodyned signal was also carried out. Figure 3.5 shows how the relative distance error between the original motion data and the tracked displacement estimations changed as more zero-padding time was added to `signalMix`. Both the 'Peak' and 'Quad' methods were used to demonstrate this relationship.

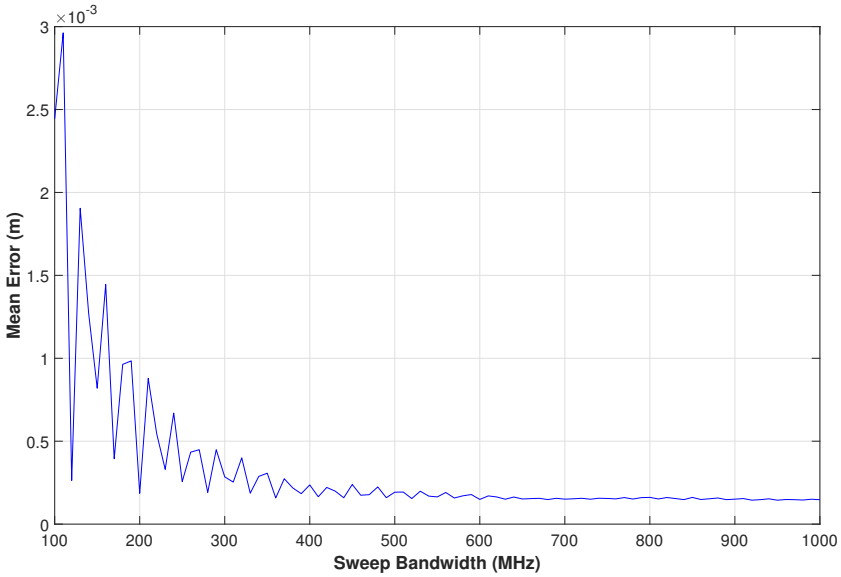

Figure 3.4: Displacement estimation accuracy is improved with increased frequency sweep bandwidth. In each case, $T_{\text{mod}} = 5\,\text{ms}$, and $f_1 = 1\,\text{GHz}$.

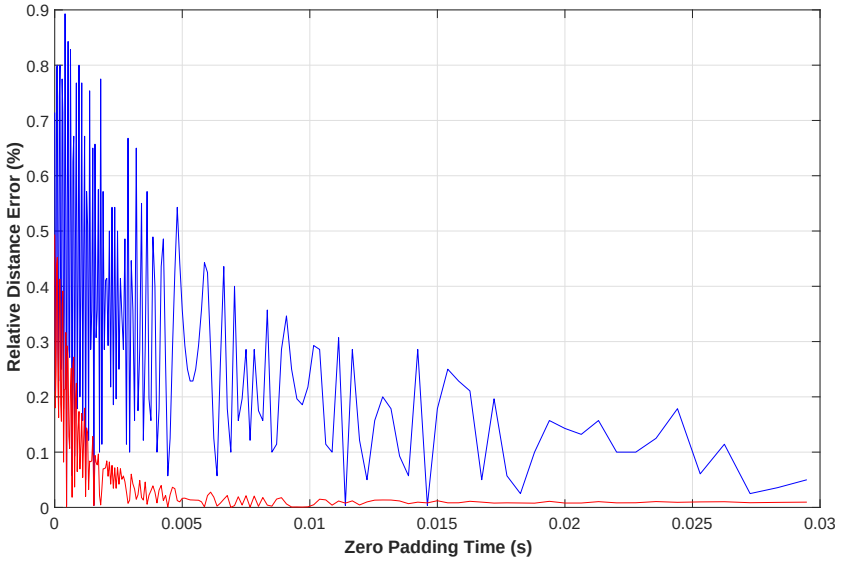

Figure 3.5: A comparison between 'Peak' (blue) and 'Quad' (red) methods with different amounts of zero-padding (relative to T_{mod}). The quadratic interpolation method is consistently better, and zero-padding the signal improves the detection accuracy.

The mean relative distance error of the four methods described in Section 3.2.2 for the data taken from the Christchurch Botanic Gardens structure during the 4$^{\text{th}}$ of September, 2010 Canterbury, New Zealand earthquake is shown in Table 3.1. Plots of the target displacement and tracked target motion are shown in Figures 3.6 to 3.9. The simulation

Table 3.1: A simulated FMCW system using 2010 Canterbury earthquake data

	Mean Error (mm)	Mean Error (%)	Error at Peak Disp. (mm)
Peak	3.792	0.0188	1.094
Quad	0.201	9.94×10^{-4}	0.433
MT	1.750	8.65×10^{-3}	2.471
CorrMT	1.761	8.70×10^{-3}	2.281

was carried out with parameters $(f_1 - f_0) = 700\,\text{MHz}$, $T_{\text{mod}} = 5\,\text{ms}$, AWGN SNR $= 20\,\text{dB}$, and T_pad was 45 ms.

3.4 Discussion

As expected, widening the sweep bandwidth almost uniformly resulted in an improved distance estimation error. This relationship had an asymptote that was determined by the level of AWGN added to the system. This outcome indicates that the larger sweep bandwidth used, the better tracking accuracy will be able to be achieved, however limitations in the ability for high-frequency signals to penetrate structural members prevent a practical prototype with multi-gigahertz bandwidths from being suitable.

Additionally, lengthening of the heterodyned vector with zero-padding also yielded smaller errors in displacement tracking. This was again an asymptotic improvement; eventually, the spectral sinc function introduced by the zero-padding of the time domain signal dominates the beat frequency peak of the heterodyned signal.

While all methods are shown to achieve the required levels of displacement estimation accuracy, both in terms of mean and peak errors, the applied signal processing techniques enable greater precision of distance estimation than naïve peak finding. In terms of mean distance error, the ‘Quad’ method was found to provide the best precision, with an error of 0.201 mm being significantly smaller than the required resolution.

The ‘Quad’ method was also found to provide the smallest peak error. Again, this error was significantly better than the level of accuracy required to provide good inputs to parametric SHM methods. These findings justified the construction and testing of a prototype FMCW device for shake table testing.

This study was limited by the difficulty of simulating a truly multipath environment. While a single-dimensional channel enabled a single target to be simulated, in reality, the transmitted signal is able to reflect off structural elements other than the target reflector. As a result, the multipath reflections that the transmitted signal could take would result in a spectral spread of the perceived target, making distance estimation noisy and imprecise. Because of the difficulty of simulating the multipath environment, there was a necessity to construct a hardware model for validation purposes.

3.5 Summary

A single target in a 1D channel was simulated, both as a stationary reflector and a moving target with motion taken from historical structural records. This process was used to simulate the testing of an FMCW radar SHM system. This simulation was performed using MATLAB. The simulation confirmed theories about the parameters of an FMCW system, namely that increasing sweep bandwidth improves the system’s distance resolution, and therefore its precision in tracking small motion typical of structural behaviour. In addition, several signal processing techniques were tested to demonstrate the improvements that can be made to displacement tracking. It was found that the system, with practical considerations made to the chosen hardware parameters, would be suitably precise to track motion in an SHM context. The displacement error of 0.201 mm found using the ‘Quad’ method was deemed to be suitably small to use in the context of parametric SHM methods.

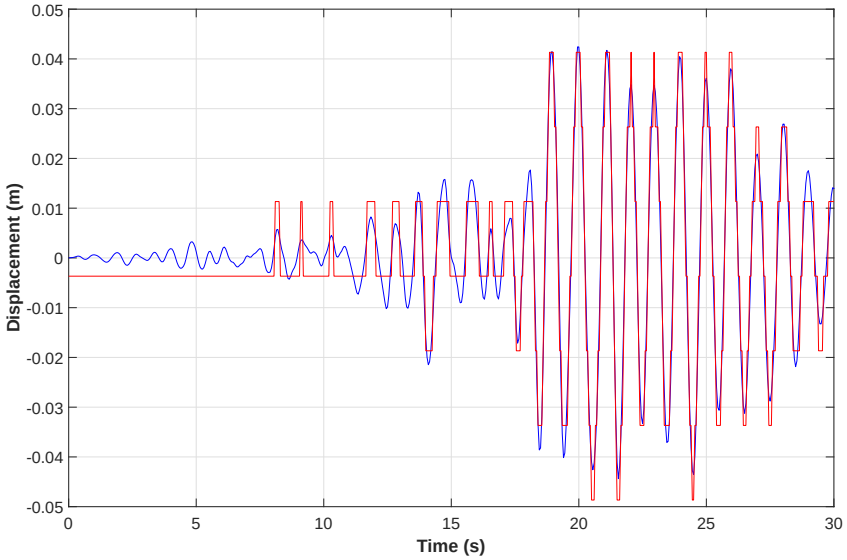

Figure 3.6: The tracking of the displacement of a target driven with structural response data (blue) with a system using the 'Peak' method (red).

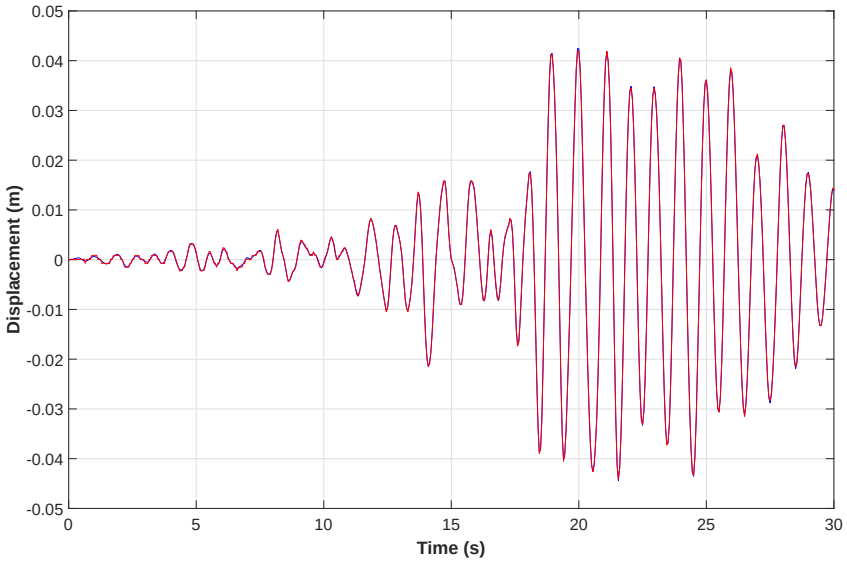

Figure 3.7: The tracking of the displacement of a target driven with structural response data (blue) with a system using the 'Quad' method (red).

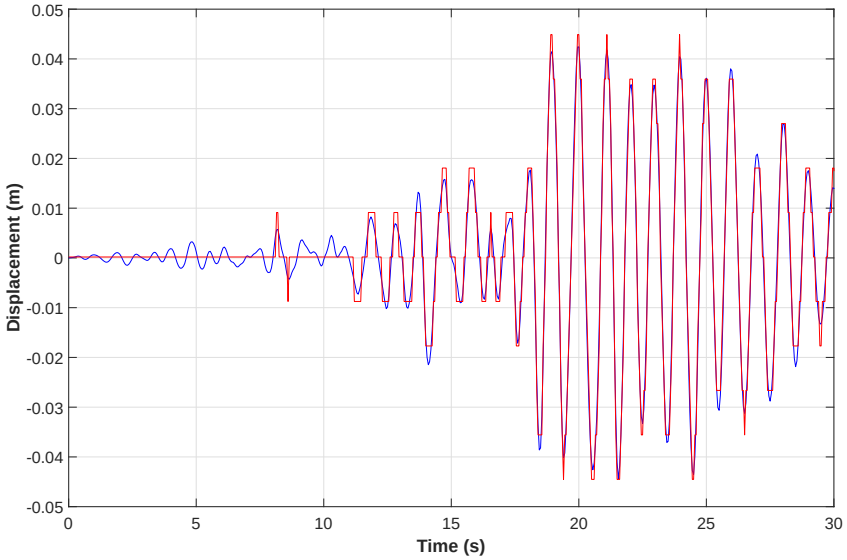

Figure 3.8: The tracking of the displacement of a target driven with structural response data (blue) with a system using the 'MT' method (red).

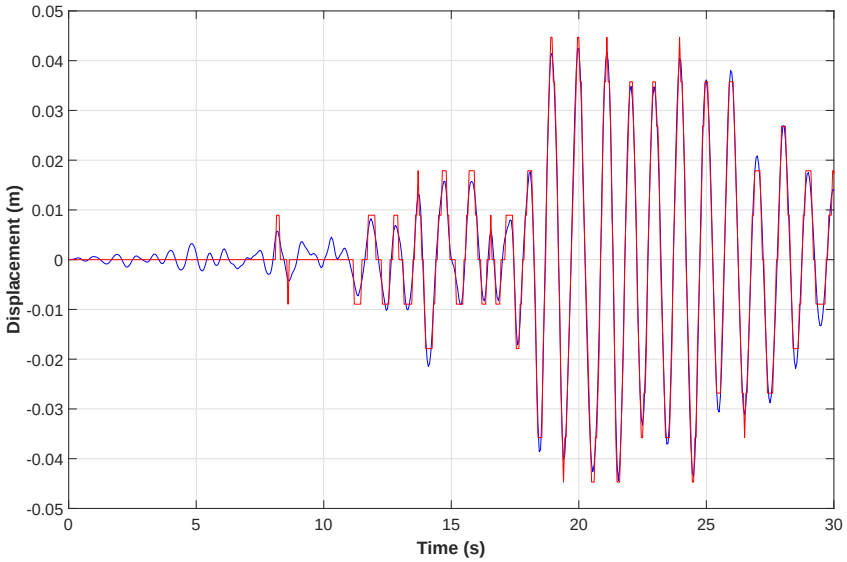

Figure 3.9: The tracking of the displacement of a target driven with structural response data (blue) with a system using the 'CorrMT' method (red).

CHAPTER 4

Development of a Prototype Radar Structural Health Monitoring Sensor

4.1 Introduction

Simulation of a single-degree of freedom (DOF) target and its tracking using a non-contact frequency-modulated continuous wave (FMCW) radar system was completed in the previous chapter. The results of this simulation were encouraging for the use of this method in the determination of interstorey displacements that a structure undergoes during seismic events. To confirm the results of the simulation were a good indication of the efficacy of this system, a hardware prototype needs to be constructed.

Simulation verified the mean interstorey drift ratio (IDR) measurement error improves with increased frequency modulation bandwidth. There are diminishing returns associated with increasing the sweep bandwidth, as the IDR error becomes asymptotic. This result provided an upper bound on the frequency range necessary for a prototype. The prototype was also designed to have the capability to output variable sweep bandwidths.

Construction of a prototype was required to ensure assumptions made during simulation allowed for a fair evaluation of the concept of FMCW radar structural health monitoring (SHM). In particular, additive white Gaussian noise (AWGN) was added to the transmission channel to simulate the effects of channel shading on the reflected signal. In reality, multipath transmissions and reflections corrupt the received signal in non-independent and correlated ways that are difficult to simulate. To verify such a system can provide accurate displacement measurements in indoor environments, a prototype was constructed for testing.

4.2 Design Requirements

The results of the simulation of an FMCW radar-based system led to the need for verification of the system for SHM. A prototype system with the necessary features needed to be designed and constructed to ensure real-world effects on signal propagation, including noise, channel shading, multipath reflections, and signal attenuation would not render such a device unable to operate to the required levels. These levels are the spatial and temporal resolutions defined in Chapter 2 required for inputs to parametric SHM models. The aforementioned signal effects were not able to be adequately simulated, so an electronic implementation was tested instead.

The electronic prototype needed to be able to generate a signal with a variable frequency, as required in an FMCW radar device. This signal needed to be able to have its frequency modulated in an automated fashion, with initial and final set points, and rise linearly between these two values. The linearity criterion was important because non-linear (i.e. stepped) increases in frequency cause errors in distance calculation Brooker (2005). The system needed to have a bandwidth sufficiently large to obtain displacement measurements with enough precision for SHM. Simulation confirmed increasing the system bandwidth improves the detection resolution of an FMCW radar system, but this improvement is asymptotic. There was no significant improvement to distance resolution when the sweep bandwidth was increased beyond 500 MHz, so a system able to handle frequency sweeps in this range is sufficient.

The centre frequency of transmission is of interest. It is defined:

$$f_{centre} = \frac{f_0 + f_1}{2} \tag{4.1}$$

The frequency at which the sweep is centred needed to be kept as small as possible. This requirement arises because an eventual implementation of an FMCW radar SHM system would be required to operate in environments with numerous obstacles between the transmitter and target, and lower frequency signals penetrate these obstacles with less attenuation than those with higher frequencies. The prototype's centre frequency also needed to avoid commonly-used frequency bands, such as the 2.4 GHz and 5 GHz WiFi bands, to avoid co-channel interference.

The signal also needed to have sufficient amplification at the transmitter and receiver stages for the mixer output to be useful for target distance calculation. A low signal-to-noise ratio (SNR) at the mixer input would limit the amplitude of the beat frequency,

making it difficult to detect. Additionally, the amplification needed to have good frequency and phase linearity across the transmission band to reduce the likelihood of phase distortion affecting the heterodyned output. The amplification needed to be sufficient for the transmission of the FMCW signal to a target up to 5 m away for proof-of-concept testing.

The transmitter and receiver needed to be limited in their directionality. Transmission of a radar signal over a wide area increases the likelihood of multipath reflections originating from sources other than the target could be confused for the target radar signature in the heterodyned output. A less-focused receiver is more likely to receive non-target reflections. The prototype was anticipated to be tested in a single DOF experiment, so the target was not anticipated to move outside a directional antennas' broadcast range. Even in a multi-DOF application, typical IDRs would allow for relatively tightly focused directional antennas to be used.

The outputs of these signals needed to be mixed together to provide a beat signal for signal transmission distance analysis. In simulation, this step was performed by simple computation of the Hadamard product, an element-wise multiplication, of the transmitted and received vectors. Frequency and target distance scaling had to be used to achieve this result due to the memory demands of storing and operating on two vectors with sample rates greater than 1 GHz. To circumvent this necessity for scaling, the analog signals needed to be mixed in hardware, and the beat signal, heterodyned output, could be captured for software manipulation.

The output signal thus needed to be captured for software analysis and manipulation. An analog-to-digital converter (ADC) needed to be employed to perform this task, with a required sample rate determined by the FMCW equation. Rearranging Equation (2.17):

$$
\begin{aligned}
x &= \frac{c \times T_{\text{mod}}}{2\,(f_1 - f_0)} f_r \\
f_r &= \frac{(f_1 - f_0)}{T_{\text{mod}}} \frac{2d}{c} \\
&= \frac{500\,\text{MHz}}{T_{\text{mod}}} \frac{2 \times 5\,\text{m}}{3 \times 10^8\,\text{m}\,\text{s}^{-1}} \\
&= \frac{50}{3T_{\text{mod}}}
\end{aligned}
\tag{4.2}
$$

For a short modulation time such as $T_{\text{mod}} = 100\,\mu\text{s}$, the beat frequency corresponding to a target 5 m away is 167 kHz. An ADC able to capture signals at a significantly faster rate than 167 kS was therefore required. Using a rule-of-thumb of digital sampling rates 20 times greater than the highest frequency component of a signal for good time domain reconstruction, a sample rate in excess of 3 MS was required.

All of these requirements for a hardware prototype were set to ensure the requirements of inputs for a parametric SHM system could be met. In particular, the resolution standards established in Chapter 2 requiring the system to be able to detect changes in IDRs as small as 0.2 % needed to be accomplished by this prototype. Additionally, the constructed prototype needed to be customisable to ensure that changing the system's parameters had the same effects on displacement measurement precision as was found in simulation. The selected components thus needed to have large linear operation bandwidths and were to be simply customisable using software settings where possible for fast prototyping.

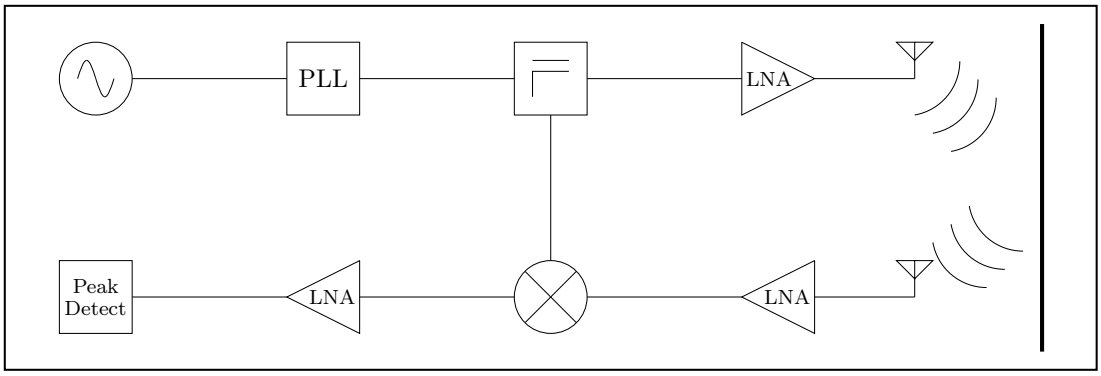

Figure 4.1: The functional layout of the FMCW system used to validate this SHM approach.

4.3 Components Selected

Figure 4.1 illustrates the functional design of the FMCW system created to validate the experimental results. The system was was designed with reference to previously instantiated radar setups, with components selected to suit the specific SHM application. The developed prototype was able to have its radar parameters (f_0, f_1, T_{mod}) configured so the effects of varying these parameters could be quantified and confirmed.

The fractional N phase-locked loop (PLL) device used to configure the output frequency modulation parameters was a Texas Instruments LMX2492. This device is able to produce signals with frequencies in the range 0.5 GHz to 14 GHz, depending on the connected voltage-controlled oscillator (VCO). The device is able to be configured to repeat patterns of up to eight frequency level transitions (Texas Instruments, 2014). Figure 4.2 shows the interface to configure these transitions. The image shows the configuration settings required to transmit a signal rising from $f_0 = 9.4\,\text{GHz}$ to $f_1 = 10.1\,\text{GHz}$ with an upsweep time $T_{\text{mod}} = 5\,\text{ms}$.

The frequency parameters were chosen because they were the limits of operation for the VCO placed on the LMX2492 evaluation kit with the loop filter components used.

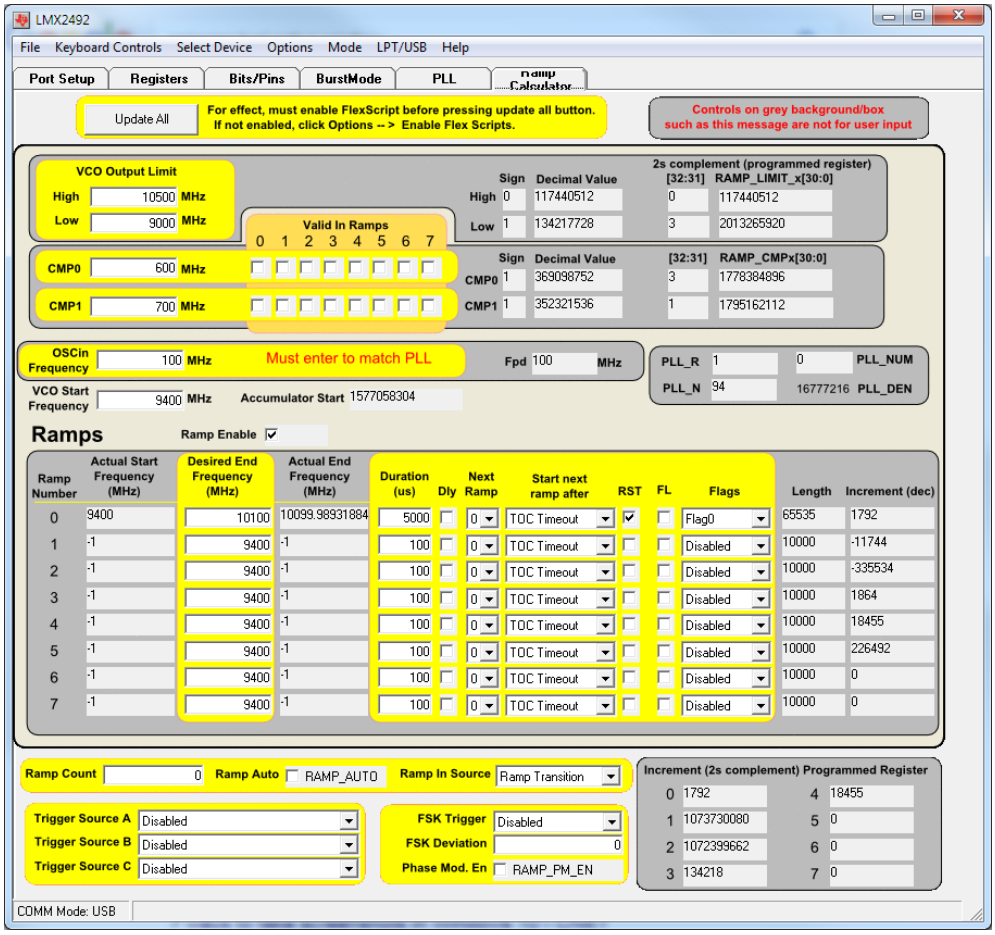

Figure 4.2: The interface for the LMX2492EVM Fractional PLL device to configure the transmitter frequency modulation parameters.

The VCO, the RFMD RFVC1843, was able to provide output in this range, and additionally had output frequency dividers for transmissions centering on 4.88 GHz and 2.44 GHz (RFMD, 2014). These settings allowed testing a range of sweep bandwidths, up to the defined bandwidth for sufficiently precise SHM data collection.

The requirements of the radar-based SHM system included antennas suited to measuring interstorey displacement. Log-periodic antennas were thus chosen due their combination of directionality and wide bandwidth operation. Specifically, Aaronia HyperLOG 60180 antennas were selected. The horizontal radiation pattern is presented in Figure 4.3, showing the narrow main lobe of broadcast for a range of input frequencies. The frequency response of this antenna across the output band of the signal generator

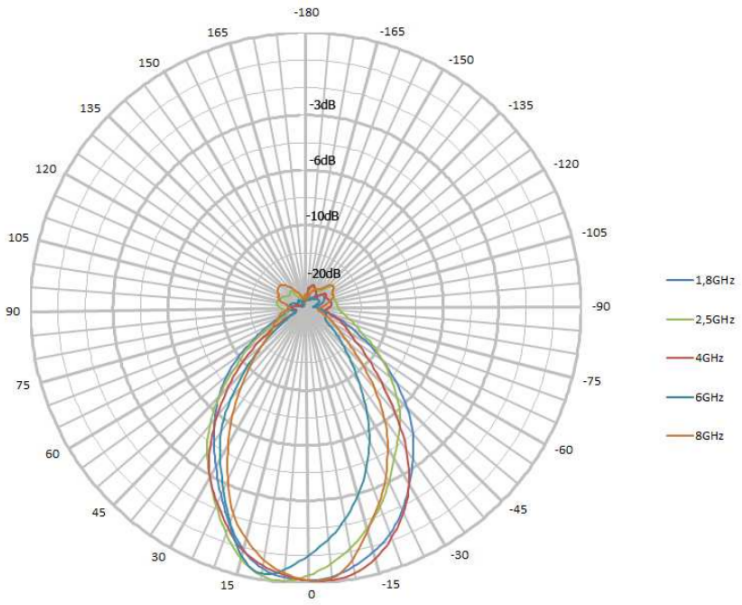

Figure 4.3: The horizontal radiation pattern for a range of broadcast frequencies for the Aaronia HyperLOG 60180 antenna (reproduced from Aaronia (2014)).

is sufficiently linear (± 1 dB).

To mix the transmitted and received signals, a wideband mixer was used. This component, the Hittite HMC1048L3CB, was chosen to passively mix the two signals due to its large input frequency range of 2 GHz to 18 GHz. The mixer output, or intermediate frequency (IF), was able to support frequencies up to 4 GHz, which was sufficient for this FMCW radar application.

The transmitted and received signals were amplified by Mini-Circuits ZVA-183+ wideband amplifiers, which provided a 26 dB gain (Mini-Circuits, 2015). The noise figure (NF) of these amplifiers, 3.0 dB, was considered low enough for use in this application. The heterodyned mixer output signal was amplified by a Texas Instruments INA118 instrumentation amplifier. The R_G pin of this device was connected to a potentiometer, allowing the gain to be configured between 1 and 10,000. This value was set to ensure the mixer output could use the entire input range of the ADC to reduce quantisation

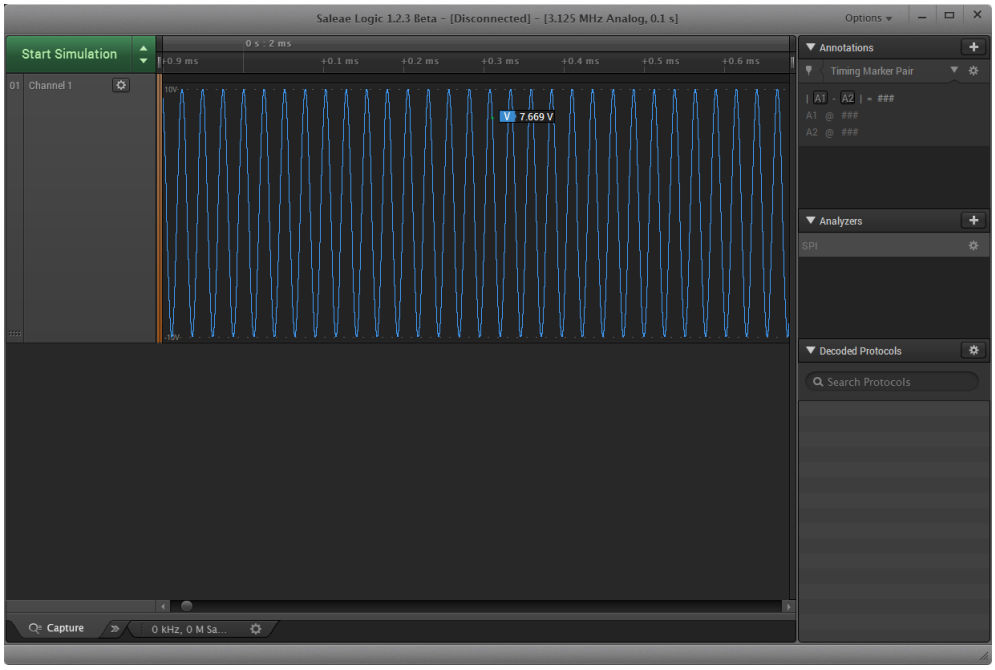

Figure 4.4: The interface for the Logic Pro 16 when configured to capture analog signals.

error.

A Saleae Logic Pro 16 logic analyser was used to collect the outputs from the electronic mixer after amplification. This device was able to capture analog signals at up to 50 MS, so it was a suitable choice for capturing the beat signal. Its input voltage range was −10 V to 10 V and it had a 12-bit ADC, making it a suitable choice for limiting quantisation error. The interface used for collecting and storing this data is shown in Figure 4.4.

These components were connected using SMA connectors and RG-405 semi-rigid coaxial cable. Care was taken to ensure all components of the prototype had 50 Ω characteristic impedance to minimise transmission line losses due to reflections. Some components are shown in Figure 4.5, and a list of the components used is presented in Table 4.1. The prototype was tested using a static sheet aluminium reflector, as shown in Figure 4.6.

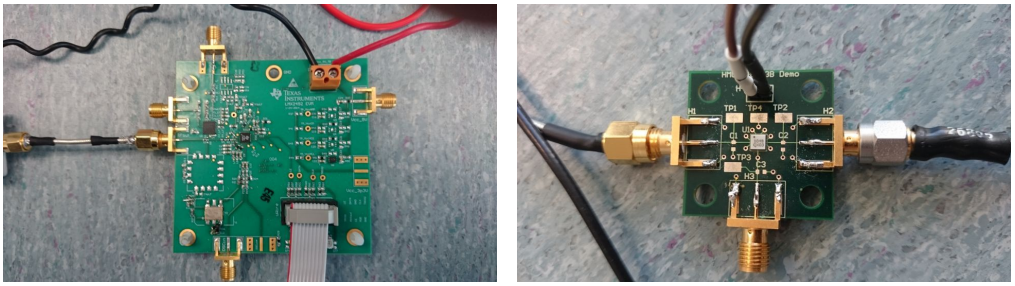

(a) (b)

(c)

Figure 4.5: Components of the FMCW radar prototype, including (a) the PLL and VCO, (b) the signal mixer, (c) and the ADC.

4.4 Reflector Design

A reflector was designed to act as a target to be tracked by the FMCW radar SHM system. A corner reflector was chosen due to several factors in its design making it a more suitable than a flat sheet reflector. The primary factor was its ability to preserve signal transmission distance regardless of the angle of incidence of the signal. Figure 4.7 shows the path of two beams to illustrate how this works. Additionally, the fact the beams exit the reflector in the same, but opposite, direction they entered, maximises its reflectivity for systems in which there is little spatial separation between transmitter and receiver.

Table 4.1: The components selected for the prototype FMCW system.

Function	Manufacturer	Component
VCO and PLL	Texas Instruments	LMX2492EVM
Power Divider	Fairview Microwave	MPR18F-2
Power Amplification	Mini-Circuits	ZVA-183+
Antennas	Aaronia	HyperLOG 60180
Mixer	Hittite Microwave	HMC1048LC3B
IF Amplification	Texas Instruments	INA118
ADC	Saleae	Logic Pro 16
Cabling	Generic	RG405

A corner reflector was also deemed to be a suitable reflector in a structural context. To measure a diagonal distance between two adjacent floors, the transceiver unit would be placed in one corner of a storey, while the reflector would be placed in the opposite corner. Due to the required corner positioning, a reflector of this shape would require the least amount of structural modification or allowance to be fitted. As such, this design was implemented for experimental testing. It was constructed using 1.6 mm aluminium sheet with an edge length of 370 mm, and is depicted in Figure 4.8. The reflector was fastened to a stand manufactured from 10 mm thick aluminium, which had holes drilled for M20 bolts to be placed through for fastening to a shake table.

4.5 Summary

After simulation of an FMCW radar-based SHM displacement measurement system had provided encouraging results, a prototype of the system needed to be constructed for validation. This prototype required the use of components that could suit the transmission of a range of sweep bandwidths towards a target up to 5 m away from the transceiver. Components were selected with the ability to perform this task in a configurable manner for testing on a shake table. A corner reflector was also built for this purpose. The corner reflector was deemed a suitable target for a radar system due to its property of parallel entry and exit signal paths and uniform reflection distance.

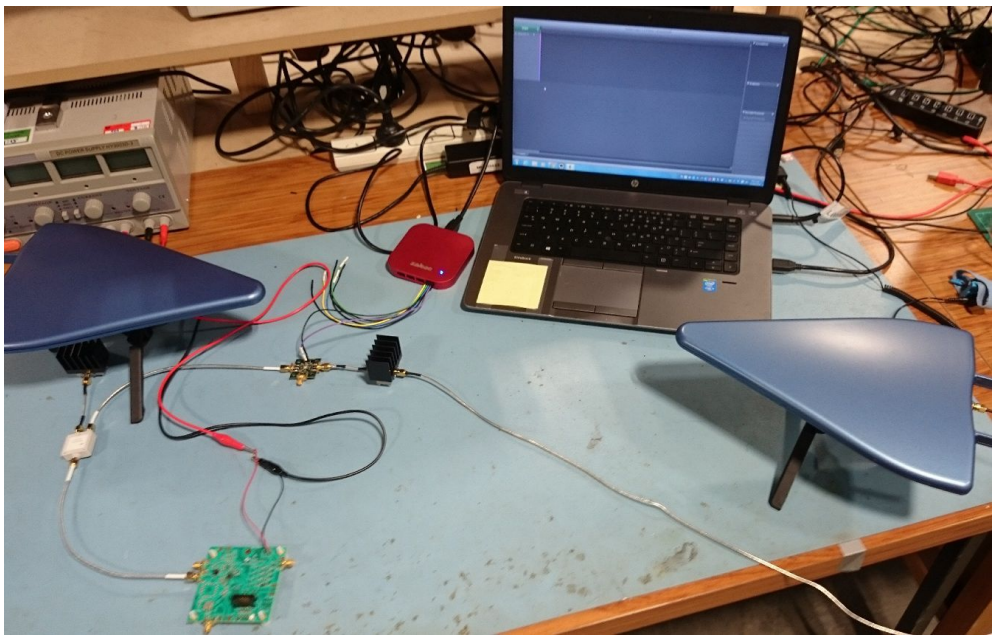

(a)

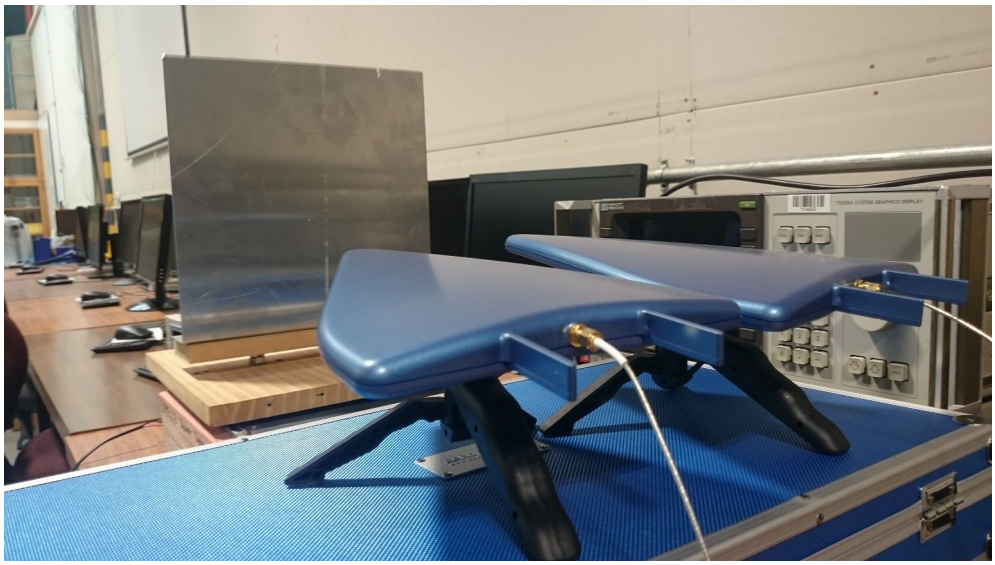

(b)

Figure 4.6: Initial verification of the prototype, with components connected in (a) and detecting a nearby static reflector in (b).

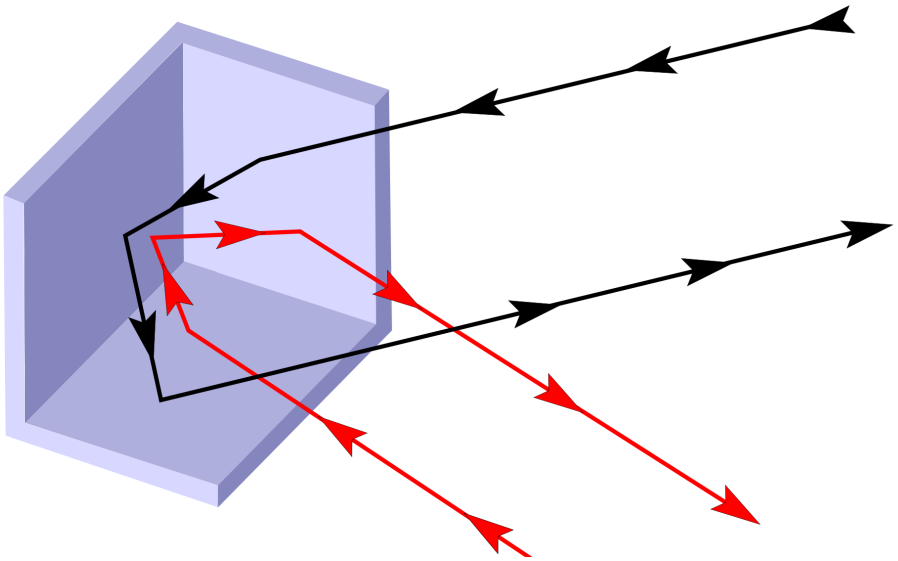

Figure 4.7: Corner reflectors reflect incoming beam paths off each of the three internal faces before returning the beam in a direction parallel to the path in which it entered the reflector. Note that regardless of the entry angle, the beam travels the same distance before it exits the reflector.

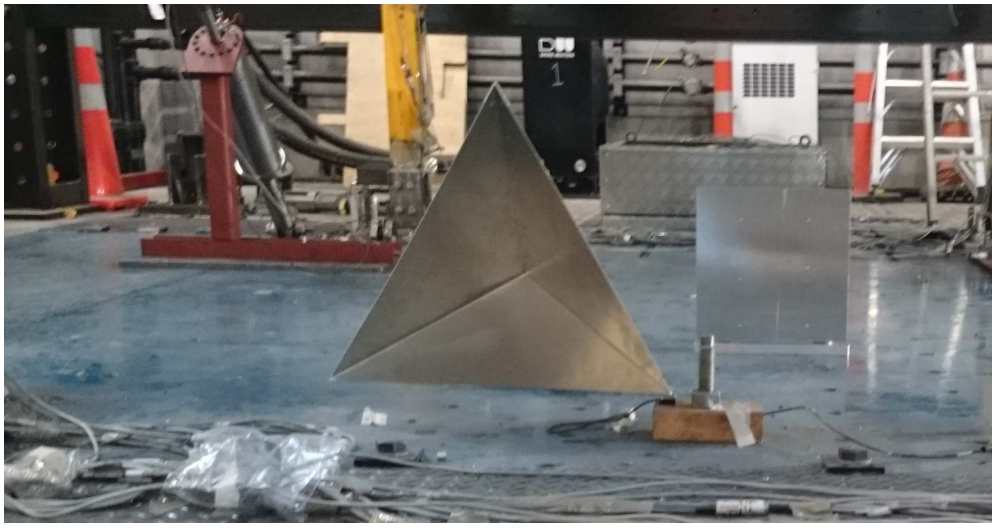

Figure 4.8: The corner reflector fixed to a shake table.

CHAPTER 5

Shake Table Validation of Prototype Radar Sensor

5.1 Introduction

The results of simulation of a frequency-modulated continuous wave (FMCW) radar system were a positive indicator that this method is capable of returning useful data for structural health monitoring (SHM). As a result of this simulation, a hardware prototype was constructed to verify that the SHM requirements set out in Chapter 2 were able to be met in the real world. The prototype components were chosen to be as configurable as possible so that the limits of operation could be evaluated. The prototype design is described in Chapter 4.

To ensure that real-world effects such as multipath interference would not significantly compromise the FMCW radar method's measurement precision, a real-world test was

devised. This experiment used a single corner reflector mounted to the shake table base, which was driven with historical earthquake data. Radar transmitting and receiving antennas were located on the laboratory floor, adjacent to the table, to record motion. The table was instrumented with linear variable differential transformer (LVDT) sensors and accelerometers in addition to the radar system. The LVDT data was used as the reference displacement for comparison with the radar output. The heterodyned signal captured by the FMCW radar system was processed using several different signal processing techniques to find the optimal algorithm. The errors obtained from the LVDT comparison for each different approach are used to confirm the suitability of the proposed FMCW radar method.

5.2 Method

The constructed prototype presented in Chapter 4 was placed on the floor adjacent to a shake table. Figure 5.1 shows the layout of the devices used in the shake table test. The transmitting and receiving antennas were placed as close to each other as possible to create a monostatic radar system. The antennas were located around 2 m from a corner reflector. This reflector was placed on the shake table and fixed using M20 bolts into adjacent holes on the table with a 200 mm pitch between hold-down bolt locations. The reflector and antennas were aligned such that the signal propagation paths were parallel to the table's direction of motion and perpendicular to the open face of the corner reflector. A photograph of the experimental setup is shown in Figure 5.2.

Fastening the reflector to the table and monitoring the shake table motion as driven with historical earthquake data was seen as a suitable substitute for monitoring structural motion for the purpose of proof-of-concept validation of the sensor concept. The frequency content (Fast Fourier Transform (FFT) spectrum) of the structural response of

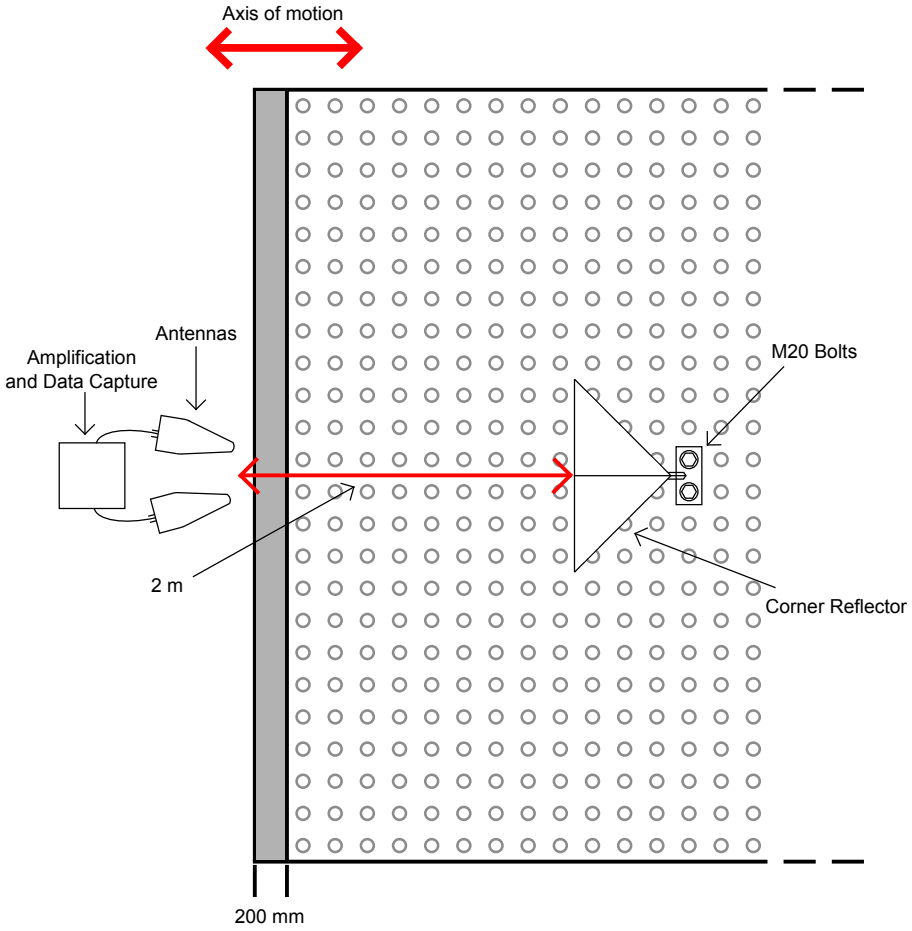

Figure 5.1: Plan view of the FMCW radar validation experimental layout, with a corner reflector fastened to the shake table and the monitoring equipment placed off-structure.

a 2.0 s-period single-degree of freedom (DOF) structure used for simulation and the corresponding frequency content of an example ground motion used to drive the shake table are shown in Figure 5.3. The similarity in spectral peaks and overall frequency content indicated that tracking ground motion rather than structural response was broadly representative of the structural response, and hence able to provide information about the efficacy of the radar system in an SHM context.

The magnitude of ground displacement is larger than the relative deflections within a structure that would be measured in a final SHM application. The table was able to be displaced $\pm$ 200 mm, while structural drifts are more typically in the range 2 mm to 50 mm. For ease of comparison with simulation results, the measured displacements

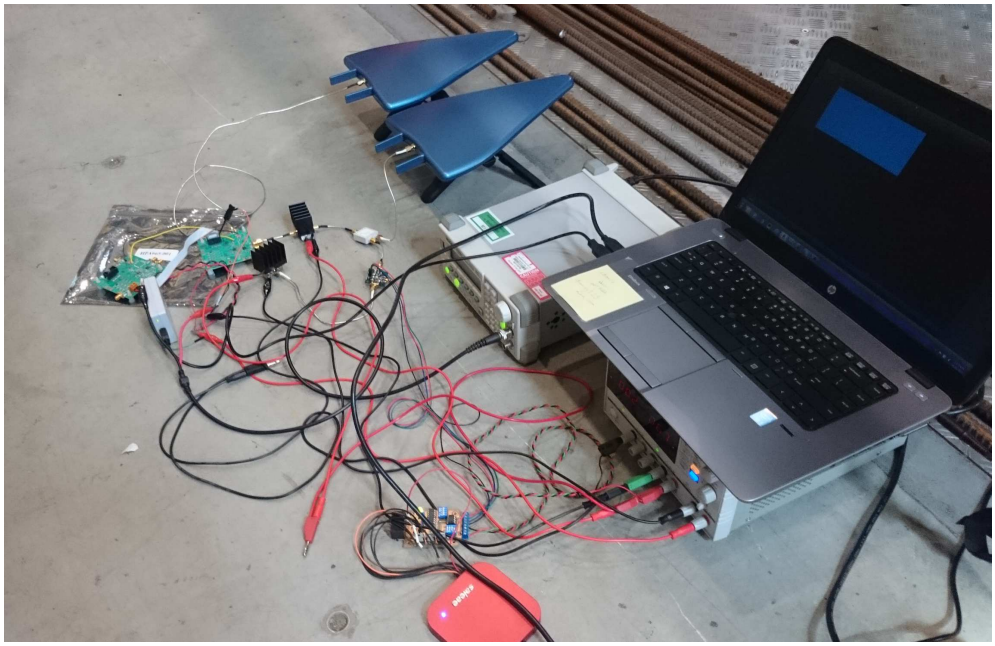

(a)

(b)

Figure 5.2: The prototype FMCW system set up to detect the motion of a shake table, and the reflector fastened to the table (far right).

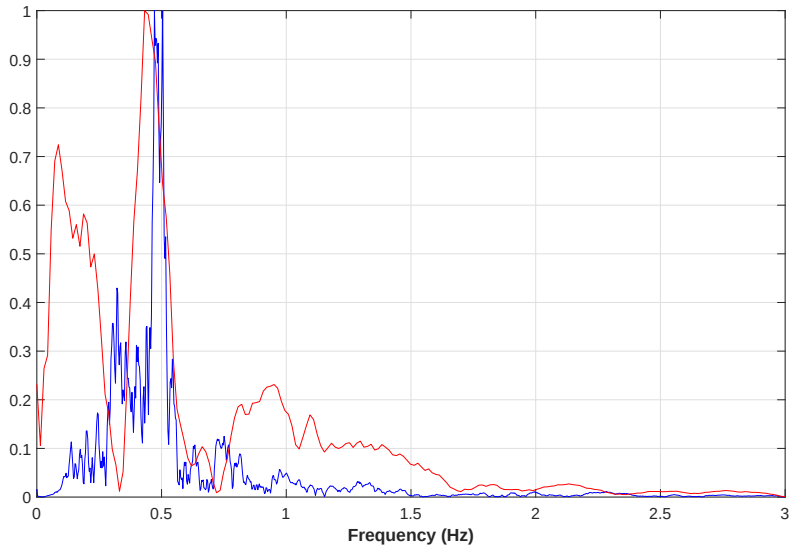

Figure 5.3: The FFT spectrum of the REHS strong motion recording (red) and the corresponding FFT spectrum of the response of a 2.0 s period single DOF structure (blue) for this input ground motion.

were scaled when converted to hypothetical interstorey drift ratios (IDRs). The scaling factor was chosen such that the peak displacement of the run corresponded to a severely-damaging IDR of 1.5 %.

Each set of seismic data was run in turn on the shake table, with an LVDT sensor used to record to reference position for accuracy validation purposes. The beat signal was captured by the FMCW system. The system's T_{mod} was set to 500 µs to match the value used in simulation for ease of comparison, and the frequency sweep generator was configured to sweep up from 9.4 GHz to 10.1 GHz, before reverting to 9.4 GHz for the next upsweep. The implication of setting T_{mod} to 500 µs was that the system's sampling rate was 2 kHz, enabling motion up to 100 Hz to be reconstructed in time series plots. This figure was deemed sufficient for testing, and for future implementation of this device. The analog-to-digital converter (ADC) was set to capture the mixed data at 1.5625 MHz, with the mixed data expected to have a maximum frequency of around 30 kHz.

5.3 Tested Data Sets

The reflector designed was fastened to a shake table, which was driven with horizontal ground acceleration data from several locations near the epicentre of the 22nd of February, 2011 earthquake in Christchurch, New Zealand. These locations include the following strong motion stations:

- Christchurch Resthaven (REHS)
- Christchurch Cathedral College (CCCC)
- Canterbury Botanical Gardens (CBGS)
- Papanui High School (PPHS)
- Christchurch Hospital (CHHC)

Further information regarding these sites can be found in Wotherspoon et al. (2013). Plots of the data sets used are visible in Figures 5.4 to 5.8. The data sets are LVDT-collected outputs from the shake table, which was driven with north-south (N-S) component acceleration data collected from the aforementioned sites. The acceleration data was band-pass filtered with transition bands of 0.05 Hz to 0.10 Hz and 24.50 Hz to 25.50 Hz. The frequency spectrum of the seismic data, in combination with the amplitude of the shake table ($\pm 0.2\,\mathrm{m}$) made this data suitable motion to validate the ability of the system to detect damaging IDRs in realistic structural responses.

These ground displacement records represented a suitable range of motion for assess-

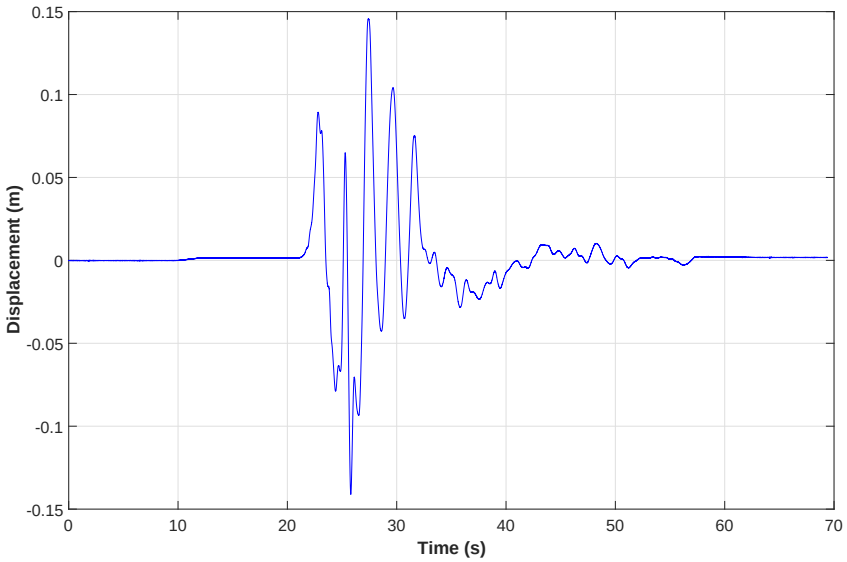

Figure 5.4: The Christchurch Resthaven (REHS) ground displacement data.

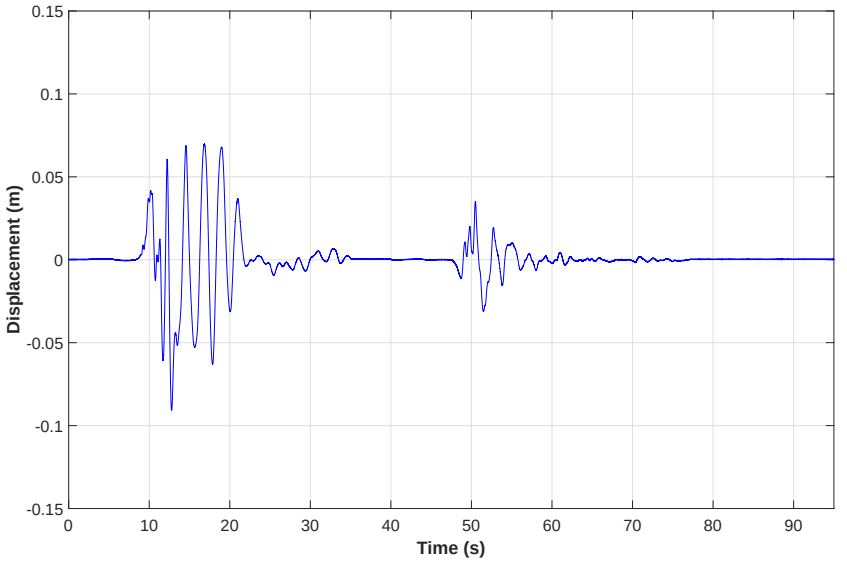

Figure 5.5: The Christchurch Cathedral College (CCCC) ground displacement data.

ment of the FMCW radar system. The maximum displacement in each of the records matches the maximum displacement typically expected to be measured by such a device. Additionally, the latter four records (CCCC, CBGS, PPHS, CHHC) each have sections of motion which are smaller in amplitude. These sections are suitable for evaluating the system's ability to accurately detect small levels of displacement that might be associated with less damaging structural motion.

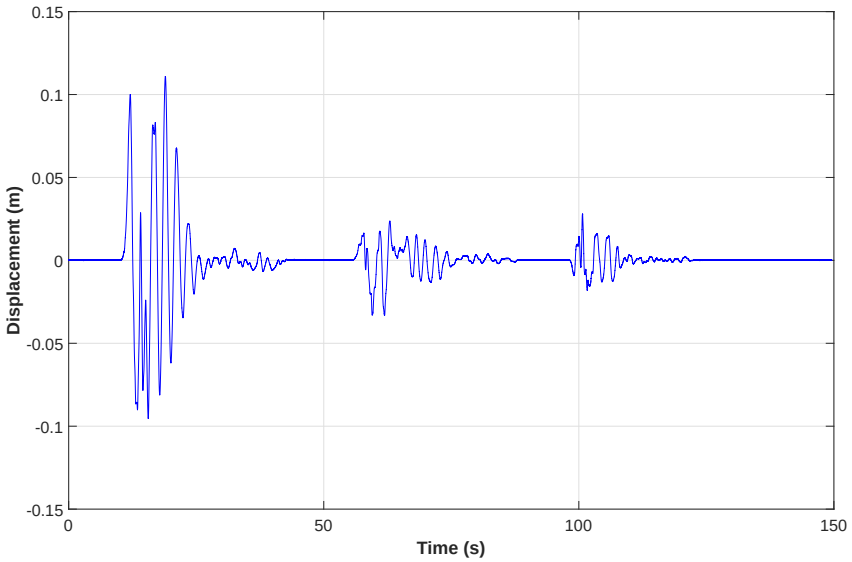

Figure 5.6: The Canterbury Botanical Gardens (CBGS) ground displacement data.

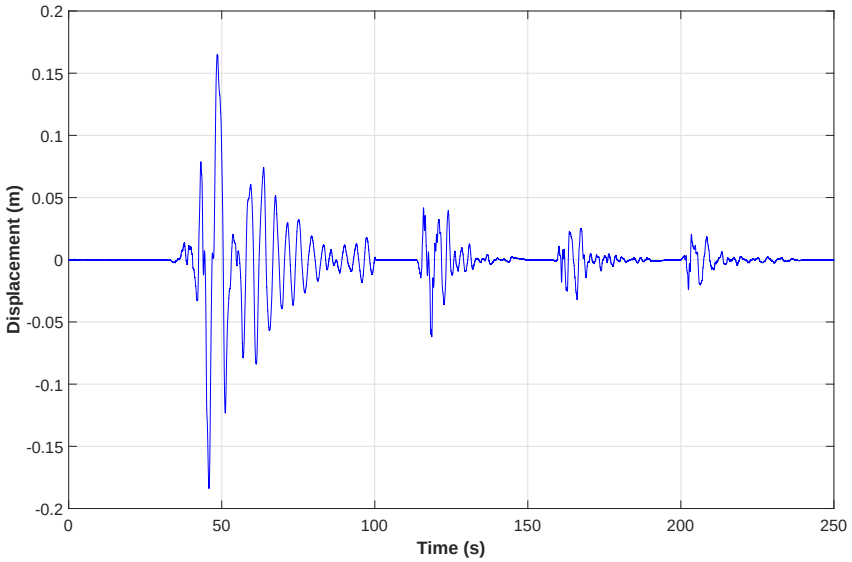

Figure 5.7: The Papanui High School (PPHS) ground displacement data.

5.4 Signal Processing Methods

The data collected by the ADC was stored for later offline processing. A single time series of data was collected from the heterodyned output, which needed to be split into sections for which signal transmission distance could be estimated. Each individual sec-

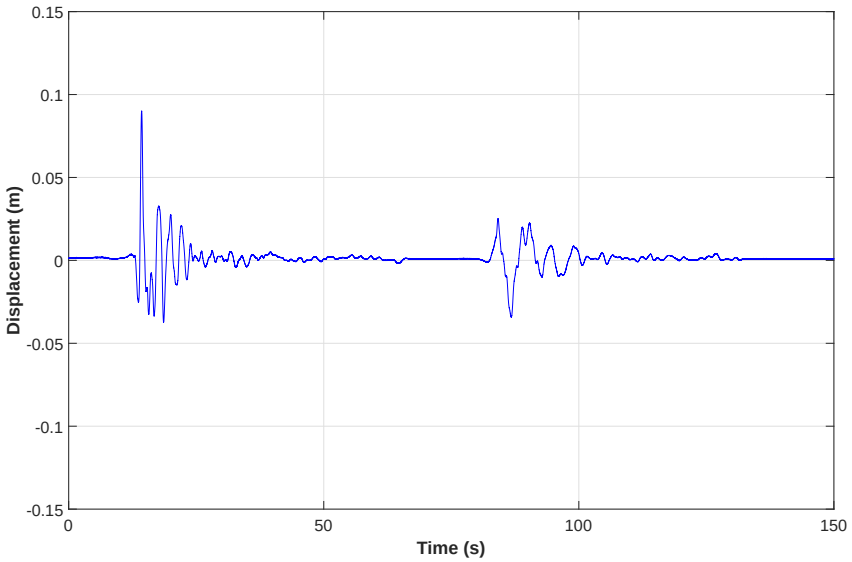

Figure 5.8: The Christchurch Hospital (CHHC) ground displacement data.

tion of the heterodyned signal was thus T_{mod} seconds in length. The individual sections were then processed separately using a variety of different methods for evaluation.

A range of different signal processing methods were used to determine the best method for obtaining precise reflector displacement estimates. As performed during simulation, zero-padding was used on each sweep section before transforming it to the frequency domain. 45 ms padding was added. This process has been shown to improve the frequency resolution of spectra significantly for the purpose of more precisely identifying particular harmonic components of signals (Abe & Smith III, 2004; Spangenberg et al., 2000).

5.4.1 'Peak' Method

The simplest displacement identification method used for the estimation of target displacement was spectral peak finding. The FFT approach was taken to transforming each individual sweep to the frequency domain. The FFT output represented the spec-

tral makeup of the heterodyned output. The magnitude of each frequency bin indicated the proportion of the received signal that had travelled a particular distance between transmitter and receiver. This relationship originates from the FMCW equation:

$$x = \frac{c \times T_{\text{mod}}}{2(f_1 - f_0)} f_r \tag{5.1}$$

The frequency scale was thus converted to a corresponding distance scale using Equation (2.17). Bins with the largest relative magnitude (i.e. the frequency peak) within an expected distance range were located for each sweep to provide a distance for each sample. The MATLAB code used to perform this is shown in Listing 5.1. The expected distance range was defined through knowledge of the experimental geometry and hardware prototype characteristics. A range of 3 m to 6 m, corresponding to a beat frequency range of 2.8 kHz to 5.6 kHz, was used. The displacements found using this approach are referred to as the 'Peak' method.

```
function [signalDFT, f] = FMCWFourierTransform(signal, f_s)

% Perform Fourier transform of mixed signal
signalDFT = fft(signal);
% Remove the negative frequency components and convert to magnitudes
N_mix = length(signal);
signalDFT = signalDFT(1:floor(N_mix/2+1), :);
f = 0:f_s/N_mix:f_s/2;
end

function distance = GetDistanceFromSpectrum(mixSpectrum, mixDistances, windowStart,
    windowEnd)

dRes = mixDistances(2) - mixDistances(1);

% Select a slice from the mixSpectrum corresponding only to distances within the
```

```
    range (windowStart, windowEnd)
mixDistancesSlice = mixDistances((round(windowStart / dRes) + 1):(round(windowEnd /
    dRes) + 1));
mixSpectrumSlice = mixSpectrum((round(windowStart / dRes) + 1):(round(windowEnd /
    dRes) + 1));

[~, maxInd] = max(abs(mixSpectrumSlice));

distance = mixDistancesSlice(maxDInd);

end

signal = [signal zeros(N_zeroPadding, 1)]; % Zero padding
[signalDFT, f] = FMCWFourierTransform(signal, f_s);
d = f .* (c * T_mod / (2 * (f_1 - f_0))); % FMCW equation
dRadarPeak = GetDistanceFromSpectrum(signalDFT, d, 3, 6);
```

Listing 5.1: Fast Fourier Transform approach to spectral analysis

Beyond the inclusion of zero-padding, different methods were applied to the spectra individually and in combination.

5.4.2 'Quad' Method

To improve the resolution of beat frequency identification, the frequency bins adjacent to the selected peak were used to create a three-point quadratic interpolation. It has been shown that this method provides a better estimate of spectrum shape (Abe & Smith III, 2004). A quadratic was fit to the frequencies $i-1$, i, $i+1$, where i is the frequency found using the 'Peak' method. The peak of this quadratic was calculated by solving its derivative. The code shown in Listing 5.2 shows how this was achieved. The distance which this frequency corresponded to was recorded, and is referred to as the

'Quad' method.

```
function distance = GetQuadDistanceFromSpectrum(mixSpectrum, mixDistances,
    windowStart, windowEnd)

dRes = mixDistances(2) - mixDistances(1);

% Select a slice from the mixSpectrum corresponding only to distances within the
    range (windowStart, windowEnd)
mDist = mixDistances((round(windowStart / dRes) + 1):(round(windowEnd / dRes) + 1));
mSpec = mixSpectrum((round(windowStart / dRes) + 1):(round(windowEnd / dRes) + 1));

[~, maxInd] = max(abs(mSpec));

% Fit a polynomial with 1000 times the sampling frequency to the points adjacent to
    maxInd
p = polyfit(mDist(maxInd - 1:maxInd + 1), mSpec(maxInd - 1:maxInd + 1)', 2);
distance = - p(2) / p(1); % Solution to derivative of polynomial

end
```

Listing 5.2: 'Quad' method used to improve spectral resolution

5.4.3 'QuadF' Method

Initial inspection of the FFT output of the collected heterodyned sweeps indicated that a significant amount of spectral noise had interfered with the signal. This noise is related to thermal Johnson-Nyquist noise and ADC quantisation. To smooth this noise, a filter was designed to be applied directly to the spectrum. The noise was observed to have periods less than 10 units per cycle. From this figure, it was deduced that a filter with a 4 Hz cut-off would be suitable. A low-pass finite impulse response (FIR) filter with a Blackman window was designed and applied to each sweep spectrum. The quadratic

method was then used on this result. This distance estimate method is shown in Listing 5.3 and is referred to as the 'QuadF' method.

```
function Hd = DFTSmooother

Fs = 0.05;              % Spectrum Sampling Rate
Fpass = 0.002;          % Normalised Passband Frequency
Fstop = 0.004;          % Normalised Stopband Frequency
Dpass = 0.057501127785; % Passband Ripple
Dstop = 0.0001;         % Stopband Attenuation
dens  = 20;             % Density Factor

% Calculate the order from the parameters using FIRPMORD.
[N, Fo, Ao, W] = firpmord([Fpass, Fstop]/(Fs/2), [1 0], [Dpass, Dstop]);

% Calculate the coefficients using the FIRPM function.
b  = firpm(N, Fo, Ao, W, {dens});
Hd = dfilt.dffir(b);
end

Hd = DFTSmoother();
signalDFTF = filtfilt(Hd.Numerator, 1, radarDFT);
dRadarQuadF = GetQuadDistanceFromSpectrum(signalDFTF, d, 3, 6);
```

Listing 5.3: 'QuadF' method used to improve spectral precision

5.4.4 'MT' Method

The Thomson multitaper method of spectral analysis (Thomson, 1982) was used as a method which could improve on the spectral precision of the Discrete Fourier Transform (DFT) method, as was shown in simulation. The code used to perform this is shown in Listing 5.4. The naïve peak finding method used to find distances for the 'Peak' method was reapplied to the multitaper transform output to find data for the

'MT' method. Similarly, the multitaper output and its filtered version were also fed into the quadratic interpolation method to obtain data henceforth referred to as 'MTQuad' and 'MTQuadF'.

```
function [signalPMTM, f] = FMCWMultitaperTransform(signal, f_s)

% Perform a Multitaper transform of mixed signal
signalPMTM = pmtm(signal, 4, [], f_s);
f = linspace(0, f_s / 2, length(signalPMTM));

end

[signalPMTM, f] = FMCWMultitaperTransform(signal, f_s);
d = f .* (c * T_mod / (2 * (f_1 - f_0))); % FMCW equation
dRadarMT = GetDistanceFromSpectrum(signalPMTM, d, 3, 6);
dRadarMTQuad = GetQuadDistanceFromSpectrum(signalPMTM, d, 3, 6);

Hd = DFTSmoother(); % Filter from Listing 3
signalPMTMF = filtfilt(Hd.Numerator, 1, signalPMTM);
dRadarMTQuadF = GetQuadDistanceFromSpectrum(signalPMTMF, d, 3, 6);
```

Listing 5.4: Multitaper method used to smooth spectra

It was observed that the sweep spectra did not have sharply-defined beat frequencies, but instead had a spread of spectral energy around the anticipated dominant frequency component. It was also observed that a target in motion caused the components of this energy spread to be shifted by an almost constant amount proportional to target displacement. A correlation-based method was thus used to determine the change in displacement between an initial sweep spectrum and subsequent sweeps. The MATLAB code used to execute this process is shown in Listing 5.5. The offset output by the cross-correlation of the spectra determines the distance through which the reflector has moved relative to its initial position. Again, a window containing the expected beat frequency was used to ensure that only frequency components relating to the reflector

were used for analysis. Frequency components resulting from crosstalk between the two antennas and reflections from objects behind the corner reflector not attached to the shake table did not have the same motion as the corner reflector and thus needed to be omitted from the cross-correlation.

```
function distance = GetDistanceFromCorrelation(sampleSpectrum, sampleDistances,
    staticSpectrum, staticDistances, windowStart, windowEnd)

dResSample = sampleDistances(2) - sampleDistances(1);

% Sections of the spectra used for analysis (between windowStart and windowEnd
    distances) are taken for cross-correlation
sampleDistancesSlice = sampleDistances((round(windowStart / dResSample) + 1):(round(
    windowEnd / dResSample) + 1));
sampleDFTSlice = abs(sampleSpectrum((round(windowStart / dResSample) + 1):(round(
    windowEnd / dResSample) + 1)));

% Slice the reference spectrum with the same parameters
staticDFTSlice = abs(interp1(staticDistances, staticSpectrum, sampleDistancesSlice));

% Normalise the spectrum slice
staticDFTSlice = staticDFTSlice * max(abs(sampleDFTSlice)) / max(abs(staticDFTSlice))
    ;

[xcorrDFT, xcorrDFTLag] = xcorr(sampleDFTSlice, staticDFTSlice);
[~, corrPeakIndex] = max(xcorrDFT);

distance = xcorrDFTLag(corrPeakIndex) .* dResSample;

end
```

Listing 5.5: Correlation-based displacement estimation method

Because no time synchronisation information was available to match the time scales of the LVDT and FMCW radar data, cross-correlation was used to objectively determine the

delay between the data from each sensor. After the displacements have been computed using each method, the cross-correlation between the radar and LVDT measurements was computed. The offset corresponding to the peak in cross-correlation was then used to recentre the time vectors, and data was trimmed such that the only overlapping section was preserved. Figure 5.9 shows an example of pre- and post-synchronisation of outputs from the two sensors. Listing 5.6 shows the code used to perform the synchronisation.

The LVDT and FMCW radar data outputs collected different measurements. The former measured the displacement of the table from its resting position, while the beat frequency of the heterodyned signal was proportional to the distance between the reflector and the transceiver unit. This discrepancy was accounted for by subtracting the difference in output in the opening few samples after synchronisation, specified by the `calibrationIndices` parameter in Listing 5.6. The calibration duration was set to 1 s.

```
function offset = ComputeOffset(vector1, vector2, calibrationIndices)

offset = mean(vector1(1:calibrationIndices)) - mean(vector2(1:calibrationIndices));

end

function dataSet = trimLVDTAndRadarDistances(dataSet, calibrationTime)

if (min(dataSet.lvdtTimeInterp) < min(dataSet.radarTime))
    validIndices = find(dataSet.lvdtTimeInterp >= min(dataSet.radarTime));
    dataSet.lvdtTime = dataSet.lvdtTime(validIndices);
    dataSet.lvdtDistance = dataSet.lvdtDistance(validIndices);
else
    validIndices = find(dataSet.radarTime >= min(dataSet.lvdtTimeInterp));
    dataSet.radarTime = dataSet.radarTime(validIndices);
    dataSet.radarDistances = dataSet.radarDistances(:, validIndices);
    % This process is repeated for all other radar data analysis methods
end
```

```
19
20 dataSet.radarTime = dataSet.radarTime - min(dataSet.radarTime);
21 dataSet.lvdtTimeInterp = dataSet.lvdtTimeInterp - min(dataSet.lvdtTimeInterp);
22
23 if (max(dataSet.lvdtTimeInterp) > max(dataSet.radarTime))
24     validIndices = find(dataSet.lvdtTimeInterp <= max(dataSet.radarTime));
25     dataSet.lvdtTimeInterp = dataSet.lvdtTimeInterp(validIndices);
26     dataSet.lvdtDistanceInterp = dataSet.lvdtDistanceInterp(validIndices);
27 else
28     validIndices = find(dataSet.lvdtTimeInterp <= max(dataSet.radarTime));
29     dataSet.radarTime = dataSet.radarTime(validIndices);
30     dataSet.radarDistances = dataSet.radarDistances(:, validIndices);
31    % This process is repeated for all other radar data analysis methods
32 end
33
34 dataSet.radarDistances = dataSet.radarDistances - ComputeOffset(dataSet.
       radarDistances, dataSet.lvdtDistanceInterp, round(calibrationTime / dataSet.
       parameters.tSweep));
35
36 end
```

Listing 5.6: Synchronisation of reference and tested sensors

5.4.5 Data Processing for System Validation

The distance calculated using the methods presented in the previous sections is equivalent to an interstorey diagonal displacement (IDD), the distance from the lower corner of a floor to its opposite upper corner. A pictorial definition of this value is shown in Figure 5.10. The mean error of this value across the entire data record was used as a metric of comparison. The error was calculated as the radar-measured reflector distance relative to the LVDT measured displacement of the shake table. Because the LVDT measurements were centred about 0 m, these measurements were calibrated using the

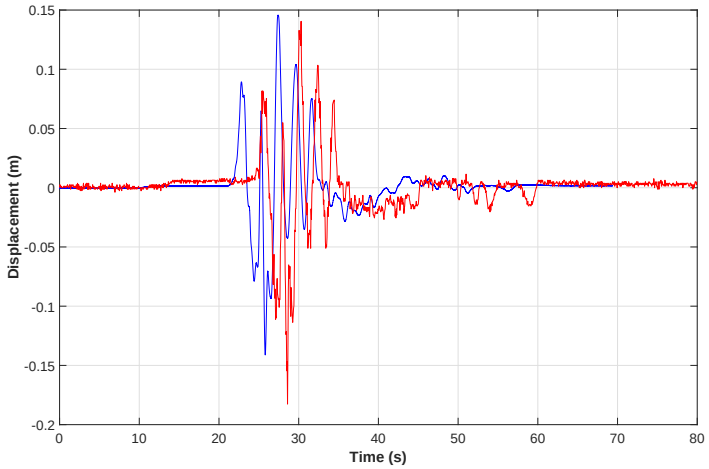

(a)

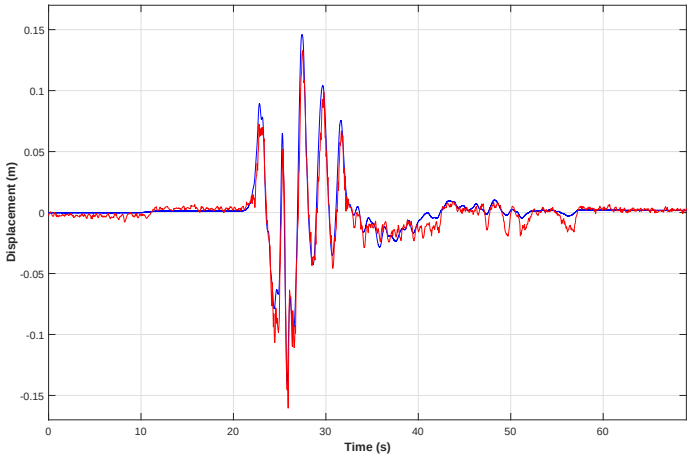

(b)

Figure 5.9: Linear variable differential transformer (blue) and radar 'CorrMT' method (red) data (a) before and (b) after time synchronisation.

initial radar measurement of the static reflector distance. The mean error for n samples was calculated as:

$$
\begin{aligned}
x_{\text{radar}} &= \frac{c \times T_{\text{mod}}}{2\left(f_1 - f_0\right)} f_r \\
\Delta\left(x[k]\right) &= \frac{\left|x_{\text{radar}}[k] - \left(x_{\text{LVDT}} + x_{\text{radar}}[0]\right)\right|}{x_{\text{LVDT}} + x_{\text{radar}}[0]} \\
\Delta x &= \sum_{k=0}^{n-1} \frac{\Delta\left(x[k]\right)}{n}
\end{aligned}
\tag{5.2}
$$

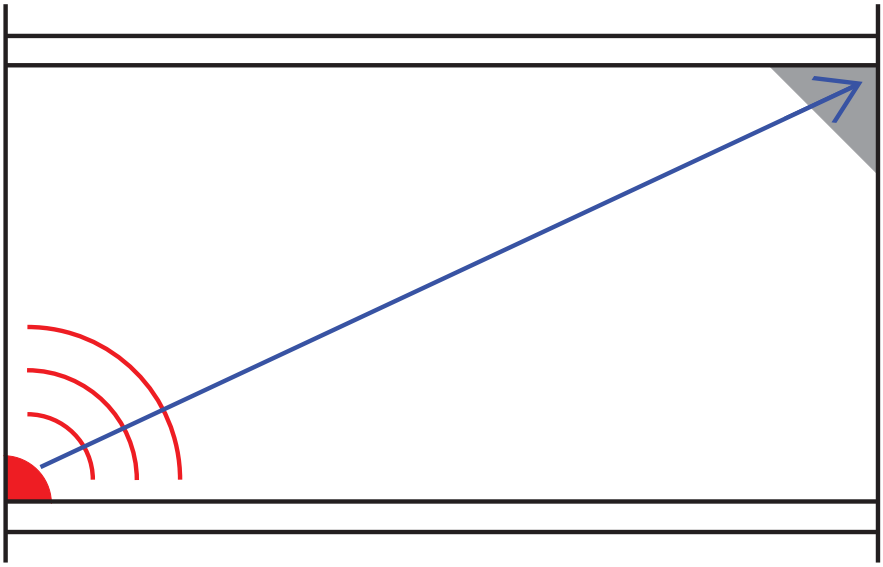

Figure 5.10: An example of a hypothetical 2D structure with a radar transceiver placed in the lower left corner and a reflector in the upper right corner. The interstorey diagonal displacement, x, is represented in blue.

To better validate the efficacy of the signal processing methods in an SHM context, the IDD errors needed to be converted to IDR errors. For IDRs to be calculated, the displacement of two consecutive storeys must be known. This value can be obtained by comparing the distance diagonally between the two storeys, defined here as the IDD. By observing how the IDD changes during a seismic event, the IDR can be calculated.

For a hypothetical two-dimensional structure with uniform floor length, l, as depicted in Figure 5.10, the corner-to-corner distance (or IDD) measured by a radar system, x, is:

$$x = \sqrt{l^2 + h_i^2}$$

When the structure is disturbed by an external force, x is altered and becomes:

$$x' = \sqrt{l'^2 + h_i'^2} \tag{5.3}$$

Assuming that l and h_i remain constant during the event, l' and h_i' are defined:

$$\begin{aligned} l' &= l + (d_i - d_{i-1}) \\ h_i' &= \sqrt{h_i^2 - (d_i - d_{i-1})^2} \end{aligned} \tag{5.4}$$

By substituting Equation (5.4) into Equation (5.3), x' becomes:

$$\begin{aligned} x' &= \sqrt{[l + (d_i - d_{i-1})]^2 + h_i^2 - (d_i - d_{i-1})^2} \\ &= \sqrt{l^2 + 2l\,(d_i - d_{i-1}) + h_i^2} \end{aligned} \tag{5.5}$$

The IDR Equation (2.11) can be rearranged to yield:

$$\delta_i h_i = d_i - d_{i-1}$$

and substituted into Equation (5.5) to give:

$$x' = \sqrt{l^2 + 2l\,(\delta_i h_i) + h_i^2}$$

Rearranging gives an expression for the IDR, δ_i:

$$\delta_i = \frac{x'^2 - l^2 - {h_i}^2}{2lh_i} \tag{5.6}$$

The relationship in Equation (5.6) allows the collected IDDs to be converted to IDRs for comparison to SHM requirements detailed in Section 2.2.4. Both the reference LVDT displacement measurements and the processed radar displacement estimates were converted using this equation. An arbitrary building length was chosen as $l = 20\,\mathrm{m}$, and the floor height was chosen such that the peak IDR was the severely damaging motion threshold $|\delta_i| = 1.5\,\%$ (h =6.0 m to 10.6 m).

The resulting mean IDR error for each data set was used as a metric to determine the effectiveness of the various signal processing methods. For n measurements in a data set, the mean absolute IDR error was calculated using the formula:

$$\begin{aligned} \Delta\left(\delta\left[k\right]\right) &= \left|\delta_{\mathrm{radar}}\left[k\right] - \delta_{\mathrm{LVDT}}\left[k\right]\right| \\ \Delta\delta &= \sum_{k=0}^{n-1} \frac{\Delta\left(\delta_{\mathrm{radar}}\left[k\right]\right)}{n} \end{aligned} \tag{5.7}$$

To determine the ability of the FMCW radar system to detect the most damaging motion over the tracking period, an additional metric was defined. Because the likelihood of structural damage has been stated to be determined by the peak IDR, the error in peak IDR estimated by each radar signal processing technique was found, relative to the peak IDR of the LVDT data, which was set at 1.5 %. This metric was thus calculated suing the formula:

$$\Delta_{\mathrm{p}}\delta = |\max(|\delta_{\mathrm{radar}}|) - 0.015| \tag{5.8}$$

5.4.6 Comparison to Accelerometers

To evaluate the suitability of FMCW radar-based SHM compared to current methods, a comparison between the efficacy of an accelerometer and the proposed system was included. This was performed by taking the output of an accelerometer fixed to the shake table, and doubly-integrating. The accelerometers used were STMicroelectronics X6-1A Micro-Electro Mechanical System (MEMS) devices with 15-bit resolution. The acceleration-derived displacement data was filtered using a band-pass Butterworth infinite impulse response (IIR) filter ($f_{c,1} = 0.1\,\mathrm{Hz}, f_{c,2} = 15\,\mathrm{Hz}, n = 2$) to remove integral drift, as is standard for accelerometer-derived displacements. The errors relative to the reference displacement data obtained from the table-mounted LVDT sensor were then computed using the same methods as applied to the radar data.

5.5 Results

Table 5.1 summarises the results. Displacements measured with the FMCW system were treated as IDDs, and then converted to IDRs using Equation (5.6). Values for h_i and l were selected such that the maximum IDR was equal to 1.5 % for ease of comparison with the simulated system. The mean error in terms of IDR for each strong motion site and data processing method is presented in Table 5.2. The peak error for each data set and processing method is shown in Table 5.3. The values in these two tables are absolute differences in IDR, where both the actual and measured IDRs are expressed as percentages.

Table 5.1: Mean absolute interstorey diagonal displacement errors as a relative percentage

	Peak (%)	Quad (%)	QuadF (%)	MTPeak (%)	MTQuad (%)	MTQuadF (%)	Corr (%)	CorrMT (%)
REHS	0.0279	0.0279	0.0305	0.0278	0.0279	0.0276	0.0274	0.0175
CCCC	0.0336	0.0333	0.0282	0.0321	0.0319	0.0287	0.0167	0.0166
CBGS	0.0310	0.0308	0.0262	0.0275	0.0274	0.0259	0.0170	0.0162
PPHS	0.0329	0.0326	0.0279	0.0280	0.0281	0.0273	0.0228	0.0195
CHHC	0.0353	0.0351	0.0338	0.0344	0.0344	0.0320	0.0142	0.0112
Mean	0.0321	0.0320	0.0293	0.0300	0.0299	0.0283	0.0196	0.0162

Table 5.2: Mean interstorey drift ratio errors as absolute difference in IDR

	Peak	Quad	QuadF	MTPeak	MTQuad	MTQuadF	Corr	CorrMT
REHS	0.0765	0.0765	0.0837	0.0761	0.0766	0.0757	0.0751	0.0479
CCCC	0.138	0.137	0.116	0.131	0.131	0.118	0.0686	0.0682
CBGS	0.106	0.105	0.0895	0.0941	0.0937	0.0885	0.0580	0.0553
PPHS	0.0779	0.0773	0.0660	0.0664	0.0666	0.0648	0.0541	0.0461
CHHC	0.145	0.145	0.139	0.142	0.142	0.132	0.0585	0.0463
Mean	0.109	0.108	0.0989	0.102	0.102	0.0957	0.0629	0.0528

Table 5.3: IDR errors at peak interstorey drift as absolute difference in IDR

	Peak	Quad	QuadF	MTPeak	MTQuad	MTQuadF	Corr	CorrMT
REHS	8.04×10^{-3}	6.13×10^{-3}	0.0199	0.0164	0.0150	0.0554	0.191	0.0834
CCCC	0.168	0.170	0.240	0.217	0.214	0.188	0.0482	0.0688
CBGS	0.114	0.111	0.235	0.0450	0.0459	0.0408	0.0851	0.0776
PPHS	0.0276	0.0278	0.0426	0.0395	0.0380	0.0468	2.78×10^{-3}	0.0369
CHHC	0.366	0.365	0.454	0.413	0.409	0.378	0.378	0.0967
Mean	0.137	0.136	0.198	0.146	0.144	0.142	0.141	0.0727

Table 5.4: Accelerometer errors

	Mean IDD Error (%)	Mean IDR Error	Error at Peak IDR
REHS	0.179	0.0688	0.226
CCCC	0.130	0.0820	0.0653
CBGS	0.137	0.0700	0.0917
PPHS	0.122	0.0375	0.218
CHHC	0.0646	0.0416	0.367
Mean	0.127	0.0600	0.194

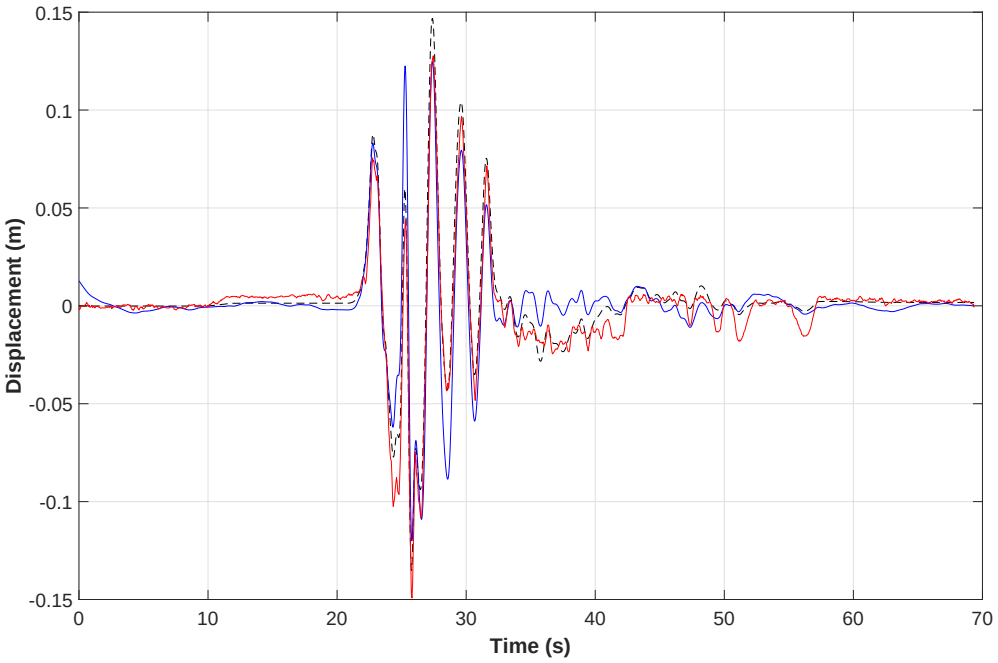

Figure 5.11: The REHS acceleration-derived displacement data (blue) and radar-derived data (red), compared to the LVDT-derived displacement (black, dashed).

Table 5.4 shows the errors of the accelerometer-derived displacements, using the metrics defined in the previous paragraph. Figures 5.11 to 5.15 show how the IDR-converted data sets compare to the radar-obtained displacement in terms of displacement estimation precision.

5.6 Discussion

The results indicated that, while the FMCW system is able to detect displacements to the accuracy necessary in SHM using naïve peak identification of zero-padded sweep

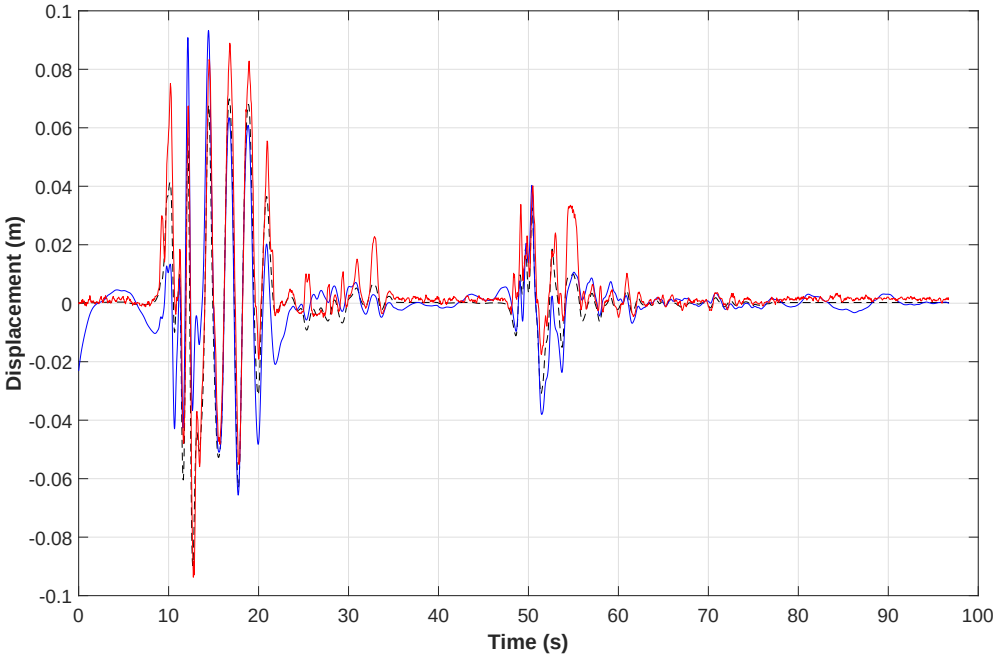

Figure 5.12: The CCCC acceleration-derived displacement data (blue) and radar-derived data (red), compared to the LVDT-derived displacement (black, dashed).

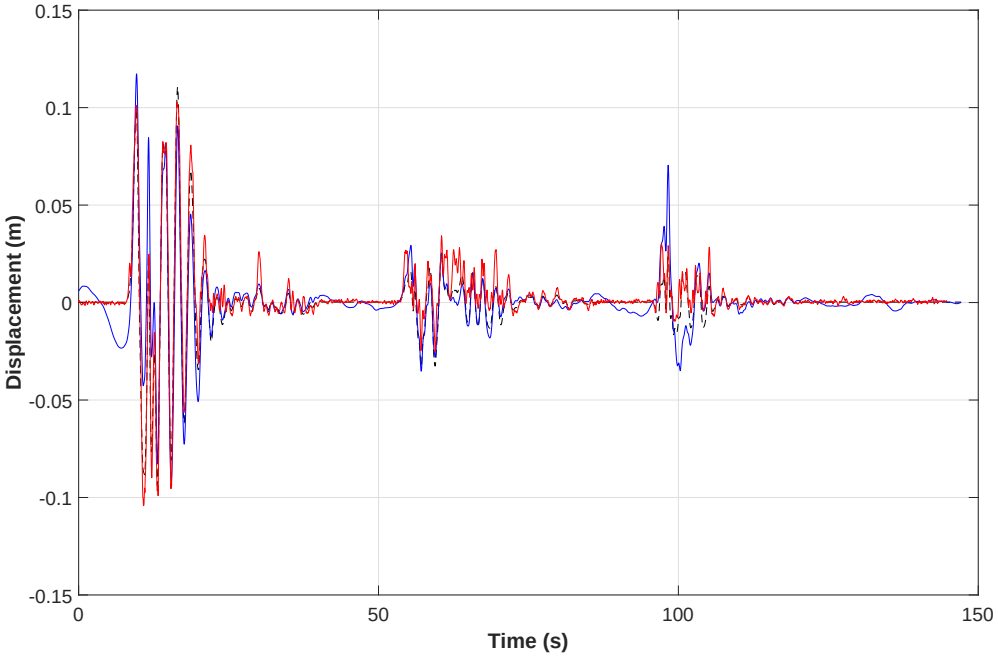

Figure 5.13: The CBGS acceleration-derived displacement data (blue) and radar-derived data (red), compared to the LVDT-derived displacement (black, dashed).

spectra, significant improvements to the IDR detection accuracy can be made using additional signal processing methods. The mean estimated IDR error using the 'Peak' method was 0.109 %. The minimum detectable IDR necessary to identify structural cracking was determined in Chapter 2 to be 0.2 %. Assuming that the system's resolu-

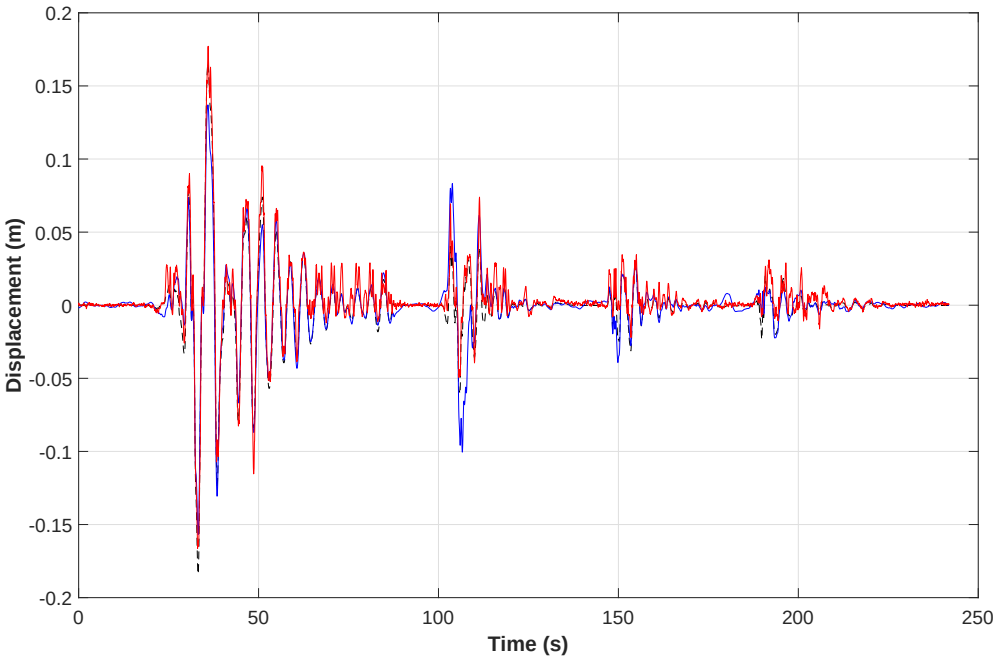

Figure 5.14: The PPHS acceleration-derived displacement data (blue) and radar-derived data (red), compared to the LVDT-derived displacement (black, dashed).

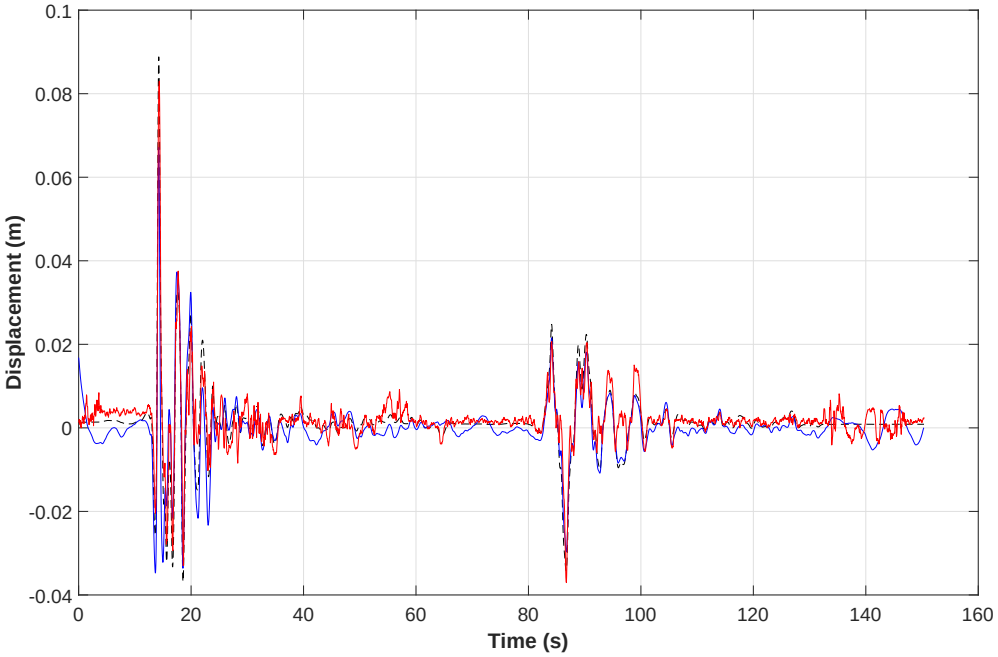

Figure 5.15: The CHHC acceleration-derived displacement data (blue) and radar-derived data (red), compared to the LVDT-derived displacement (black, dashed).

tion is comparable to its mean error, small displacements measured using this method are likely to have a significant error factor. This error limits the ability of the 'Peak' method to provide useful response data in slightly damaging events. The best achievable error of 0.0528 % was found using the 'CorrMT' method, and was more than twice

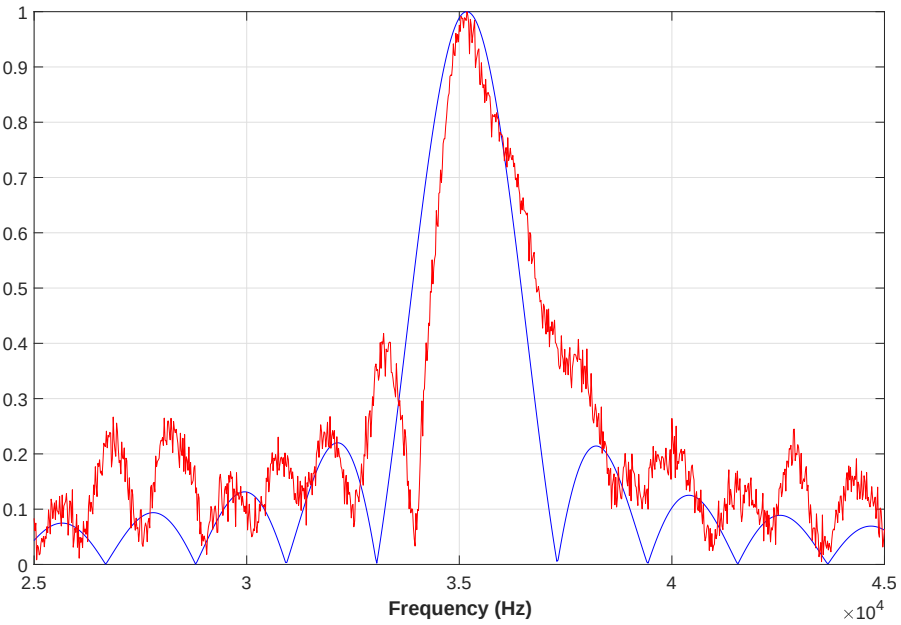

Figure 5.16: A comparison of sweep spectra from simulation (blue) and experimental (red) data. In both cases, the FFT method was used.

as accurate as the naïve method and much more suitable for SHM use. In addition, the peak IDR error was improved by a factor of 88 % when 'CorrMT' was used.

There were several reasons why the accuracy of these results was not quite able to match previously simulated data presented in Chapter 3. While the error in terms of raw distance estimation during simulation was 0.29 mm, the best achievable error during experimentation was 0.62 mm. The main issue is the difficulty of simulating a multipath environment. The variety of signal propagation paths due to other objects in the laboratory caused a spread in spectral energy around the bin corresponding to the target, which limited the device's ability to detect the specific motion of the target. Figure 5.16 shows a comparison of DFT spectra from simulation and experimentation.

As a result of the spread of spectral energy, there was little difference in amplitude between the most prominent frequency bin and those adjacent to it. This resulted in the 'Quad' method and related methods finding a peak beat frequency almost identical to

the most prominent bin, reducing the methods' effectiveness. Therefore, there was negligible difference between displacements calculated by the 'Peak' and quadratic methods. This similarity can be seen in the small discrepancy between the mean and peak IDR errors.

Figure 5.16 also shows the cause of the reduced precision of the 'Peak' detection method when compared to its simulated result. The well-defined, sharp peak in the simulated spectrum makes peak detection, and thus distance estimation, trivial. Conversely, the artifacted and less smooth experimental spectrum means that accurate distance estimation is more difficult.

Of particular interest is the fact that the 'CorrMT' method outperformed the 'Quad' method in terms of mean IDR estimation. This differs from the result found in simulation, and can be related to the multipath nature of the real-world transmission channel. The window of the spectrum used for correlation includes reflections from objects other than the fixed corner reflector, including the table itself, and the structure mounted on the table which was simultaneously undergoing testing. Because these objects were constrained in their motion along the same single-DOF axis, and were all driven by the same source, it follows that their motion is strongly correlated. The implication for the spectrum of the heterodyned signal is that the entire correlation window shifts as the peak shifts. This allowed for the correlation-based methods to have improved accuracy in practice.

Because real seismic events lack this single-DOF constraint, and structures have multiple DOF responses during such events, motion in directions other than the one being measured may significantly alter the radar transmission channel, and thus the heterodyned spectrum. This could reduce the effectiveness of correlation-based methods in practice. Further testing on a real-world structure is required, but due to the intercon-

nected nature of structural members, the correlation methods should still hold validity. However, these differences between shake table and real-world testing should not affect the 'Peak' or 'MTQF' methods' ability to identify the reflector.

While the accuracy of the 'CorrMT' method represents the best achievable IDR error by this hardware prototype, other configurations could improve the detection accuracy yet further. As stated by Equation (2.18), simple increases to the sweep bandwidth can improve the detection resolution, which would improve detection error. These increases would require more expensive components to generate a wider frequency sweep. In addition, higher bandwidths would require higher frequency signals to be transmitted, resulting in the need for stronger signal amplification.

The radar method compared favourably with the results obtained using accelerometers. The mean accelerometer IDR error (0.0600 %) is slightly worse than the mean error found using the 'MTCorr' radar method (0.0528 %). The peak acclerometer IDR error is much greater than the peak error of the radar system regardless of the signal processing method used. This difference in performance was primarily due to the difficulty of removal of integral drift in the doubly-integrated accelerations without losing important response data. The IIR filter removed integral drift, but low-frequency motion was then lost. An example of this loss of data is visible in the REHS data shown in Figure 5.11 between 35 s to 40 s.

In addition, introduced oscillations into the displacement which reduced accuracy. FIR filters are typically used to limit passband ripple. The use of an FIR filter was not possible in this application due to the high filter order required to remove very low frequencies from the data. Instead, an IIR filter was used.

Through experimentation, it was found that the accelerometer error was significantly

reduced when the LVDT data was filtered with the same passband filter used to remove integral drift. This result highlights the problem with obtaining displacement measurements from accelerometer outputs, because the error in displacement tracking is due to low frequency oscillations which can be indicative of structural damage. The measurement of ground acceleration records with a final displacement of 0 mm, as was the case with tested data sets, is also ideal for accelerometers because there is no permanent recentering which would be filtered out when integral drift is removed. In real-world structures, a recentering of a floor can be a key indicator of structural damage. While more sophisticated baseline correction algorithms may be able to improve the accelerometers' displacement tracking precision, this result justifies the validity of the novel method of SHM presented in this thesis when compared to contemporary approaches.

In practical terms, this sensing method requires a heterodyned signal sampling rate of significantly larger than the largest frequency component of the FMCW spectrum. For appropriate time series reconstruction, a sampling rate 20 times greater than this component would be sufficient. If the FMCW parameters used in this test are chosen, a sample rate around $1.0\,\mathrm{MS\,s^{-1}}$ is required. A hardware-based multitaper transform solution could be developed to perform the beat frequency identification using a field-programmable gate array (FPGA) or an application-specific integrated circuit (ASIC). This approach would reduce the sampling requirements significantly.

5.7 Summary

An experiment was conducted using physical hardware to verify that FMCW radar could be used as a method of SHM. A prototype device was aimed at a reflector attached to a shake table, which was driven with historical earthquake ground displacement

data. The displacement of the target was obtained using a variety of signal processing techniques to improve precision to the levels necessary for SHM. The system was found to be able to measure structural IDR equivalents to a mean error of 0.0528 %. This was deemed to be a suitable resolution to detect even slightly damaging motion. These results compared favourably to measurements obtained from an accelerometer. The results of this experiment led to the development of a scheme to fully instrument a multistorey structure.

CHAPTER 6

Sensor Placement and Identification in a Multistorey Structure

6.1 Introduction

Frequency-modulated continuous wave (FMCW) radar has been shown to be a viable method of sensing structural displacement at magnitudes appropriate for structural health monitoring (SHM). These results are encouraging, and lead to further questions regarding the implementation of an FMCW radar system for in-structure monitoring. In particular, the necessary arrangement of sensors for complete monitoring of a multistorey structure requires investigation to determine how such a system would be implemented for the least expensive and most precise structural monitoring.

The experimentation described in Chapter 5 indicated that an FMCW radar system, when configured appropriately and with the use of a combination of signal processing techniques, is able to detect interstorey diagonal displacements (IDDs) to a precision of 0.02 %. These IDDs correspond to absolute interstorey drift ratio (IDR) errors of 0.0528 %. These IDRs were derived from a model relating IDRs to IDDs in Chapter 5 for a hypothetical two-dimensional structure, with some assumptions made about the rigidity of structural members and thus the geometry of the perturbed building. The shake table motion was taken as the structural drift in this case. Equivalent IDRs were calculated by making the assumption that the table motion was an example of severely damaging displacement.

To ensure the suitability of FMCW radar as a complete, on-structure SHM system could be evaluated, the two-dimensional model of IDD needed to be reimagined in a three-dimensional case. This task was completed to determine the number and positioning of sensors required to extract interstorey drift for both north-south (N-S) and west-east (W-E) directions in a structure. An alternative method is also proposed using a centrally-located transmitter/receiver unit to reduce the cost of implementing a complete SHM solution using this sensor technology. The benefits and limitations of each system are compared.

6.2 Requirements

Parametric models of structural behaviour are a common method of understanding structural properties. The dynamics of a structure are used as inputs to a mass, stiffness, and damping-based model, where the stiffness parameters are allowed to vary (Chase et al., 2004). The model for a structure undergoing external earthquake loading is expressed using the equation:

$$\boldsymbol{M} \cdot \ddot{v} + \boldsymbol{C} \cdot \dot{v} + \boldsymbol{K} \cdot v = -\boldsymbol{M} \cdot \ddot{x}_g$$

In Equation (6.2), v, $\dot{v}$, and $\ddot{v}$ are vectors representing the storey-by-storey displacement, velocity, and acceleration response measurements or estimates. M is a diagonal matrix representing the masses of each level of the structure, and C and K are matrices representing the damping and stiffness relationships between adjacent structural levels. $\ddot{x}_g$ is the ground acceleration applied to the structure. This equation can be expanded for a n-storey structure, yielding:

$$\begin{bmatrix} m_1 & 0 & \dots & 0 \\ 0 & m_2 & \dots & 0 \\ \vdots & \vdots & \ddots & \vdots \\ 0 & 0 & \dots & m_n \end{bmatrix} \begin{bmatrix} \ddot{v}_1 \\ \ddot{v}_2 \\ \vdots \\ \ddot{v}_n \end{bmatrix} + \begin{bmatrix} c_1 + c_2 & -c_2 & \dots & 0 & 0 \\ -c_2 & c_2 + c_3 & \dots & 0 & 0 \\ \vdots & \vdots & \ddots & \vdots & \vdots \\ 0 & 0 & \dots & -c_n & c_n \end{bmatrix} \begin{bmatrix} \dot{v}_1 \\ \dot{v}_2 \\ \vdots \\ \dot{v}_n \end{bmatrix} + \begin{bmatrix} k_1 + k_2 & -k_2 & \dots & 0 & 0 \\ -k_2 & k_2 + k_3 & \dots & 0 & 0 \\ \vdots & \vdots & \ddots & \vdots & \vdots \\ 0 & 0 & \dots & -k_n & k_n \end{bmatrix} \begin{bmatrix} v_1 \\ v_2 \\ \vdots \\ v_n \end{bmatrix} = - \begin{bmatrix} m_1 \\ m_2 \\ \vdots \\ m_n \end{bmatrix} \ddot{x}_g \quad (6.1)$$

Equation (6.1) is a model for expected behaviour. Structural response which does not match this model can be related to changes in stiffness, using Equation (2.6), rewritten here:

$$\boldsymbol{M} \cdot \ddot{v} + \boldsymbol{C} \cdot \dot{v} + (\boldsymbol{K} + \Delta \boldsymbol{K}) \cdot v = -\boldsymbol{M} \cdot \ddot{x}_g \quad (6.2)$$

The $\triangle \boldsymbol{K}$ parameter is a time-varying change in structural stiffness. Rearrangement of Equation (6.2) leads to the extraction of per-storey model errors being related to changes in stiffness, multiplied by interstorey drift. It follows that the more precisely and accurately an SHM can measure the IDRs of a structure, the better the model error will reflect changes in stiffness. Damage indication by SHM systems thus requires accurate displacement measurement to be most useful. This latter statement indicates the motivation for the research presented in this thesis.

In particular, parametric SHM model error is determined by the difference between model estimation of displacement and measured displacement between adjacent floors. This displacement change is normalised by storey height. Hence, the radar-based structural displacement measurement method must be able to measure the displacement floor-by-floor to be used in many SHM models so they can provide data related to metrics of structural damage and best localise damage.

Inspection of members recovered from a range of structures post-earthquake has allowed models of damage related to various measurable quantities of structural behaviour (Pagni & Lowes, 2006). Damage types and states were ranked on a scale 0 to 12, with 0 indicating an undamaged sample, and a value of 12 representing failure due to: (a) buckling of column longitudinal reinforcement; (b) loss of beam reinforcement anchorage within the joint; or (c) pull-out of discontinuous beam longitudinal reinforcement. The samples were categorised and plotted against a number of metrics. These plots are reproduced in Figure 6.1.

The coefficient of determination (r^2) for a log-normal fit to these scatter plots were calculated. A comparison of these values indicates that among single-metric damage relationships, IDRs provide the most strongly-correlated relationship between measurement metric and damage state. This resultfurther reinforces that the error in the model

in Equation (6.2) based on changes in stiffness, observable through changes in interstorey displacement, is a suitable method for SHM.

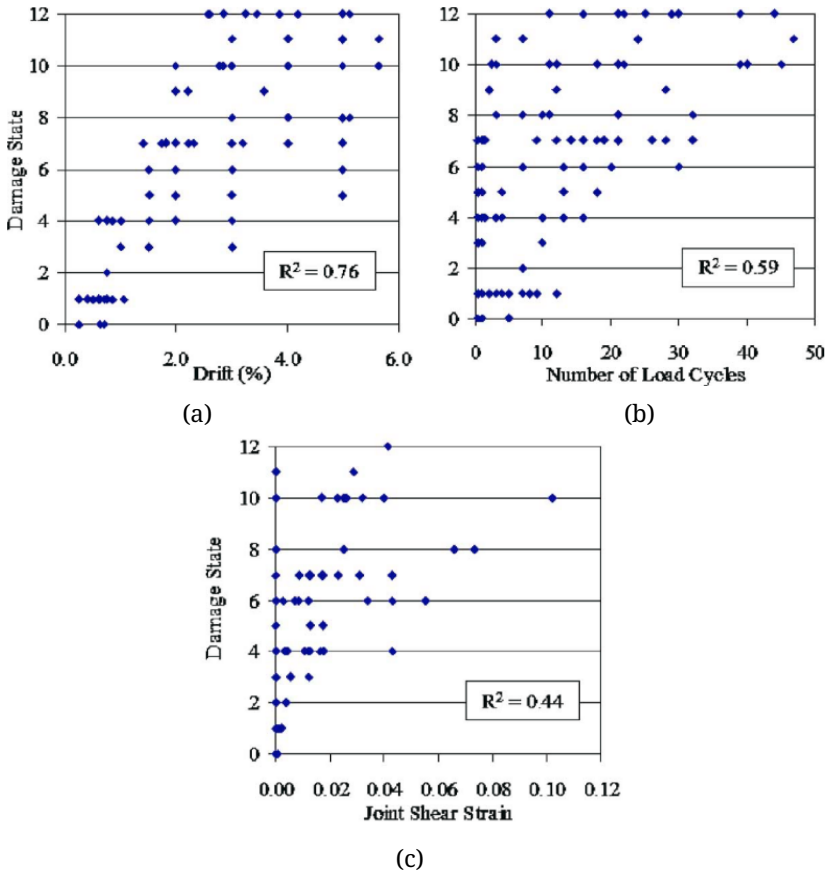

Figure 6.1: Empirical damage state data based on (a) interstorey drift ratio, (b) load cycles, and (c) joint shear strain engineering demand parameters with associated coefficients of determination (Pagni & Lowes, 2006).

Seismic ground motion, is not restricted in direction from source-to-site, and can arrive at a particular damage site from unpredictable directions (Bradley & Baker, 2014). Because of this lack of predictability in ground motion arrival angle, no assumptions can be made about the direction of interstorey drift. As such, for full instrumentation of a structure to be achieved, structural drift must be able to be measured omnidirectionally. This motion is represented by two orthogonal components. With the assumption made that the structure is of a regular rectangular form, the axes of motion are defined as running along two adjacent and perpendicular walls, with one corner of the structure identified as the origin. Drifts along these axes are referred to as N-S and W-E. A diagram showing the definition of these directions is shown in Figure 6.2. These drifts

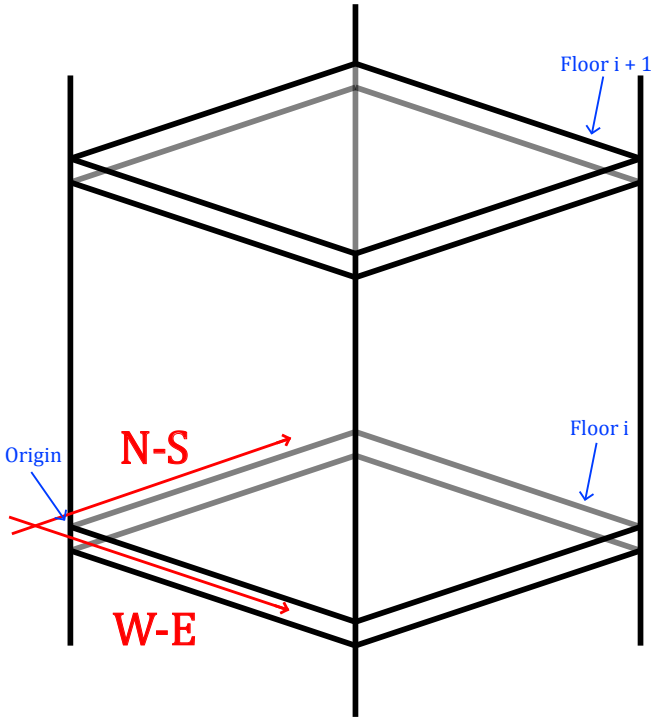

Figure 6.2: The definition of North-South and West-East axes in a three dimensional, multistorey structure.

can be used as inputs to SHM parametric models for the determination of damage state and location (C. Zhou, Chase, Rodgers, & Iihoshi, 2017).

6.3 Placement Options

The aim of the placement options detailed in this section is to fully instrument a multistorey structure. To meet the requirements of full instrumentation, it is preferable that damage severity is able to be determined for all storeys and/or bays of a structure to best localise damage. The data from this complete instrumentation is used as inputs to a parametric SHM model which relates the metric(s) measured by the sensor network to expected response.

These instrumentation patterns are intended to appropriately balance the required

number of sensors and the displacement precision of the measurements collected by these sensors. The former requirement is important to consider because the intent of the methods presented in this thesis is to provide a cost-effective method justfying retrofit to existing structures. The majority of the expense of this radar-based SHM system is in the component cost of the transmitter/receiver unit. Hence, a reduction in the required number of transceiver units significantly reduces the cost of instrumentation.

6.3.1 Mapping Interstorey Diagonal Displacements to Three Dimensions

The simplified two dimensional case for mapping structural motion of a single degree of freedom (DOF) structure to IDRs used in the validation of an SHM system can be extended to the real-world three dimensional case. The use of radar to determine structural motion requires a method of mapping a measured target displacement to an IDR, as defined in Equation (2.11).

Measurement of the relative motion between adjacent storeys requires the proposed FMCW radar based method to have transmitting and receiving antennas located on one floor, and a reflective target on either the next or previous storey. This layout assumes a monostatic radar configuration is used, because this particular radar application lacks the geometric properties for which a bistatic system would be advantageous (Jackson, 1986).

This requirement to measure between two consecutive floors led to the IDD-based arrangement of the FMCW radar sensor implementation depicted in Figure 6.3. For a structure with floor length, l, and separation between storeys, h_i, it follows the IDD of the resting structure using Pythagoras' Theorem (Heath, 1956) is defined:

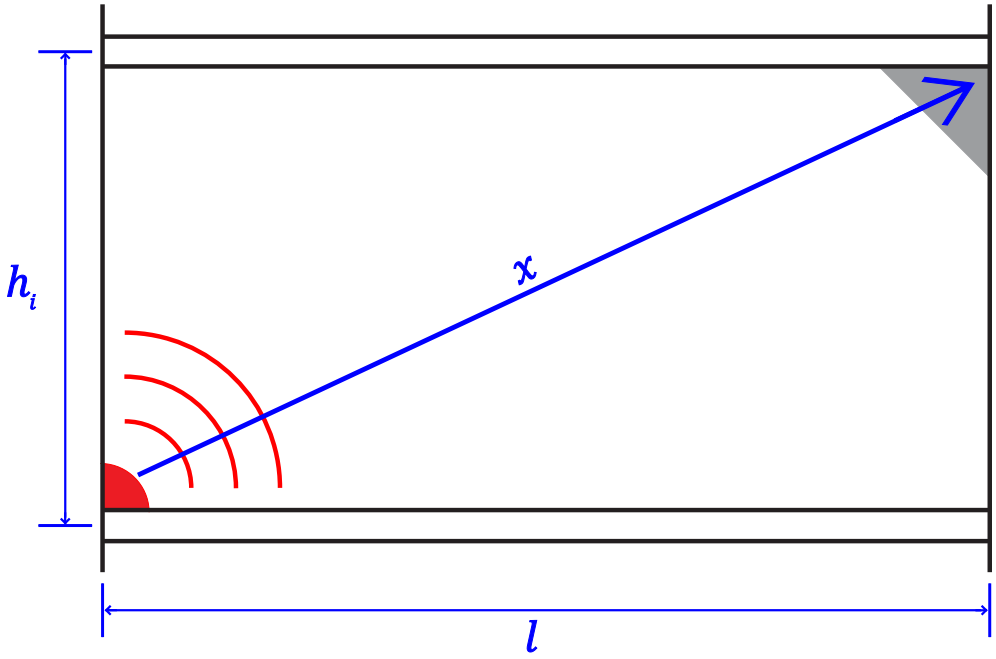

Figure 6.3: The interstorey diagonal displacement, shown as x, of a hypothetical two dimensional structure.

$$x = \sqrt{l^2 + h_i^2} \tag{6.3}$$

When the structure is perturbed, the relative alignment between storeys changes, altering the IDD. This change in alignment is shown in Figure 2.1. Assuming rigidity in the beams and axial stiffness of the columns of the structure, the floors remain parallel, but the effective values of l and h_i change. The value of the perturbed IDD is now defined:

$$\begin{aligned} x' &= \sqrt{[l + (d_i - d_{i-1})]^2 + h_i^2 - (d_i - d_{i-1})^2} \\ &= \sqrt{l^2 + 2l\,(d_i - d_{i-1}) + h_i^2} \end{aligned} \tag{6.4}$$

Equation (2.11) can be rearranged and substituted into Equation (6.4) to provide the relationship between IDD and IDR:

$$\delta_i = \frac{x'^2 - l^2 - {h_i}^2}{2lh_i} \tag{6.5}$$

Because the structural parameters l and h_i are known, IDR can be calculated. These principles can be extended to a three dimensional structure. Figure 6.4 shows how IDDs, x_1 and x_2, are defined in three dimensions for a uniformly rectangular multistorey structure, where l is the length of the building along the W-E axis, and w is the width of the building along the N-S axis. Note that the transceiver units are placed on a common edge of the structure.

The resting IDDs are equal and defined:

$$x_1 = x_2 = \sqrt{w^2 + l^2 + h_i^2} \tag{6.6}$$

When undergoing seismic loading, the structure has some interstorey drift. Because of this motion, adjacent floors become offset, but remain effectively parallel. There is thus a drift along both the N-S and W-E axes for each floor, meaning the effective dimensions determining x_1' and x_2' are defined:

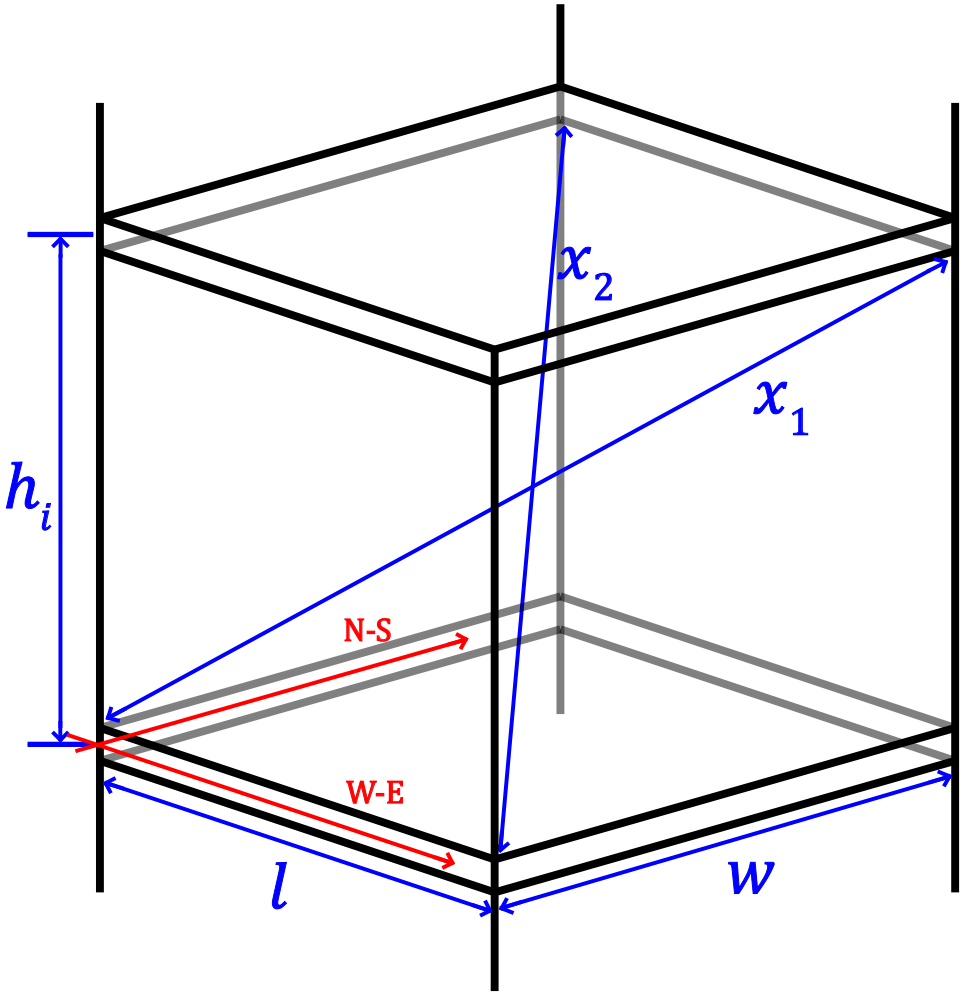

Figure 6.4: The definition of interstorey diagonal displacements in a three dimensional structure.

$$
\begin{aligned}
w &= w + (d_{w_i} - d_{w_{i-1}}) && = w + \Delta w \\
l_1 &= l + (d_{l_i} - d_{l_{i-1}}) && = l + \Delta l \\
l_2 &= l - (d_{l_i} - d_{l_{i-1}}) && = l - \Delta l \\
h_i' &= \sqrt{h_i^2 - (d_{w_i} - d_{w_{i-1}})^2 - (d_{l_i} - d_{l_{i-1}})^2} && = \sqrt{h_i^2 - (\Delta w)^2 - (\Delta l)^2}
\end{aligned}
$$

Here, l_1 is the effective length of the structure for IDD x_1', while l_2 is the effective length of the structure for x_2'. These values substitute into Equation (6.6) to form the IDD equa-

tions:

$$\begin{aligned} x_1' &= \sqrt{(w+\Delta w)^2 + (l+\Delta l)^2 + \left(h_i^2 - (\Delta w)^2 - (\Delta l)^2\right)} \\ &= \sqrt{w^2 + 2w\Delta w + (\Delta w)^2 + l^2 + 2l\Delta l + (\Delta l)^2 + h_i^2 - (\Delta w)^2 - (\Delta l)^2} \\ &= \sqrt{w^2 + l^2 + h_i^2 + 2w\Delta w + 2l\Delta l} \end{aligned} \tag{6.7}$$

$$\begin{aligned} x_2' &= \sqrt{(w+\Delta w)^2 + (l-\Delta l)^2 + \left(h_i^2 - (\Delta w)^2 - (\Delta l)^2\right)} \\ &= \sqrt{w^2 + 2w\Delta w + (\Delta w)^2 + l^2 - 2l\Delta l + (\Delta l)^2 + h_i^2 - (\Delta w)^2 - (\Delta l)^2} \\ &= \sqrt{w^2 + l^2 + h_i^2 + 2w\Delta w - 2l\Delta l} \end{aligned} \tag{6.8}$$

Squaring and adding these expressions for the IDD (Equations (6.7) and (6.8) together gives:

$$\begin{aligned} \left(x_1'\right)^2 + \left(x_2'\right)^2 &= w^2 + l^2 + h_i^2 + 2w\Delta w + 2l\Delta l + w^2 + l^2 + h_i^2 + 2w\Delta w - 2l\Delta l \\ &= 2w^2 + 2l^2 + 2h_i^2 + 4w\Delta w \\ &= 2w^2 + 2l^2 + 2h_i^2 + 4w\left(d_{w_i} - d_{w_{i-1}}\right) \end{aligned} \tag{6.9}$$

This relationship can be rearranged in terms of drift in one direction:

$$d_{w_i} - d_{w_{i-1}} = \frac{(x_1')^2 + (x_2')^2 - 2w^2 - 2l^2 - 2h_i^2}{4w} \tag{6.10}$$

Using the IDR Equation (2.11), Equation (6.10) can be equated to:

$$\begin{aligned} \delta_{w_i} h_i &= \frac{(x_1')^2 + (x_2')^2 - 2w^2 - 2l^2 - 2h_i^2}{4w} \\ \delta_{w_i} = \delta_{\text{N-S}_i} &= \frac{(x_1')^2 + (x_2')^2 - 2w^2 - 2l^2 - 2h_i^2}{4wh_i} \end{aligned} \tag{6.11}$$

Substituting a rearrangement of Equation (6.9) into Equation (6.7) allows for the formulation of an expression for δ_{l_i}:

$$\begin{aligned} (x_1')^2 &= w^2 + l^2 + h_i^2 + 2l\Delta l + \frac{(x_1')^2 + (x_2')^2}{2} - w^2 - l^2 - h_i^2 \\ (x_1')^2 &= 2l\Delta l + \frac{(x_1')^2 + (x_2')^2}{2} \\ \Delta l = d_{l_i} - d_{l_{i-1}} &= \frac{(x_1')^2 - (x_2')^2}{4l} \\ \delta_{l_i} = \delta_{\text{W-E}_i} &= \frac{(x_1')^2 - (x_2')^2}{4lh_i} \end{aligned} \tag{6.12}$$

The expressions for IDRs in Equations (6.11) and (6.12) are in terms of only known structural parameters of the building's geometry (w, l, and h_i), and the IDDs measured using the FMCW radar systems placed in the lower corners of the storey (x_1' and x_2'). Estimates of the IDR experienced for the i^{th} storey are thus able to be decoupled using two sensors placed in this manner, with corner reflectors placed in the upper corners of the storey opposite to the transceiver unit locations. These IDRs can be independently fed

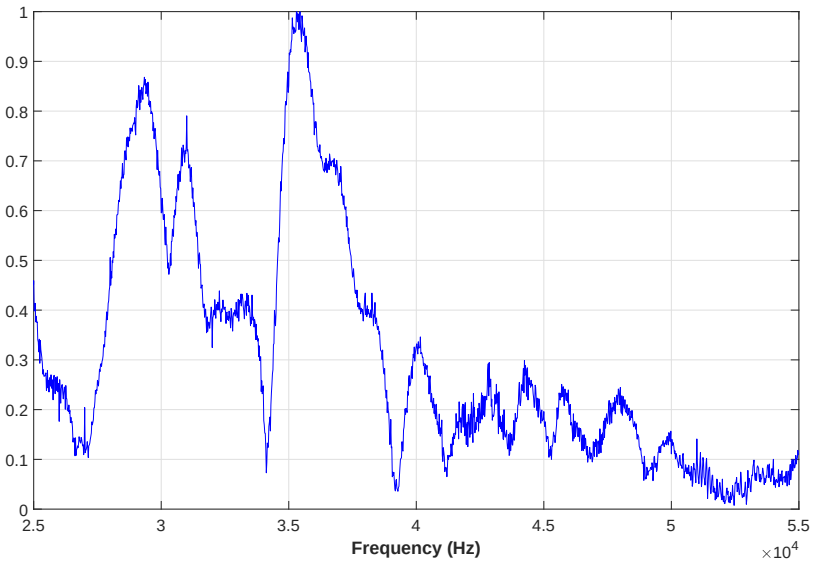

Figure 6.5: An artificially generated example of a beat spectrum containing two prominent reflecting targets.

into parametric models specific to the structure and materials used for an assessment of damage severity after a seismic event.

The use of two sensor-reflector pairs on the same floor, while being necessary to decouple the interstorey drift directionality in a structure, means two particularly reflective targets will be detected by each radar transceiver unit. Previous experimentation presented in Chapter 5 was conducted with a single corner reflector mounted to a shake table. The radar signature of this reflector was a prominent feature of the beat signal spectrum near its expected beat frequency. With a two-reflector arrangement, there will be two radar signatures present in the spectrum of the heterodyned FMCW radar signal.

An example what a spectrum with two prominent objects looks like is visible in Figure 6.5. The incidence of the transmitted radar signal on each reflector results in a defined peak appearing in the beat signal spectrum, in addition to a spread of spectral energy around this peak due to multipath propagation between the radar transceiver

and reflector. In cases where $w >> l$ or $l >> w$, the geometry of the building becomes more rectangular, and the apparent separation between reflectors is minimised. The spreading of spectral energy corresponding to each of the reflectors is then able to collide, making accurate peak detection impossible.

To avoid this problem of radar signature collision, transmitting and receiving antennas are chosen to be directional, thus having narrow beam widths. The benefits to this choice are two-fold. First, the narrow beam width limits multipath reflections of the transmitted signal from being detected by the receiving antenna. Second, reflections from the non-corresponding corner reflector have a reduced amplitude in the heterodyned spectrum. This choice allows the IDDs to be measured distinctly for the purpose of precise IDR estimation.

6.3.2 Centrally-Located Transceiver Monitoring

An alternative scheme for the arrangement of FMCW radar devices for the purposes of SHM used a single transceiver unit located on the floor of one storey, and two reflectors placed in adjacent upper corners of that same storey (i.e. fixed below the floor of the next storey). This scheme is intended to halve the number of radar units required to achieve complete instrumentation of a structure, dramatically reducing the cost of the monitoring system. In addition, installation can be simplified due to the reduced number of sensors that need to be installed.

To use this method to estimate IDRs, the distances between the sensor and the upper corners of the storey, referred to as the interstorey centre-to-corner displacement (ICCD), must be defined. These distances are shown in Figure 6.6 as the values y_1 and y_2. When the monitored structure is at rest, the values of y_1 and y_2 will be equal:

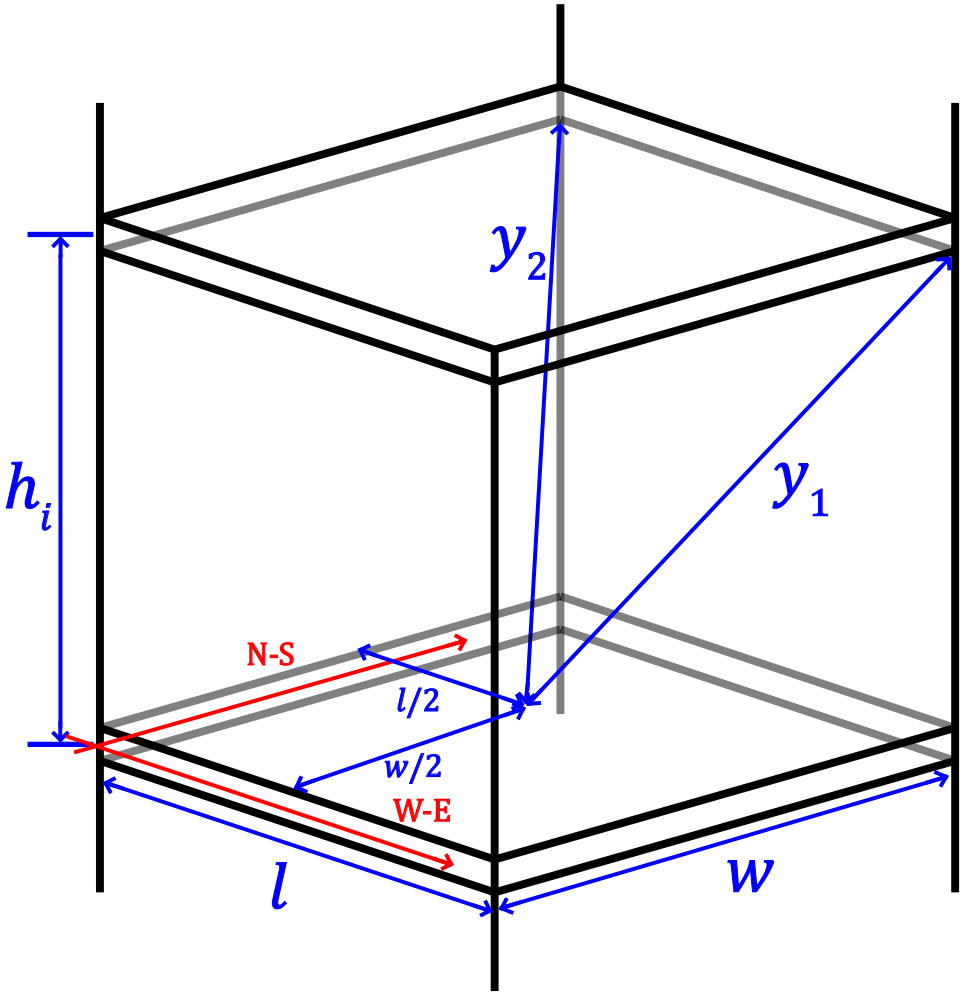

Figure 6.6: The definition of interstorey centre-to-corner displacements in a three dimensional structure.

$$y_1 = y_2 = \sqrt{\left(\frac{w}{2}\right)^2 + \left(\frac{l}{2}\right)^2 + h_i^2} = \sqrt{\frac{w^2}{4} + \frac{l^2}{4} + h_i^2} \tag{6.13}$$

When undergoing seismic motion, the change in structural geometry causes an imbalance in the ICCDs:

$$\begin{aligned} y_1' &= \sqrt{\left(\frac{w}{2}+\Delta w\right)^2+\left(\frac{l}{2}+\Delta l\right)^2+\left(h^2-(\Delta w)^2-(\Delta l)^2\right)} \\ &= \sqrt{\frac{w^2}{4}+w\Delta w+(\Delta w)^2+\frac{l^2}{4}+l\Delta l+(\Delta l)^2+h_i^2-(\Delta w)^2-(\Delta l)^2} \\ &= \sqrt{\frac{w^2}{4}+\frac{l^2}{4}+h_i^2+w\Delta w+l\Delta l} \end{aligned} \tag{6.14}$$

$$\begin{aligned} y_2' &= \sqrt{\left(\frac{w}{2}+\Delta w\right)^2+\left(\frac{l}{2}-\Delta l\right)^2+\left(h^2-(\Delta w)^2-(\Delta l)^2\right)} \\ &= \sqrt{\frac{w^2}{4}+w\Delta w+(\Delta w)^2+\frac{l^2}{4}-l\Delta l+(\Delta l)^2+h_i^2-(\Delta w)^2-(\Delta l)^2} \\ &= \sqrt{\frac{w^2}{4}+\frac{l^2}{4}+h_i^2+w\Delta w-l\Delta l} \end{aligned} \tag{6.15}$$

Through the same methods used in Section 6.3.1, the definitions of y_1' and y_2' can be used to find expressions for the N-S and W-E IDRs:

$$\delta_{w_i} = \delta_{\text{N-S}_i} = \frac{2\left(y_1'\right)^2+2\left(y_2'\right)^2-w^2-l^2}{4wh_i}-\frac{h_i}{w} \tag{6.16}$$

$$\delta_{l_i} = \delta_{\text{W-E}_i} = \frac{\left(y_1'\right)^2-\left(y_2'\right)^2}{2lh_i} \tag{6.17}$$

The expressions in Equations (6.16) and (6.17) again relate components of interstorey drift to structural geometry dimensions and radar-measured displacements, in this case, the ICCDs. These quantities are obtained through structural analysis of the frequency spectrum of the heterodyned signal from the single mixer output. The transceiver system thus must be able to transmit and receive radar signals to both reflective targets

simultaneously, requiring wide beam width antennas must be used.

When measuring structural drift with this method, the spread of spectral energy resulting from multipath signal propagation causes a collision in radar signatures of the two reflectors when the drift ratios are small. When the structure is at rest or experiencing small magnitudes of ground acceleration, the spectral spread causes radar signatures to collide in the heterodyned signal spectrum. More specifically, the signals returned from each reflector have similar frequencies. Only when the drift is significant will these signatures become distinct and be measurable, as shown by the example in Figure 6.5. This collision phenomenon limits the system's ability to detect small IDRs without the application of sophisticated signal processing methods to the heterodyned spectrum for peak identification.

The frequency spectrum of the heterodyned signal necessarily contains radar reflection signatures from multiple sources. Due to the equidistant positioning of the transceiver unit relative to the targets, these signatures will have similar prominence in the heterodyned signal spectrum. There is thus some difficultly in distinguishing which radar signature corresponds to y_1 and which corresponds to y_2. This difficulty does not limit the method's ability to provide accurate IDR estimations, because structural deformation can be inferred from the difference between measured ICCDs. However, the correct mapping of N-S and W-E IDRs requires some inference based on ground acceleration direction and the resulting expected structural behaviour.

6.3.3 Method Comparison

Each method described requires sensors and reflectors to be placed on each storey of a structure for complete instrumentation. Because the IDR equation is expressed in

terms of the relative motion of consecutive storeys, structural displacement measurements necessary for parametric SHM methods can not be interpolated between pairs of monitored storeys. Any storeys without FMCW radar sensing equipment are unable to be monitored and only a multi-storey IDR would be available across these storeys.

The IDD-based method requires radar signals to be propagated along a path twice the length of the storey's hypotenuse. Because of the length of this path, and the likelihood of destructive interference due to structural and non-structural features on this path, significant signal amplification is required. The gain required on the power amplification stage of the FMCW radar transceiver unit is also made larger by increased precision requirements, because improved precision requires larger sweep bandwidths and higher transmission frequencies. These higher frequencies are attenuated more significantly due to the Free Space Path Loss formula (Abhayawardhana, Wassell, Crosby, Sellars, & Brown, 2005):

$$\mathrm{FSPL}_{\mathrm{dB}} = 20 \log 10 \left(\frac{4\pi d}{\lambda} \right) \tag{6.18}$$

where λ is the signal wavelength.

The Free Space Path Loss Formula shows a relationship between signal attenuation and frequency of transmission. This relationship means that for more precise monitoring, which requires larger bandwidths and higher centre transmission frequencies due to the IDR Equation (2.11), more signal amplification is required, where greater amplification is expensive in terms of financial and power requirements. While this relationship applies to both methods presented in this chapter, the ICCD method requires shorter signal transmission distances for structures with equal w, l, and h parameters and is thus less limited by available amplification.

Experimentation in Chapter 5 identified correlation-based spectral analysis methods outperform peak-finding methods in terms of IDR measurement precision. The former methods were found to be almost twice as precise for the measured data sets when measuring IDRs equivalent to 1.5 %. However, a limitation of this experiment was it sought to simply track the displacement of a single target driven with a single DOF. This restriction allowed the radar signature of a static target to isolated and compared to subsequent measurement spectra to measure the target's shift.

The ICCD-based method of drift measurement presented in Section 6.3.2 relies on the detection of two signatures in a single sweep spectrum. The signatures are expected to have a similar amplitude. In the presented multi-DOF model, the change in position of the two targets is not necessarily correlated, so simple cross-correlation between a static spectrum and subsequent spectra will not reveal the displacement of the targets. This inability to utilise the most effective signal processing technique for target identification limits the ICCD method's ability to measure IDRs precisely. The IDD-based method presented in Section 6.3.1 is a suitable application for the correlation displacement estimation method because of the directionality of its antennas and different relative amplitudes of its target radar signatures.

The ability to place the transceiver unit in the centre of a floor rather than in a corner may be advantageous and feasible for certain structural designs. Any indoor radar system's effectiveness is susceptible to the effects of multipath propagation and channel shading. Larger structures which use centralised load-bearing columns are likely to have a large concentration of reflective materials, particularly steel, in line with the radar transmission path of the IDD method. To overcome these problems, an implementation can require the use of lower sweep frequencies resulting in reduced measurement precision, or significantly increased signal amplification. In these circumstances, the ICCD method with a centrally or near-centrally located transceiver unit is the more

Table 6.1: Prototype transceiver unit cost

Item	Unit Price (NZD)	Qty	Total (NZD)
Antenna	$2570	2	$5140
Power Amplifier	$1450	2	$2900
Mixer	$180	1	$180
Signal Generator	$280	1	$280
Instrumentation Amplifier	$10	1	$10
Cabling	$20	1 m	$20
Total			$8530

appropriate choice of monitoring scheme.

The two presented schemes are thus suitable in different contexts. In situations where the signal transmission paths from lower corners to opposing upper corners of storeys are unimpeded by strongly reflective materials, and the increased cost of $2n$ transceiver units is an acceptable trade-off for the improved IDR resolution afforded by improved signal processing techniques, then the IDD method is most appropriate. The additional cost of implementing this method with the prototype hardware discussed in Chapter 4 is NZ$8530 per floor. An itemised price list is shown in Table 6.1. When the structural layout prevents such a scheme being implemented, the ICCD-based method can be used. This approach should be used with the understanding that the IDR resolution of this system is inferior to that of the IDD method, though still twice as good as deemed necessary for use with parametric SHM methods.

For complete monitoring of a structure, it is probable that radio frequency (RF) interference would affect the signal-to-noise ratio (SNR) of the transmitted signals. The effects of interference can be limited with the use of highly directional antennas, but this is only a suitable approach when using the IDD method. To limit channel shading due to cross-signal interference between devices on adjacent storeys, a set of upsweep bandwidth and centre frequency settings can be distributed to the array of sensors. These FMCW parameters would be distributed such that each sensor is transmitting a different frequency gradient at a given time. An example of this method is detailed by Son,

Sung, and Heo (2018), who found a significantly improved correct detection probability using this method for all interference-to-noise ratios up to 0 dB.

6.4 Summary

The efficacy of a non-contact, displacement-measuring SHM instrumentation method using FMCW radar has been validated to be able to measure distance with the levels of accuracy necessary for this implementation. This chapter described how these sensors can be arranged for the purposes of providing useful inputs to parametric SHM methods, which is a novel application of radar-based SHM. Two different instrumentation schemes were explained and compared.

The interstorey diagonal displacement-based method uses two radar transceiver units placed in adjacent corners of a floor, with target reflectors placed in opposing corners. Highly directional antennas allow the corresponding reflectors' radar signatures to be easily identified. This method was seen to be precise, due to the ability to use superior correlation-based signal processing methods on its sweep spectra, but more expensive to implement due to its reliance on $2n$ transceiver units for an n-storey structure.

The second method presented is the interstorey centre-to-corner displacement-based method, which uses a single, centrally-located transceiver unit to instrument each floor. This method is unable to take advantage of correlation-based signal processing methods, but is cheaper to implement due to only using a single transceiver unit. This configuration is appropriate where low-cost, but less precise monitoring is required, particularly in structures with significant structural columns located in the centre of the building.

CHAPTER 7

Utilising Existing Wireless Protocols for Structural Displacement Measurement

7.1 Introduction

Chapter 6 detailed the methods of instrumenting a building for non-contact structural health monitoring (SHM) using frequency-modulated continuous wave (FMCW) radar sensor devices. These schemes require the installation of transceiver units, which with the hardware used for the prototype discussed in Chapter 4, have a unit cost of NZ$8530. While specialised hardware and economies of scale can reduce this price significantly, the installation of dedicated hardware may be prohibitive in some instances. To circumvent this problem, a method of using alternative radio frequency (RF)-transmitting

devices was sought.

Structures that might be suitable for SHM installation typically have WiFi access points already installed. These devices can transmit and receive signals over a range of frequencies, so they can act as FMCW radar transceiver units during seismic events for structural monitoring while otherwise operating as wireless local area network (WLAN) access points. This sharing of hardware could provide a meas to significantly reduce the cost of implementing SHM. This chapter investigates how such a monitoring system might be implemented, and presents simulation of the system with a single-degree of freedom (DOF) target to prove the initial concept.

7.2 Existing Protocols

The aim is to utilise existing wireless hardware to significantly reduce the cost of implementing non-contact, displacement-based SHM instrumentation. To verify if WiFi devices might provide a suitable method for performing this task, a review of existing standards is needed. The outcomes of this research allow us to know what the limits of operation of wireless devices is, so simulation can be carried out to validate the overall concept.

The Institute of Electrical and Electronics Engineers (IEEE) 802.11 standard is a set of specifications for the operation of wireless data transmission devices. The most ubiquitous categories within these guidelines are 802.11g, 802.11n, and 802.11ac. The former two specifications have the ability to broadcast signals in the 2.4 GHz range. The specific frequencies at which these signals can be broadcast with 802.11 devices in New Zealand are listed in Table 7.1 (IEEE, 2016). The 11 channels each have a fixed bandwidth of 20 MHz and centre frequencies evenly spaced at a pitch of 5 MHz.

Table 7.1: IEEE 802.11 WLAN channels in the 2.4 GHz band

Channel	Centre Frequency (MHz)	Frequency Range (MHz)	Bandwidth (MHz)
1	2412	2402–2422	20
2	2417	2407–2427	20
3	2422	2412–2432	20
4	2427	2417–2437	20
5	2432	2422–2442	20
6	2437	2427–2447	20
7	2442	2432–2452	20
8	2447	2437–2457	20
9	2452	2442–2462	20
10	2457	2447–2467	20
11	2462	2452–2472	20

IEEE 802.11n and 802.11ac devices are also capable of transmitting in the 5 GHz band. The available channels for New Zealand devices in this range are shown in Table 7.2 (IEEE, 2016; Radio Spectrum Management NZ, 2016). These channels are not uniformly spaced, nor have uniform bandwidths. However, the range of broadcastable frequencies is significantly larger than in the 2.4 GHz band. This increase is a potentially useful property when using these devices in a radar-based SHM context, due to the inverse relationship between sweep bandwidth and displacement resolution outlined in Chapters 2 and 3.

Previous research into the use of WiFi devices for radar applications has focused on the measurement of the velocity of targets using Doppler radar. These methods have investigated methods of analysis of radar spectra to identify people moving within a monitored space (Chetty, Smith, & Woodbridge, 2012; Colone, Falcone, Bongioanni, & Lombardo, 2012; Falcone, Colone, Bongioanni, & Lombardo, 2010). The implementations used in this research are unsuitable for SHM because they attempt to identify targets based on their velocity rather than displacement. Because parametric SHM methods require displacement inputs for damage identification and localisation, data obtained in this manner would face similar limitations as measurements obtained from accelerometers due to integral drift.

Table 7.2: IEEE 802.11 WLAN channels in the 5 GHz band

Channel	Centre Frequency (MHz)	Frequency Range (MHz)	Bandwidth (MHz)	Channel	Centre Frequency (MHz)	Frequency Range (MHz)	Bandwidth (MHz)
34	5170	5150–5190	40	114	5570	5490–5650	160
36	5180	5170–5190	20	116	5580	5570–5590	20
38	5190	5170–5210	40	118	5590	5570–5610	40
40	5200	5190–5210	20	120	5600	5590–5610	20
42	5210	5170–5250	80	122	5610	5570–5650	80
44	5220	5210–5230	20	124	5620	5610–5630	20
46	5230	5210–5250	40	126	5630	5610–5650	40
48	5240	5230–5250	20	128	5640	5630–5650	20
50	5250	5170–5330	160	132	5660	5650–5670	20
52	5260	5250–5270	20	134	5670	5650–5690	40
54	5270	5250–5290	40	136	5680	5670–5690	20
56	5280	5270–5290	20	138	5690	5650–5730	80
58	5290	5250–5330	80	140	5700	5690–5710	20
60	5300	5290–5310	20	142	5710	5690–5730	40
62	5310	5290–5330	40	144	5720	5710–5730	20
64	5320	5310–5330	20	149	5745	5735–5755	20
100	5500	5490–5510	20	151	5755	5735–5775	40
102	5510	5490–5530	40	153	5765	5755–5775	20
104	5520	5510–5530	20	155	5775	5735–5815	80
106	5530	5490–5570	80	157	5785	5775–5795	20
108	5540	5530–5550	20	159	5795	5775–5815	40
110	5550	5530–5570	40	161	5805	5795–5815	20
112	5560	5550–5570	20	165	5825	5815–5835	20

7.3 Simulation

Previously, simlation of an FMCW radar system was shown to be sufficiently accurate for SHM. This chapter uses simulation of a WLAN and FMCW radar-based implementation to test its feasibility. Because the aim of such a method is to reduce the cost of implementation of SHM by using existing hardware, the simulated radar parameters were restricted to values supported by IEEE 802.11-compliant hardware. It was assumed this hardware would be able to have its firmware altered to support the transmission of arbitrary signals with centre frequencies equal to those of canonical WLAN channels. Such a software change would impose negligible cost overall and could be readily added to existing standards.

The 5 GHz band was identified to be the most suitable band to simulate. Simulation results in Chapter 3 showed narrow bandwidth FMCW radar systems are unable to offer the distance and interstorey drift ratio (IDR) resolution required for use in parametric SHM methods. The range of centre frequencies of channels in the 2.4 GHz band is 50 MHz, which corresponds to a mean IDR error of 0.3 %. The 5 GHz band's range of channel centre frequencies is 655 MHz, which is a comparable bandwidth to the hardware prototype tested in Chapter 5. Equally, 5 GHz WLAN is increasingly ubiquitous due to its higher data rates in support of modern devices and apps.

7.3.1 Method

The simulation of the static target was carried out in much the same manner the dedicated FMCW radar system was modelled in Chapter 3. A chirp signal was generated to model the transmitted, frequency-modulated signal, and a delay based on target motion

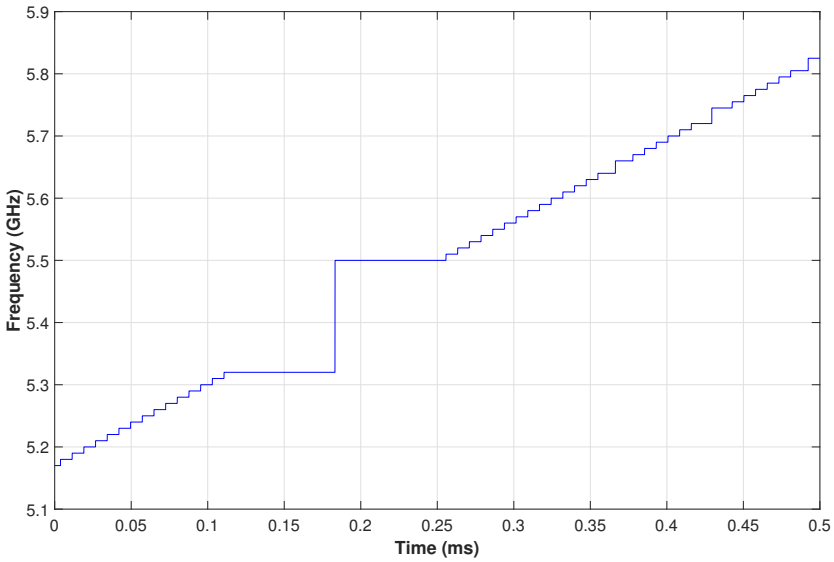

Figure 7.1: A frequency upsweep when the frequencies are limited to the centre frequencies of the channels available to IEEE 802.11-compliant hardware in the 5 GHz band.

was added to the signal. The chirp generation was modified to ensure the only frequencies broadcast were centre frequencies of the standard WLAN channels by performing a nearest-neighbour interpolation on a linearly-increasing frequency sweep over the set of allowable frequencies.

A plot of the time-varying frequency of a chirp is shown in Figure 7.1. The large jump in available channel centre frequency between channels 64 and 100 is visible at 5.48 GHz. The inconsistent spacing between particular pairs of channels is also shown. The larger the difference in frequency between two consecutive channels, the longer the system transmits using those channels to maintain linearity in the output.

This method made an assumption about the modelled hardware, which may not hold for all devices. The simulation models a device with the capability of transmitting at precise frequencies, specifically the channel center frequencies. However, this level of precision is not specified by the IEEE 802.11 standard, and thus cannot be assumed. In reality, devices transmit signals with a spread of spectral energy in the band specified

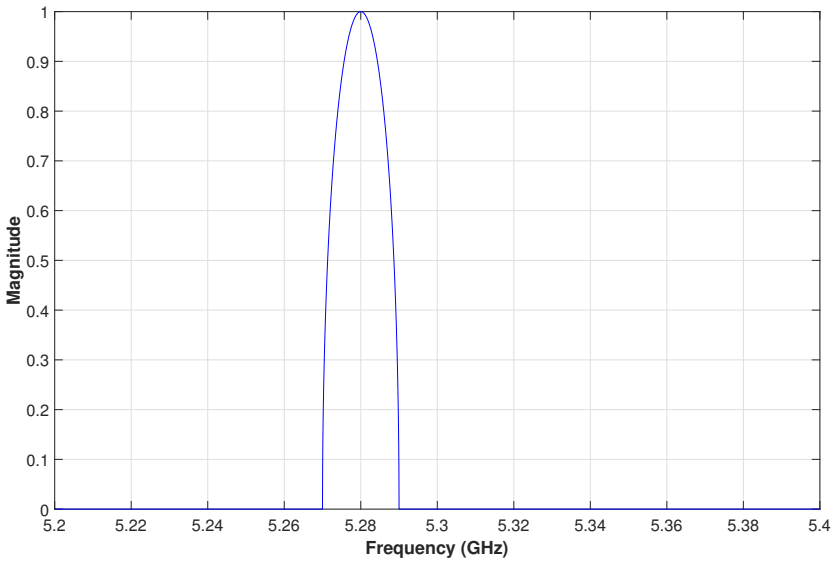

Figure 7.2: The created spectrum for 5.0 GHz channel 56, which was run through an inverse FFT for chirp generation.

for each channel in Table 7.2. This range is the spectral mask of each channel, which defines the spectral domain outside which frequencies are attenuated by at least 50 dB.

To simulate of this property, an approximation of each channel was generated. One such channel, channel 56, centred on 5.28 GHz, is represented in Figure 7.2. The channel was generated by creating an ellipse with a major axis radius of half the channel bandwidth, and a minor axis radius of 1. These spectra were then run through an inverse Fast Fourier Transform (FFT), and concatenated together to create a chirp signal with length T_{mod}.

To obtain distance measurements from the mixed signal, the 'CorrMT' method of signal analysis, as described in Section 5.4.4, was used. This method was demonstrated to have the smallest mean and peak IDR error in the experiments in Chapter 5. The mixed signals were transformed using the Thomson multitaper method (Thomson, 1982), and then cross-correlated with the multitaper transform of the initial sweep. The offset of the cross-correlation corresponded to the distance of the target from the simulated

transceiver.

7.3.2 Results

The simulation of a single DOF target with motion taken from a structure with response period 1.0 s in the Christchurch Botanic Gardens during the 4$^{\text{th}}$ of September, 2010 Canterbury, New Zealand earthquake was carried out. This motion is the same as those used in Chapter 3. The radar simulation parameters were $f_0 = 5.17$ GHz, $f_1 = 5.825$ GHz, $T_{\text{mod}} = 0.5$ ms, and T_pad = 49.5 ms. The structural motion was mean-adjusted to 20 m, while leaving the amplitude of motion unchanged from source.

Assuming the transmitter could broadcast signals at precisely the centre frequency of each IEEE 802.11n 5 GHz channel listed in Table 7.2, the target was able to be tracked with a mean absolute error of **3.23 mm**, corresponding to a relative error of **0.0161 %**. The error in peak displacement of the simulated target was **2.10 mm**. The tracking of this target is shown in Figure 7.3.

Simulation of the target was then performed with a non-ideal transmitter, using the same radar parameters as in the ideal case. The transmitter sweep function was derived from spectra with non-distinct channel frequencies, as described in Section 7.3.1. The target was tracked with a mean absolute error of **5.05 mm**, corresponding to a relative error of **0.0253 %**. The error in peak displacement of the simulated target with non-ideal radar transmission was **9.59 mm**. The tracking of this target is shown in Figure 7.4.

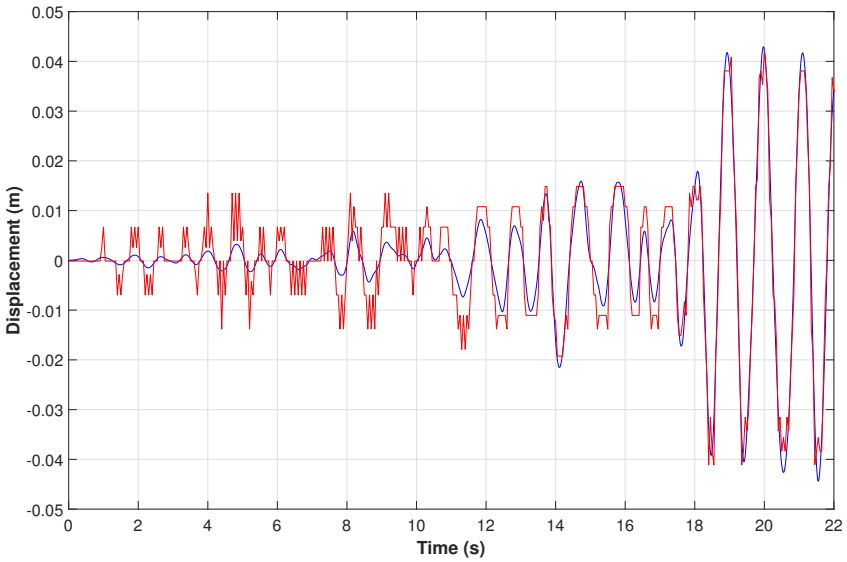

Figure 7.3: The simulated tracking (red) using 'CorrMT' of a single DOF target driven with structural response data (blue). The target is tracked using a WiFi-based FMCW radar system.

7.3.3 Discussion

When simulated with ideal broadcast frequencies, the system achieved a mean absolute displacement error of 3.23 mm. Detection of motion to this precision would be sufficient for use as inputs to parametric SHM methods. The minimum displacement required to be detected is 5 mm, per the requirements specified in Chapter 2.

Simulation of non-ideal broadcast channels, as is typical of IEEE 802.11-compliant hardware showed a modest increase in the mean absolute error of the system. This error was almost equal to the minimum displacement detection required for SHM. Because changes in structural parameters are related to IDR, rather than absolute displacement, the minimum detection magnitude and thus allowable error increases with structure size, so this method is sufficiently accurate for all but the smallest structures.

Exploratory simulation of static targets showed the displacement error can be signifi-

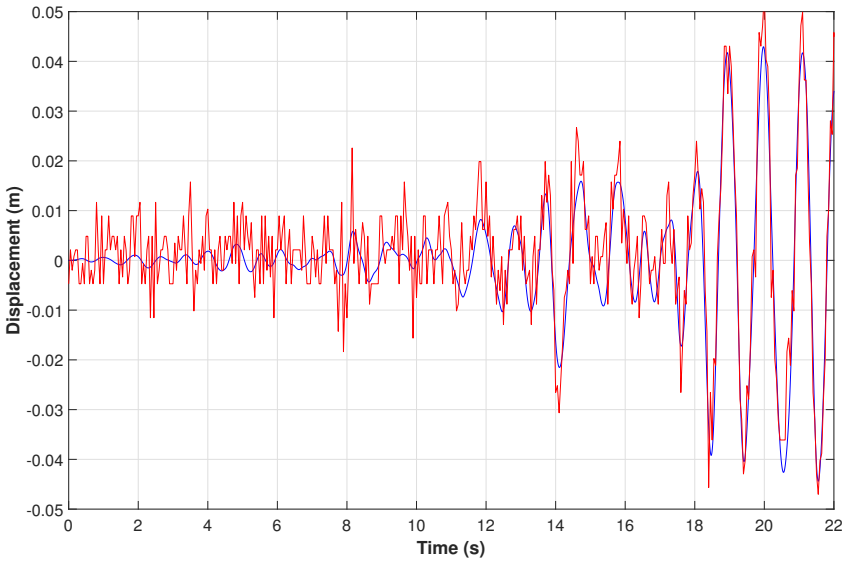

Figure 7.4: Another example of simulated tracking (red) using 'CorrMT' of a single DOF target driven with structural response data (blue). The target is tracked using a Wi-Fi-based FMCW radar system with non-ideal broadcast channels.

cantly increased if the beat frequency corresponding to the target coincides with a large gap in the 5 GHz band. Taking channel 100 as an example: if the beat frequency, f_r, is equal to 5.40 GHz − 5.17 GHz = 230 MHz, then any perturbation of the target will result in the same beat frequency. There is thus a detection deadzone at this range. If such a scheme is to be implemented, it is important to ensure there is no chance the target falls into this range during a damaging seismic event. The large deadzone in the 5 GHz band effectively limits the maximum possible bandwidth of the system. The largest continuous grouping of broadcasts is the group of channels listed in Table 7.2 from 102 to 165. These channels have a cumulative bandwidth of 315 MHz.

An assumption in this simulation is that WiFi hardware would be able to switch broadcast channels instantaneously and seamlessly. In reality, some wireless transmitter chips may have a delay between receiving and actioning requested channel changes. In a wireless router's typical application as a wireless connection handler, the ability to change channels instantaneously is not required. An inability to change channels in this manner reduces the device's output linearity, increasing the error in displacement

measurement (Brooker, 2005). However even if dedicated and specialised routers were used, their relatively low cost still offers significant possible cost savings.

Another assumption made is the WiFi-based FMCW radar SHM hardware only having the minimum channel spectrum broadcasting ability stipulated by the IEEE 802.11 standard. In reality, the attenuation of frequencies away from a channel's centre frequency might be significantly greater than the standard requires, particularly in more expensive hardware. The error of such a system would be closer to that found in the simulation of ideal channel broadcasting.

WiFi routers have different design aims to purpose-built FMCW radar sensors. WiFi devices aim to broadcast to a large number of devices located at in a hemispherical space, so they are equipped with antennas with omnidirectional radiation patterns. Radar devices for SHM require directionality in their antennas so target reflectors can be identified and multipath reflections can be minimised. WiFi routers also lack the required hardware to perform mixing in an analog manner. Instead, the device's microcontroller would be required to perform a digital Hadamard product on two vectors. The task of identifying a radar signature corresponding to a particular target with increased multipath reflections is a more challenging task that may require further advanced signal processing techniques, including machine learning applications.

WiFi routers and access points are also typically located centrally on floors to maximise their broadcast range for particular signal amplification. Continued use of these placements would require the use of the interstorey centre-to-corner displacement (ICCD) method of installation established in Section 6.3.2. Care would also need to be taken to ensure the signal strength is sufficient of the device's use in SHM. WiFi signals are transmitted by client devices for the return hop to the router, whereas in an SHM application, the signal would need enough amplification to be returned to the device through

passive reflection alone. Hardware built for the dual purpose of IEEE 802.11-adherent data transmission and SHM would be suitable to circumvent many of the problems that simple firmware changes would encounter.

7.4 Summary

Most modern structures that would be candidates for SHM instrumentation already have RF-transmitting devices installed for internet connectivity. This chapter investigated the possibility of using this hardware for the dual purpose of transmitting WiFi signals and the measurement of structural displacement during seismic events. It was identified that using the 5 GHz channels specified by IEEE 802.11 would allow for a system with sufficient bandwidth for the measurement of displacement to the necessary precision for use in SHM. Simulation of a single-DOF target indicated that such a device has the ability to measure damaging structural motion. This result prompts the development of firmware for a WiFi router to test the hypothesis in a real-world application.

CHAPTER 8

Conclusions

This thesis explored the suitability of a frequency-modulated continuous wave (FMCW) radar-based structural health monitoring (SHM) method. This method was seen to fill a need in contemporary SHM methods, because parametric SHM methods require displacement inputs. Currently, these inputs are obtained by doubly-integrating structural acceleration records obtained from accelerometers, and baseline correcting the result. This process filters out important displacement information, allowing damaging motion to remain undetected. The use of FMCW radar allows displacement to be measured directly, and in a robust manner, without any structural modification requirements for installation.

The interstorey drift ratio (IDR) metric was found to be the required data input for model-based SHM methods. This metric is a height-normalised measure of the relative displacement between adjacent floors of a structure. A range of requirements in terms of displacement and IDR for an FMCW radar system were determined. These requirements included a minimum detectable IDR and minimum IDR resolution of 0.2 %, and

a minimum sample rate of 50 Hz. This minimum sample rate allows for modal identification of structural response. Sample rates exceeding 200 Hz are required for proper time series reconstruction of structural motion, allowing data to be used with parametric approaches.

To verify the method was suitable for tracking structural displacement, a single target in a 1D channel was simulated, driven with motion taken from historical structural records. This simulation was performed using MATLAB. The simulation confirmed increasing sweep bandwidth of an FMCW system improves the system's distance resolution, and thus its precision in tracking small motion typical of structural behaviour. In addition, it was found that the system's resolution could be improved with the application of signal processing methods, such as quadratic interpolation and multitaper transforms. The displacement error of 0.201 mm found using the quadratic interpolation method significantly bettered the requirements of an input to parametric SHM methods.

A hardware prototype was constructed to test the FMCW radar SHM system on a shake table. The prototype used components that were suitable for the transmission of a range of sweep bandwidths towards a target up to 5 m away from the transceiver. Components were selected with the ability to perform this task in a configurable manner. A corner reflector was chosen due to its properties of parallel entry and exit signal paths, and uniform reflection distance. The reflector was fixed to a shake table and the hardware prototype antennas were aimed at it. The table was driven with historical earthquake ground motion data. The displacement of the target was obtained using a variety of signal processing techniques to improve precision to the levels necessary for SHM. The system was found to be able to measure structural IDR equivalents to a mean error of 0.0528 %. This result compared favourably to measurements obtained from an accelerometer and was within the required precision limits for SHM.

The arrangement of FMCW radar SHM sensors for full instrumentation of a structure was examined. Two schemes were devised with different strengths. The first method utilises two radar transceiver units placed in adjacent corners of a floor, with target reflectors placed in opposing corners. Highly directional antennas allow the corresponding reflectors' radar signatures to be easily identified. This method was considered to be the more precise approach due to its ability to utilise superior correlation-based signal processing methods on its sweep spectra, but more expensive to implement due to its requirement of $2n$ transceiver units for an n-storey structure. The second method uses a single, centrally-located transceiver unit to instrument each storey. This method is unable to take advantage of correlation-based signal processing methods, but is cheaper to implement due to requiring only a single transceiver unit per storey, and is suitable for use in structures with significant structural columns located in the centre of the building.

Most modern structures that would be candidates for SHM instrumentation already have radio frequency (RF)-transmitting devices installed for internet connectivity. Simulation of an FMCW radar system that adhered to Institute of Electrical and Electronics Engineers (IEEE) 802.11 standards in the 5 GHz range was carried out. The results of this simulation showed WiFi in this band has sufficient bandwidth for the precise measurement of displacement, despite its non-continuous broadcast channels. This result prompts the development of firmware for a WiFi router to test the hypothesis in a real-world application.

CHAPTER 9

Future Work

Completion of the work presented in this thesis prompted further questions about the the implementation of a non-contact displacement-measuring structural health monitoring (SHM) method. While the work in this thesis confirms such a method is feasible to implement using frequency-modulated continuous wave (FMCW) radar devices, and would provide suitable precision for inputs to parametric SHM models, improvements can be made to the system to ensure it becomes a viable product for the verification of the security of structures to save lives.

First, testing the prototype on a multiple-degree of freedom (DOF) structure would be a suitable next step in confirming the efficacy of the FMCW radar system. In particular, the implementation of two sensor units on a shake table-mounted structure in the interstorey diagonal displacement (IDD) arrangement detailed in Chapter 6 would verify the ability of the sensor unit to detect both north-south (N-S) and west-east (W-E) components of interstorey drift on an unconstrained structure.

The implementation of two or more sensor units in a shake table test would also allow for the effects of radio frequency (RF) interference to be investigated. In particular, the requirements of per-device chirp sequences could be determined with respect to the necessary bandwidths and centre frequencies for the expected distance measurement precision to be preserved. This testing is particularly relevant for testing of the inter-storey centre-to-corner displacement (ICCD) approach, because this method cannot be instantiated with narrow beamwidth antennas.

Further, the implementation of these sensors on a structure designed to undergo plastic deformation would allow the particular strength of displacement-based measurement to be demonstrated. Displacements obtained from the double integration of acceleration measurements must be high-pass filtered to remove integral drift. This process inevitably removes low-frequency components of structural response. A comparison of measurements taken with both FMCW radar and accelerometers on a structure which recentres after a seismic event should show the former method's ability to detect motion the components of motion most likely to be damaging.

Obtaining the heterodyned response from the mounting of FMCW radar SHM sensors on a multiple-DOF structure would also allow for better simulation of this method in the future. One of the significant assumptions made in the simulation of a single-DOF target in Chapter 3 was that noise was purely Gaussian. This assumption allowed a 1D channel to be used. In reality, multipath propagation effects were found to be the dominant source of noise and interference in sweep spectra. Collection of this data would allow for better modelling of an FMCW radar system in a busy environment.

It would be interesting to use the data obtained from a real-world test of the FMCW radar SHM to develop a model of the reflection and interference patterns resulting from various objects in an SHM environment. Modelling of such complex environments, par-

ticularly in a structure in motion, would be invaluable for the future simulation of target detection algorithms. It would also be useful to understand how much particular obstacles restrict SHM precision, and whether there is any predictability in this restriction depending on clutter density.

The installation of an FMCW radar-based SHM system on a real structure would allow for testing of the effects of multipath signal propagation on system performance. One of the limitations of the shake table test documented in Chapter 5 was that the table itself may have helped the detection of the target due to its radar signal reflectivity. It is proposed that reflective structural components such as beams, columns, and floor decks also move in a correlated manner during seismic motion. Installation in a structure would allow this theory to be tested.

Currently, beat frequencies are obtained by spectral analysis of sweeps. These Fourier and Thomson Multitaper transform-derived spectra are processed using a variety of techniques to more precisely identify the peak within a given range. Solutions to this problem could be further improved with the implementation of machine learning. Supervised learning could be used to create a regression model for displacement based on a dataset containing many spectral inputs and outputs taken from linear variable differential transformer (LVDT) sensors. Unsupervised techniques may also be suitable for the classification of types of motion based on sweep spectra inputs.

The tested prototype offered a proof-of-concept for the use of FMCW radar in SHM. Due to the exploratory nature of the research presented in this thesis, the components selected for the prototype needed to be as configurable as possible. The overall cost of a single sensor unit is thus quite high. It would be interesting to find out how cheaply a sensor could be constructed on a single printed circuit board (PCB), and how closely the cost of a sensor can be reduced to that of a wireless local area network (WLAN) router.

Chapter 7 explored the possibility of using wireless routers as radar transceiver units. The development of firmware for a wireless router to verify the simulation would be interesting. It would also be valuable to determine what component modifications could be made to improve the system. In particular, the antennas of the WLAN device could be replaced with, or used in conjunction with a more strongly-directive one, such as a log-periodic antenna as was used in the FMCW radar hardware prototype.

References

Aaronia. (2014). *Precompliance test antenna series HyperLOG 60xxx [Datasheet].*

Abe, M., & Smith III, J. O. (2004). Design criteria for the quadratically interpolated FFT method (i): Bias due to interpolation. *no. STAN-M-114*.

Abhayawardhana, V. S., Wassell, I. J., Crosby, D., Sellars, M. P., & Brown, M. G. (2005). Comparison of empirical propagation path loss models for fixed wireless access systems. In *2005 ieee 61st vehicular technology conference* (Vol. 1, p. 73-77 Vol. 1).

Al-Khalidy, A., Noori, M., Hou, Z., Carmona, R., Yamamoto, S., Masuda, A., & Sone, A. (1997). Health monitoring systems of linear structures using wavelet analysis. In F.-K. Chang (Ed.), *International workshop on structural health monitoring* (p. 164-178). Stanford, CA: Technomic.

Antonik, P. A., Griffiths, H., Weiner, D. D., & Wicks, M. C. (2001). *Novel diverse waveforms* (In-House Report). Air Force Research Laboratory.

Ardo, H., Astrom, K., & Berthilsson, R. (2007). Real time Viterbi optimization of Hidden Markov Models for multi target tracking. In *Ieee workshop on motion and video computing* (p. 2). Austin, TX: IEEE.

Arulampalam, M. S., Maskell, S., Gordon, N., & Clapp, T. (2002). A tutorial on particle filters for online nonlinear/non-Gaussian Bayesian tracking. *IEEE Transactions on Signal Processing*, *50*(2), 174-188.

Bernal, D., & Gunes, B. (2000). Observer/Kalman and subspace identification of the UBC

benchmark structural model. In *Proceedings of the 14th asce engineering mechanics conference* (p. 21-24). Austin, Texas.

Boore, D. M., Stephens, C. D., & Joyner, W. B. (2002). Comments on baseline correction of digital strong-motion data: Examples from the 1999 Hector Mine, California, earthquake. *Bulletin of the Seismological Society of America*, *92*(4), 1543-1560.

Bouc, R. (1967). *Forced vibration of mechanical systems with hysteresis*.

Bradley, B. A., & Baker, J. W. (2014). Ground motion directionality in the 2010–2011 Canterbury earthquakes. *Earthquake Engineering & Structural Dynamics*, *44*(3), 371-384.

Brincker, R., Zhang, L., & Andersen, P. (2000). Modal identification from ambient responses using frequency domain decomposition. In *Proc. of the 18th international modal analysis conference (IMAC)*. San Antonio, Texas.

Brooker, G. M. (2005). Understanding millimetre wave FMCW radars. In *1st international conference on sensing technology* (p. 152-157). Palmerston North, New Zealand: IEEE.

Brownjohn, J. M. W. (2007). Structural health monitoring of civil infrastructure. *Philosophical Transactions of the Royal Society A: Mathematical, Physical and Engineering Sciences*, *365*(1851), 589.

Brownjohn, J. M. W., Xia, P.-Q., Hao, H., & Xia, Y. (2001). Civil structure condition assessment by FE model updating:: methodology and case studies. *Finite Elements in Analysis and Design*, *37*(10), 761-775.

Caicedo, J. M., Dyke, S. J., & Johnson, E. A. (2004). Natural excitation technique and eigensystem realization algorithm for phase i of the IASC-ASCE benchmark problem: Simulated data. *Journal of Engineering Mechanics*, *130*(1), 49-60.

Chan, T. H. T., Yu, L., Tam, H. Y., Ni, Y. Q., Liu, S. Y., Chung, W. H., & Cheng, L. K. (2006). Fiber Bragg grating sensors for structural health monitoring of Tsing Ma bridge: Background and experimental observation. *Engineering Structures*, *28*(5), 648-659.

Chang, P. C., & Liu, S. C. (2003). Recent research in nondestructive evaluation of civil infrastructures. *Journal of Materials in Civil Engineering*, *15*(3), 298-304.

Chase, J. G., Hudson, N. H., Lin, J., Elliot, R., & Sim, A. (2005). Nonlinear shake table identification and control for near-field earthquake testing. *Journal of Earthquake Engineering*, *9*(04), 461-482.

Chase, J. G., Hwang, K. L., Barroso, L. R., & Mander, J. B. (2004). A simple LMS-based approach to the structural health monitoring benchmark problem. *Earthquake Engineering & Structural Dynamics*, *34*(6), 575-594.

Chetty, K., Smith, G. E., & Woodbridge, K. (2012). Through-the-wall sensing of personnel using passive bistatic wifi radar at standoff distances. *IEEE Transactions on Geoscience and Remote Sensing*, *50*(4), 1218-1226.

Chiu, H.-C. (1997). Stable baseline correction of digital strong-motion data. *Bulletin of the Seismological Society of America*, *87*(4), 932-944.

Colone, F., Falcone, P., Bongioanni, C., & Lombardo, P. (2012). WiFi-based passive bistatic radar: Data processing schemes and experimental results. *IEEE Transactions on Aerospace and Electronic Systems*, *48*(2), 1061-1079.

Cunha, A., & Caetano, E. (2006). Experimental modal analysis of civil engineering structures. *Journal of Sound and Vibration*, *40*(6), 12-20.

Curadelli, R. O., Riera, J. D., Ambrosini, D., & Amani, M. G. (2008). Damage detection by means of structural damping identification. *Engineering Structures*, *30*(12), 3497-3504.

Dana, P. H. (2000). *The Global Positioning System.* `http://www.colorado.edu/geography/gcraft/notes/gps/gps_f.html`.

Deacon, P., Hunt, R., Koenigsknecht, D., Leonard, C., & Oakley, C. (2011). *Frequency modulated continuous wave (FMCW) radar.* `http://www.egr.msu.edu/classes/ece480/capstone/fall11/group06/style/Technical%20Presentation.pdf`.

Doebling, S. W., Farrar, C. R., Prime, M. B., & Shevitz, D. W. (1996). *Damage identification*

and health monitoring of structural and mechanical systems from changes in their vibration characteristics: a literature review (Tech. Rep.). Los Alamos National Lab., NM (United States).

Çelebi, M., & Sanli, A. (2002). GPS in pioneering dynamic monitoring of long-period structures [Journal Article]. *Earthquake Spectra, 18*(1), 47-61. Retrieved from https://doi.org/10.1193/1.1461375 doi: 10.1193/1.1461375

Falcone, P., Colone, F., Bongioanni, C., & Lombardo, P. (2010). Experimental results for OFDM WiFi-based passive bistatic radar. In *2010 ieee radar conference* (p. 516-521).

Fritzen, C.-P. (2014). *Vibration-based methods for SHM* (Tech. Rep. No. STO-EN-AVT-220-05). North Atlantic Treaty Organization Science and Technology Organization.

Fritzen, C. P., Jennewein, D., & Kiefer, T. (1998). Damage detection based on model updating methods. *Mechanical Systems and Signal Processing*, *12*(1), 163-186.

Garmatyuk, D., & Kauffman, K. (2009, Sept). *Radar and data communication fusion with UWB-OFDM software-defined system.*

Garmatyuk, D., Schuerger, J., & Kauffman, K. (2011). Multifunctional software-defined radar sensor and data communication system. *Sensors Journal, IEEE, 11*(1), 99-106.

Garmatyuk, D., Schuerger, J., Kauffman, K., & Spalding, S. (2009, May). *Wideband OFDM system for radar and communications.*

Gentile, C. (2009). Radar-based measurement of deflections on bridges and large structures: advantages, limitations and possible applications. In *Iv eccomas thematic conference on smart structures and materials.* Porto, Portugal.

Geok, T. K., Choy, L. S., & Peng, T. C. (2009). Investigation of non-Taylor-series based positioning method for hybrid GPS. *International Journal of Electronics*, *96*(8), 877-885.

Gierlich, R., Huttner, J., Dabek, A., & Huemer, M. (2007). Performance analysis of FMCW synchronization techniques for indoor radiolocation. In *2007 european conference*

on wireless technologies (p. 24-27). Munich, Germany: IEEE.

Heath, T. L. (1956). *The thirteen books of Euclid's Elements*. Mineola, N.Y., U.S.A.: Dover Publications.

Hoshyarmanesh, H., Abbasi, A., Moein, P., Ghodsi, M., & Zareinia, K. (2017). Design and implementation of an accurate, portable, and time-efficient impedance-based transceiver for structural health monitoring. *IEEE/ASME Transactions on Mechatronics*, *22*(6), 2809-2814.

Hou, Z., Noori, M., & Amand, R. S. (2000). Wavelet-based approach for structural damage detection. *Journal of Engineering Mechanics*, *126*(7), 677-683.

Huang, N. E., Shen, Z., Long, S. R., Wu, M. C., Shih, H. H., Zheng, Q., ... Liu, H. H. (1998). The empirical mode decomposition and the hilbert spectrum for nonlinear and non-stationary time series analysis. *Proceedings of the Royal Society of London. Series A: Mathematical, Physical and Engineering Sciences*, *454*(1971), 903-995.

IEEE. (2016). IEEE standard for information technology–telecommunications and information exchange between systems local and metropolitan area networks–specific requirements - part 11: Wireless LAN medium access control (MAC) and physical layer (PHY) specifications. *IEEE Std 802.11-2016 (Revision of IEEE Std 802.11-2012)*, 1-3534.

Jackson, M. C. (1986). The geometry of bistatic radar systems. *Communications, Radar and Signal Processing, IEE Proceedings F*, *133*(7), 604-612.

Jaishi, B., & Ren, W.-X. (2005). Structural finite element model updating using ambient vibration test results. *Journal of Structural Engineering*, *131*(4), 617-628.

Jardak, N., & Samama, N. (2009). Indoor positioning based on GPS-repeaters: Performance enhancement using an open code loop architecture. *IEEE Transactions on Aerospace and Electronic Systems*, *45*(1), 347-359.

Jenn, D. (2007). *Radar fundamentals.* Naval Postgraduate School.

Jeon, H., Myeong, W., Shin, J. U., Park, J. W., Jung, H. J., & Myung, H. (2014). Experimental validation of visually servoed paired structured light system (ViSP) for structural

displacement monitoring. *IEEE/ASME Transactions on Mechatronics*, *19*(5), 1603-1611.

Jiang, H. J., & Kubo, T. (2008). Maximum floor displacement profiles for the displacement-based seismic design of reinforced concrete frames. In *14th world conference on earthquake engineering*.

Jo, H., Sim, S.-H., Mechitov, K. A., Kim, R., Li, J., Moinzadeh, P., ... Nagayama, T. (2011). Hybrid wireless smart sensor network for full-scale structural health monitoring of a cable-stayed bridge. In *Sensors and smart structures technologies for civil, mechanical, and aerospace systems* (Vol. 7981). San Diego, CA: SPIE.

Jo, H., Sim, S.-H., Tatkowski, A., Spencer, B. F., & Nelson, M. E. (2012). Feasibility of displacement monitoring using low-cost GPS receivers. *Structural Control and Health Monitoring*, *20*(9), 1240-1254.

Juang, J. N., & Pappa, R. S. (1985). An eigensystem realization algorithm for modal parameter identification and model reduction. *Journal of Guidance, Control, and Dynamics*, *8*(5), 620-627.

Kaloop, R. M., Elbeltagi, E., Hu, W. J., & Elrefai, A. (2017). Recent advances of structures monitoring and evaluation using GPS-time series monitoring systems: A review. *ISPRS International Journal of Geo-Information*, *6*(12).

Khoo, L. M., Mantena, P. R., & Jadhav, P. (2004). Structural damage assessment using vibration modal analysis. *Structural Health Monitoring*, *3*(2), 177-194.

Kim, H., & Adeli, H. (2004). Hybrid control of smart structures using a novel wavelet-based algorithm. *Computer-Aided Civil and Infrastructure Engineering*, *20*(1), 7-22.

Kim, J.-T., Ryu, Y.-S., Cho, H.-M., & Stubbs, N. (2003). Damage identification in beam-type structures: frequency-based method vs mode-shape-based method. *Engineering Structures*, *25*(1), 57-67.

Kinemetrics. (2013). *OASIS (On-line Alerting of Structural Integrity and Safety System).* `http://www.kinemetrics.com/wp-content/uploads/2017/04/oasis-system-overview.pdf`.

Ko, H.-H., Cheng, K.-W., & Su, H.-J. (2008, Oct). *Range resolution improvement for FMCW radars.*

Kuang, A., Sridhar, A., Garven, J., Gutschmidt, S., Rodgers Geoffrey, W., Chase, J. G., ... MacRae Gregory, A. (2016). Christchurch Women's Hospital: Performance analysis of the base-isolation system during the series of Canterbury earthquakes 2011–2012. *Journal of Performance of Constructed Facilities*, *30*(4), 04015096.

Küpper, A. (2005). *Location-based services: Fundamentals and operation*. John Wiley.

Kushki, A., Plataniotis, K. N., & Venetsanopoulos, A. N. (2012). *WLAN positioning systems*. Cambridge University Press.

Lanzisera, S., Lin, D., & Pister, K. (2006). RF time of flight ranging for wireless sensor network localization. In *2006 international workshop on intelligent solutions in embedded systems* (p. 1-12). IEEE.

Lee, J. J., & Shinozuka, M. (2006). A vision-based system for remote sensing of bridge displacement. *NDT & E International*, *39*(5), 425-431.

Li, H.-N., Li, D.-S., & Song, G.-B. (2004). Recent applications of fiber optic sensors to health monitoring in civil engineering. *Engineering Structures*, *26*(11), 1647-1657.

Luş, H., Betti, R., Yu, J., & De Angelis, M. (2004). Investigation of a system identification methodology in the context of the ASCE benchmark problem. *Journal of Engineering Mechanics*, *130*(1), 71-84.

Lynch, J. P., & Loh, K. J. (2006). A summary review of wireless sensors and sensor networks for structural health monitoring. *Shock and Vibration Digest*, *38*(2), 91-130.

Maia, N. M. M., Silva, J. M. M., Almas, E. A. M., & Sampaio, R. P. C. (2003). Damage detection in structures: From mode shape to frequency response function methods. *Mechanical Systems and Signal Processing*, *17*(3), 489-498.

Majumder, M., Gangopadhyay, T. K., Chakraborty, A. K., Dasgupta, K., & Bhattacharya, D. K. (2008). Fibre Bragg gratings in structural health monitoring – present status and applications. *Sensors and Actuators A: Physical*, *147*(1), 150-164.

Mangal, L., Idichandy, V. G., & Ganapathy, C. (1996). ART-based multiple neural networks for monitoring offshore platforms. *Applied Ocean Research*, *18*(2), 137-143.

Masri, S. F., Smyth, A. W., Chassiakos, A. G., Caughey, T. K., & Hunter, N. F. (2000). Application of neural networks for detection of changes in nonlinear systems. *Journal of Engineering Mechanics*, *126*(7), 666-676.

Mayer, L., Yanev, B. S., Olson, L. D., & Smyth, A. W. (2010). Monitoring of the Manhattan Bridge for vertical and torsional performance with GPS and interferometric radar systems. In *Transportation research board 89th annual meeting*. Washington, DC, USA: Transport Research Board.

McNeff, J. (2002). The Global Positioning System. *IEEE Transactions on Microwave Theory and Techniques*, *50*(3), 645-652.

Mini-Circuits. (2015). Super ultra wideband amplifier ZVA-183+ [Datasheet].

Miranda, E. (1999). Approximate seismic lateral deformation demands in multistory buildings. *Journal of Structural Engineering*, *125*(4), 417-425.

Miranda, E., & Akkar, S. (2006). Generalized interstory drift spectrum. *Journal of Structural Engineering*, *132*(6), 840-852.

Moschas, F., Avallone, A., Saltogianni, V., & Stiros, S. C. (2014). Strong motion displacement waveforms using 10-Hz precise point positioning GPS: an assessment based on free oscillation experiments. *Earthquake Engineering & Structural Dynamics*, *43*(12), 1853-1866.

Mottershead, J. E., & Friswell, M. I. (1993). Model updating in structural dynamics: A survey. *Journal of Sound and Vibration*, *167*(2), 347-375.

Mottershead, J. E., Link, M., & Friswell, M. I. (2011). The sensitivity method in finite element model updating: A tutorial. *Mechanical Systems and Signal Processing*, *25*(7), 2275-2296.

Moyo, P., Brownjohn, J. M. W., Suresh, R., & Tjin, S. C. (2005). Development of fiber Bragg grating sensors for monitoring civil infrastructure. *Engineering Structures*, *27*(12), 1828-1834.

Naeim, F., Hagie, S., & Alimoradi, A. (2005). *Automated post-earthquake damage assessment and safety evaluation of instrumented buildings* (JAMA Report). John A. Martin & Associates, Inc. Research & Development Department.

Nayyerloo, M. (2011). *Real-time structural health monitoring of nonlinear hysteretic structures* (Ph.D. thesis). Univ. Canterbury.

Nayyerloo, M., Chase, J. G., Millane, A., Muller, C., Malherbe, A., Chen, X. Q., & MacRae, G. A. (2011). Seismic structural displacement measurement using a line-scan camera: camera-pattern calibration and experimental validation. *Journal of Civil Structural Health Monitoring*, *1*(3), 113-124.

Ozsoy, K., Bozkurt, A., & Tekin, I. (2013). Indoor positioning based on global positioning system signals. *Microwave and Optical Technology Letters*, *55*(5), 1091-1097.

Pagni, C. A., & Lowes, L. N. (2006). Fragility functions for older reinforced concrete beam-column joints. *Earthquake Spectra*, *22*(1), 215-238.

Park, J., Lindberg, C. R., & Vernon, F. L. (1987). Multitaper spectral analysis of high-frequency seismograms. *Journal of Geophysical Research: Solid Earth*, *92*(B12), 12675-12684.

Piras, M., & Cina, A. (2010). Indoor positioning using low cost GPS receivers: Tests and statistical analyses. In *1st international conference on indoor positioning and indoor navigation (ipin)* (p. 1-7). IEEE.

Priestley, M. J. N., & Kowalsky, M. J. (2000). Direct displacement-based seismic design of concrete buildings. *Bulletin of the New Zealand National Society of Earthquake Engineering*, *33*(4), 421-444.

Pu, Q., Gupta, S., Gollakota, S., & Patel, S. (2013). Whole-home gesture recognition using wireless signals. In *Proceedings of the 19th annual international conference on mobile computing & networking* (p. 27-38). Miami, Florida, USA: ACM.

Qiao, L., Esmaeily, A., & Melhem Hani, G. (2012). Signal pattern recognition for damage diagnosis in structures. *Computer-Aided Civil and Infrastructure Engineering*, *27*(9), 699-710.

Radio Spectrum Management NZ. (2016). *Important information for users of WiFi devices in the 5GHz band.* https://www.rsm.govt.nz/consumers/pdf-and-documents-library/Wi-Fi%20Devices%20using%20the%205%20GHz%20Band.pdf. Ministry of Business, Innovation & Employment,.

Ren, W.-X., & Chen, H.-B. (2010). Finite element model updating in structural dynamics by using the response surface method. *Engineering Structures*, *32*(8), 2455-2465.

RFMD. (2014). *RFVC1843 MMIC VCO [Datasheet].*

Rice, J. A., Li, C., Gu, C., & Hernandez, J. C. (2011). A wireless multifunctional radar-based displacement sensor for structural health monitoring. In *Sensors and smart structures technologies for civil, mechanical, and aerospace systems* (Vol. 7981). San Diego, CA: SPIE.

Roveri, N., & Carcaterra, A. (2012). Damage detection in structures under traveling loads by hilbert–huang transform. *Mechanical Systems and Signal Processing*, *28*, 128-144.

Saddik, G. N., Singh, R., & Brown, E. (2007). Ultra-wideband multifunctional communications/radar system. *Microwave Theory and Techniques, IEEE Transactions on*, *55*(7), 1431-1437.

Sayrafian-Pour, K., & Perez, J. (2007). Robust indoor positioning based on received signal strength. In *2nd international conference on pervasive computing and applications* (p. 693-698). IEEE.

Son, Y.-S., Sung, H.-K., & Heo, S. W. (2018). Automotive frequency modulated continuous wave radar interference reduction using per-vehicle chirp sequences. *Sensors*, *18*(9).

Song, M., Lee, S. B., Choi, S. S., & Lee, B. (1997). Simultaneous measurement of temperature and strain using two fiber Bragg gratings embedded in a glass tube. *Optical Fiber Technology*, *3*(2), 194-196.

Spangenberg, S. M., Scott, I., McLaughlin, S., Povey, G. J. R., Cruickshank, D. G. M., & Grant, P. M. (2000). An FFT-based approach for fast acquisition in spread spectrum

communication systems. *Wireless Personal Communications*, *13*(1), 27-55.

Sridhar, A., Kuang, A., Garven, J., Gutschmidt, S., Chase, J. G., Gavin, H. P., ... MacRae, G. A. (2013). Christchurch Women's Hospital: Analysis of measured earthquake data during the 2011–2012 Christchurch earthquakes. *Earthquake Spectra*, *30*(1), 383-400.

Sun, Z., & Chang, C. C. (2002). Structural damage assessment based on wavelet packet transform. *Journal of Structural Engineering*, *128*(10), 1354-1361.

Texas Instruments. (2014). *LMX2492/LMX2492-Q1 14 GHz low noise fractional N PLL with ramp/chirp generation [Datasheet].*

Thenozhi, S., Yu, W., & Garrido, R. (2012). A novel numerical integrator for structural health monitoring. In *5th international symposium on resilient control systems (isrcs)* (p. 92-97). Salt Lake City, UT: IEEE.

Thomson, D. J. (1982). Spectrum estimation and harmonic analysis. *Proceedings of the IEEE*, *70*(9), 1055-1096.

Thorbjornsen, B., White, N., Brown, A., & Reeve, J. (2010). Radio frequency (RF) time-of-flight ranging for wireless sensor networks. *Measurement Science and Technology*, *21*(3), 035202.

Torrence, C., & Compo, G. P. (1998). A practical guide to wavelet analysis. *Bulletin of the American Meteorological Society*, *79*(1), 61-78.

Wang, G., Gu, C., Inoue, T., & Li, C. (2013). Hybrid FMCW-interferometry radar system in the 5.8 GHz ISM band for indoor precise position and motion detection. In *Ieee mtt-s international microwave symposium digest* (p. 1-4). Seattle, WA: IEEE.

Wen, Y.-K. (1976). Method for random vibration of hysteretic systems. *Journal of Engineering Mechanics*, *102*(2), 249-263.

Wotherspoon, L. M., Orense, R., Bradley, B. A., Cox, B. R., Wood, C., & Green, R. A. (2013). *Geotechnical characterization of Christchurch strong motion stations* (Tech. Rep.). Earthquake Commission (EQC).

Yan, Y. J., Cheng, L., Wu, Z. Y., & Yam, L. H. (2007). Development in vibration-based

structural damage detection technique. *Mechanical Systems and Signal Processing*, *21*(5), 2198-2211.

Yigit, C. O., & Gurlek, E. (2017). Experimental testing of high-rate GNSS precise point positioning (PPP) method for detecting dynamic vertical displacement response of engineering structures. *Geomatics, Natural Hazards and Risk*, *8*(2), 893-904.

Zhang, H., Li, L., & Wu, K. (2008). Software-defined six-port radar technique for precision range measurements. *Sensors Journal, IEEE*, *8*(10), 1745-1751.

Zheng, Y., Shi, Z., Lu, R., Hong, S., & Shen, X. (2013). An efficient data-driven particle PHD filter for multitarget tracking. *Industrial Informatics, IEEE Transactions on*, *9*(4), 2318-2326.

Zhou, C., Chase, J., Rodgers, G., Xu, C., & Tomlinson, H. (2015). Overall damage identification of flag-shaped hysteresis systems under seismic excitation. *Smart Structures and Systems*, *16*(1), 163-181.

Zhou, C., Chase, J. G., Rodgers, G. W., & Iihoshi, C. (2017). Damage assessment by stiffness identification for a full-scale three-story steel moment resisting frame building subjected to a sequence of earthquake excitations. *Bulletin of Earthquake Engineering*, *15*(12), 5393-5412.

Zhou, C., Chase, J. G., Rodgers, G. W., Kuang, A., Gutschmidt, S., & Xu, C. (2015). Performance evaluation of CWH base isolated building during two major earthquakes in Christchurch. *Bulletin of the New Zealand Society for Earthquake Engineering*, *48*(4), 264-273.

Zhou, G.-D., & Yi, T.-H. (2013). Recent developments on wireless sensor networks technology for bridge health monitoring. *Mathematical Problems in Engineering*, *2013*, 33.

Zou, Y., Tong, L., & Steven, G. P. (2000). Vibration-based model-dependent damage (delamination) identification and health monitoring for composite structures — a review. *Journal of Sound and Vibration*, *230*(2), 357-378.